Mechanical Changes in the Epithelial to Mesenchymal Transition

Haruka Yoshie

Department of Bioengineering
McGill University, Montreal

October 2019

A thesis submitted to McGill University in partial fulfilment
of the requirements of the degree of Doctor of Philosophy

Abstract

Cell motility is essential in many physiological events such as embryonic morphogenesis and tissue repair. Abnormal cell migration can lead to various pathological events including cancer metastasis. Therefore, understanding physical changes associated with cell migration is important to our understanding of many biological processes. One specific biological transformation with far ranging cell motility impact in physiology and pathology is the Epithelial to Mesenchymal Transition (EMT); in this process, epithelial cells lose cell-cell contacts and become more migratory and invasive mesenchymal cells. While important for diverse biological processes, this transition is believed to be a key phenomenon in cancer metastasis. Therefore, studying physical changes that cells undergo during EMT is critical for understanding the metastatic hallmark of increased cancer cell migration.

In this thesis, I studied the changes in contractile forces and work during EMT utilizing a new soft silicone-based Traction Force Microscopy (TFM) assay that I developed to study contractile forces that adherent crawling cells apply on their environment. Using our new polydimethylsiloxane (PDMS) assay, I found there was a significant increase in contractile work and stress. Furthermore, I observed that cells change actin architecture and increase their shear moduli as they transition from epithelial phenotype to mesenchymal phenotype. To better understand how migratory behavior of the cells changes during this transition, I examined motility of individual cells in a monolayer sheet by tracking nuclei of cells, revealing a transition from diffusive to ballistic movement during EMT. Together, these studies help us to have a more comprehensive knowledge of biophysics of EMT and cancer metastasis. This may open the door to new biophysical approaches to diagnosis and therapy for the disease. Beyond EMT, I also

demonstrate that this PDMS TFM methodology is broadly applicable in diverse scenarios to quantify cell contractility as a metric of cell health, and a tool for screening therapeutic agents.

Résumé

La motilité cellulaire est essentielle pour de nombreux évènements physiologiques tels que la morphogenèse embryonnaire et la réparation tissulaire. Une migration aberrante des cellules peut entraîner divers processus pathologiques, notamment des métastases cancéreuses. Ainsi, l'étude des changements physiques associés à la migration cellulaire est importante pour notre compréhension de nombreux processus biologiques. Une transformation biologique concrète ayant un impact considérable sur la physiologie et la pathologie est la transition épithélio-mésenchymateuse (TEM), un processus par lequel les cellules épithéliales perdent leur adhésion cellule-cellule et deviennent des cellules mésenchymateuses plus migratrices et potentiellement invasives. Quoique nécessaire pour diverses fonctions biologiques, ce mécanisme est considéré étant crucial pour les métastases cancéreuses. L'étude des changements physiques attribués à la TEM est importante pour élucider le comportement invasif des cellules cancéreuses durant la métastase.

Dans le cadre de cette thèse, j'ai étudié les changements des forces contractiles et du travail durant la TEM en utilisant une nouvelle technique de microscopie de force de traction basée sur la silicone souple dont j'ai développé dans le but d'étudier les forces contractiles que les cellules adhérentes rampantes exercent sur leur environnement. En utilisant cette nouvelle procédure basée sur le PDMS, j'ai trouvé qu'il existe une augmentation significative du travail contractile et la contrainte mécanique. De plus, j'ai observé des modifications à l'architecture du réseau d'actine et une augmentation du module de cisaillement lorsque les cellules passent d'un phénotype épithélial à un phénotype mésenchymateux. Afin de mieux comprendre les changements liés à la migration des cellules durant cette transition, j'ai examiné les mouvements de cellules individuelles dans des monocouches en suivant leur noyau, révélant ainsi une transition d'un mouvement diffusif à un

mouvement balistique au cours de la TEM. Ensemble, ces études nous permettent une connaissance plus profonde des mécanismes biophysiques de la TEM et de la métastase cancéreuse. Ces résultats pourraient inspirer de nouvelles approches biophysiques pour le diagnostic et traitement de maladies. À part l'étude de la TEM, j'ai démontré aussi que la méthodologie présentée de la microscopie de force de traction basée sur le PDMS est amplement applicable dans divers scénarios pour quantifier la contractilité cellulaire en tant que mesure de viabilité des cellules et en tant qu'outil de détection d'agents thérapeutiques.

Acknowledgment

I would first like to thank my supervisor, Dr. Allen Ehrlicher, for his mentorship, guidance, advice, and encouragement throughout my graduate degrees. I appreciate all the time he took to discuss my project and challenging problems. Through him, I have learned many important scientific skills and I have grown both professionally and academically.

I would like to thank Dr. Peter Siegel and Dr. Amine Kamen for serving on my advisory committee. I appreciate all the time they took and meaningful feedback throughout my graduate degree.

I would like to thank all my co-authors and collaborators. Special thank you to the members of Dr. Peter Siegel's laboratory for helping me with my research project, especially on biological aspects. I would also like to thank Dr. R. Krishnan and Sumati Ram-Mohan for sharing their expertise in data analysis in traction force microscopy.

I am sincerely grateful for the facilities and laboratory environment that UQÀM has provided, allowing me to pursue my research. Thank you to Denis Flipo for all his time and help with imaging.

I could not have completed this thesis without continuous support from all the members of my lab family. Their warm support and confidence in me have helped me to keep going especially during challenging times.

I would like to express my sincere gratitude to the wonderful staff of Department of Bioengineering and Department of Biomedical engineering, particularly Xavier Elisseeff, Antonella Fratino, Pina Sorrini, Aimee Jabour, and Luisa Seidl, for all the time, advice and support you provided me throughout my graduate studies.

I am very grateful for the opportunity to meet so many kind and fun people in the Bioengineering department. Thank you all for all the support you provided me with and all the fun times we have shared.

I would also like to thank the funding agencies, FRQNT, FRQS, CIHR CCS, and NSERC for the great opportunities to work on my research project, and to pursue my research goals.

Finally, I would like to express my love and thanks to my family and friends who supported and encouraged me throughout the years. I am deeply grateful to my parents for their unconditional love and support in all my endeavors. Otosan & Okasan, Arigato.

Contribution of Authors

The present thesis consists of three manuscripts - two published (Chapter 2 and Chapter 3) and one to be submitted (Chapter 4). I am the first author of all three manuscripts. The contributions of all authors to each manuscript are listed below.

Chapter 2. Traction Force Screening Enabled by Compliant PDMS Elastomers

Published in *Biophysical Journal* 2018, 114 (9)

- Authors: Yoshie, H.; Koushki, N.; Kaviani, R.; Tabatabaei, M.; Rajendran, K.; Dang, Q.; Husain, A.; Yao, S.; Li, C.; Sullivan, J. K.; Saint-Geniez, M.; Krishnan, R.; Ehrlicher, A. J.
- Contributions: Experiment design: HY, RK (Krishnan), AJE; Developed methodology: HY, RK (Krishnan), AJE, Performed experiments: HY, NK, RK (Kaviani), MT, KR, SY, QD, CL, JKS, AH; Analysis and discussion of research: HY, MT, KR, SY, QD, CL, JKS, AH, MSG, RK (Krishnan), AJE; Manuscript writing: HY, MSG, RK (Krishnan), AJE; Manuscript revision: all authors, AJE; Reagents: MSG, RK (Krishnan), AJE

Chapter 3. High Throughput Traction Force Microscopy using PDMS Reveals Dose-Dependent Effects of Transforming Growth Factor-β on the Epithelial-to-Mesenchymal Transition.

Published in *The Journal of Visualized Experiments* 2019, (148)

- Authors: Yoshie, H.; Koushki, N.; Molter, C.; Peter M Siegel; Krishnan, R.; Ehrlicher, A. J.

- Contributions: Experiment design: HY, RK, AJE; Developed methodology: HY, RK, AJE, Performed experiments: HY, NK, CM; Analysis and discussion of research: HY, NK, PMS, RK, AJE; Manuscript writing: HY, RK, AJE; Manuscript revision: all authors; Reagents: PMS, RK, AJE

Chapter 4. Mechanical and Migratory Changes during the Metastatic Epithelial to Mesenchymal Transition

In preparation for submission to *Proceedings of the National Academy of Sciences of the United States of America*

- Authors: Yoshie, H.; Ghagre, A.; Tirgar, P.; Tao, Y.; Ou, J.; Huang, Y.; Mochulska, V.; Hayer, A.L.; Siegel P. M.; Ehrlicher, A. J.
- Contributions: Experiment design: HY, AJE; Performed experiments: HY, PT, AG; Analysis and discussion of research: all authors; Manuscript writing: HY, AJE; Reagents: ALH, PMS, AJE

Contribution to Original Knowledge

The study in Chapter 2 introduces a novel traction force microscopy device based on a soft PDMS substrate, which enables a multi-well format and high-throughput measurements. This methodology will help transform a lab technique into a biomedical methodology. The new device was used as a force screening assay to study contractile response of ASM cells, where contractile agonist activity was quantified, demonstrating this methodology's utility in applications such as diagnostics and pharmacological assays.

The study in Chapter 3 applies the above novel assay to study EMT utilizing an EMT-inducible cell line, NMuMG cells with TGF-β1 treatment. To my knowledge, this was the first comprehensive study to investigate traction stresses and strain energies of monolayer sheets of NMuMG cells with broadly different exposure times and concentrations of TGF-β1, providing exceptional detail into the biochemically regulated mechanical changes of EMT. Moreover, a video component and detailed protocol accompanied this manuscript; this will ensure others have the information necessary to utilize this approach in their research while also demonstrating my commitment to open translational science.

The study in Chapter 4 explores the physical cell changes, including motility, actin structure, and traction stress and strain energy changes during EMT in multi-cellular systems in depth. This detailed and comprehensive quantification of mechanical changes of epithelial cells during EMT provides a uniquely complete study into how cells behave collectively and offers new insight into mechanical changes of monolayer systems in cancer metastasis.

List of Abbreviations

ASM	Airway Smooth Muscle
CFS	Contractile Force Screening
DCIS	Ductal Carcinoma in Situ
ECM	Extracellular Matrix
FTTC	Fourier Transform Traction Cytometry
MSD	Mean Squared Displacement
MSM	Monolayer Stress Microscopy
MTC	Magnetic Twisting Cytometry
NMuMG	Normal Murine Mammary Gland
PAA	Polyacrylamide
PDMS	Polydimethylsiloxane
TFM	Traction Force Microscopy
TGF-β1	Transforming Growth Factor-β1
2D	Two Dimentional
RMS	Root Mean Squared
RMST	Root Mean Squared Traction

Contents

Chapter 1: **: General Introduction**

Cell motility is essential for a wide range of biological processes, including embryonic development, wound healing, and immune response.[1] For cells in complex multicellular organisms, coordination of these movements is essential to elicit the appropriate physiological responses. The diversity and ubiquitous nature of these responses are beyond the scope of this thesis; however, I will briefly highlight some of these processes.

Cells undergo both local and long-range migration in the formation of tissues and organs during embryonic development, and defects in this motion are related to numerous pathologies.[2] Immune cells migrate to protect the organism from infections and carry out the inflammatory response.[3] During wound healing processes, fibroblast cells migrate into the damaged area to repair wounds.[1, 3] Cell migration is also critical in pathological conditions such as cancer metastasis. Increased movement is a crucial biophysical property of metastatic cancer cells.[4]

1.1 Cell Motility and Forces

Given the importance and breadth of cell movement in biology, it is not surprising that a vast assortment of motility modes has been identified. Cells in suspension may swim by wiggling their flagellar tails, and bacteria swim by rotating their flagellar motors.[3, 5] In this work, I am examining the movement of cells adhered to a two-dimensional (2D) substrate. One of the models of the movement to describe the adherent locomoting cells is called “cell crawling.”[6] A wide variety of mammalian cells exhibits this mode of movement, which may be principally characterized by acto-myosin contractility along the axis of movement. Despite the existence of other types of cell movement, the aspect of cell crawling movement is the primary focus of this thesis. In the next section, I will discuss the basic principles of cell crawling in more detail.

1.1.1 Cell Crawling

Individual crawling cells continuously undergo the following sequence of events: (1) Extension of the membrane at the leading edge, (2) attachment to the substrate at the leading edge and detachment at the rear end, and (3) translocation of cell body as shown in Figure 1-1.

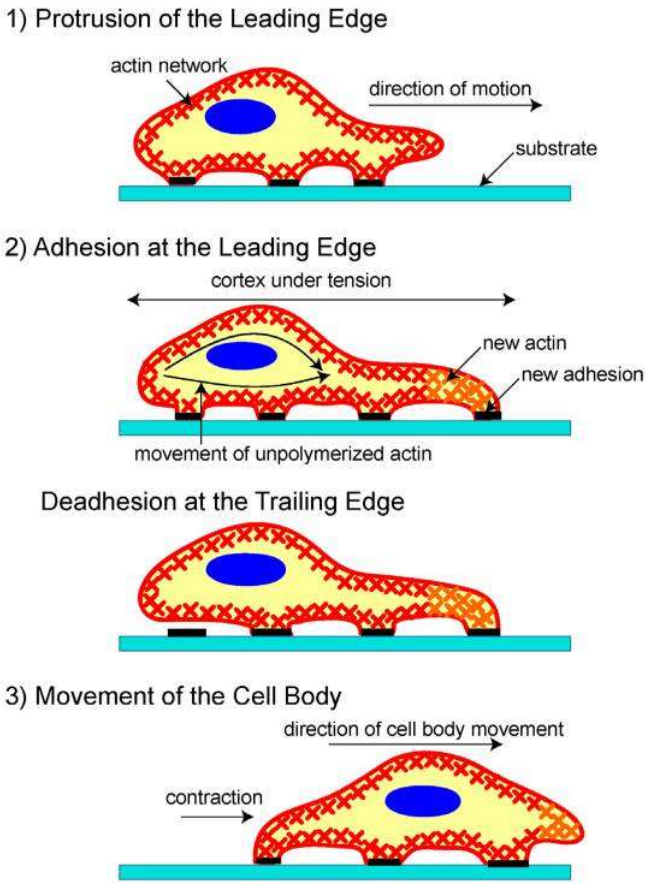

Figure 1-1: A schematic diagram of cell crawling model adapted from "The Forces Behind Cell Movement." by R. Ananthakrishnan and A. Ehrlicher, 2007, *International Journal of Biological Sciences*, *3* (5), 303-317 Copyright (2007), with permission from The Company of Biologists.[6] The cell first extends its leading edge and adheres to the underlying substrate. The cell detaches itself at the opposite end. In the final step, the cell translocates its body forward by pulling on the underlying substrate generating contractile forces.

(1) Membrane extension

There are several different kinds of membrane protrusions.[3] For example, lamellipodia have thin and broad sheet-like structures with branching actin filament networks and are often formed at the leading edge of the moving cells.[3, 7] Another example of membrane protrusion is filopodia. Filopodia have a thin and spike-like structure with long parallel actin bundles.[8] Cells also form stress-fibers, which are the bundles of actin filaments that transmit forces across the cell and bridge distal adhesion sites in the translocation step.[6, 9]

(2) Attachment and detachment

For cells to move across the surface, they must form adhesions with underlying substrates. Protrusions at the leading edge adhere to the underlying substrate.[3] These adhesion sites between cells and the extracellular matrix (ECM) are called focal adhesions.[10] The focal adhesions connect the actin cytoskeleton to the extracellular matrix in cells cultured on 2D substrate surfaces. For adherent cells to move forward over the surface, detachment must occur. While cell-substrate adhesions are formed at the leading edge, focal adhesions are disassembled at the trailing edge for the translocation of the cell body.[6]

(3) Translocation

Cells migrate by translocating the rest of the body. Traction force is the force that migrating cells apply to their underlying substrate during this translocation.[6] This contractile force that cells apply to their surroundings while pulling themselves against the substrate surface primarily arises from acto-myosin contraction. Myosin is a motor protein which produces energy by converting chemical energy to mechanical energy in an ATP-dependent process.[3, 9] These forces are crucial in many cellular functions such as cell proliferation and

differentiation[11], wound healing[12], and migration[13]; hence studying and measuring traction forces are critical in better understanding of many biological events.

1.1.2 Traction Force Microscopy (TFM)

Traction Force Microscopy (TFM) is a method to quantify contractile forces exerted by cells on the underlying substrate. The field of TFM began in the 1980s, where researchers employed thin-film wrinkling assays[14], and since then there has been a large number of significant advancements in this technology[15-16]. Although there are many different methodologies to measure traction forces, this thesis employs the most commonly used approach employing soft elastic substrates with flat continuum surfaces. In this continuous substrate approach, cells are cultured on soft elastic substrates with known elastic moduli. Fiduciary particles, usually fluorescent microbeads, are embedded in the elastic substrate. The underlying elastic substrate is deformed as adherent cells on the substrate surface pull on the substrate. These cell-induced deformations of the elastic substrate are quantified from the displacement of the beads. Displacement of the beads is calculated by comparing bead positions with the cells adhered to the substrate and bead positions without cells (null force image). To obtain the null force images, cells are detached from the substrate. With the displacement calculated along with the known Young's modulus of the elastic substrate, the traction stresses applied by cells on the substrate are calculated. This is most simply described by Hooke's law of an elastic spring, $\boldsymbol{F}=-k\boldsymbol{x}$.[16] In this case, $\boldsymbol{F}$ is the contractile force that cells apply, k is the elastic modulus of the substrate that cells are cultured on, and $\boldsymbol{x}$ is the bead displacement (cell-induced deformation). In the commonly used procedure, Fourier Transform Traction Cytometry (FTTC) introduced by Butler *et al.*[17], tractions are computed in Fourier space. This approach is computationally more efficient than the previous brute-force vector TFM analysis method introduced by Dembo and Wang[18]. More details may be found in the Appendix.

TFM substrates are fabricated with different compliant materials, one of the most common ones being polyacrylamide (PAA) gels. PAA gels have been advantageous in substrate preparations for TFM studies due to easily-tunable physiologically relevant stiffness of 100 Pa – 100 kPa.[19-21] Despite the biophysically practical range of stiffness, PAA being a hydrogel also has disadvantages. Due to the large volume content of water, PAA gels are sensitive to osmolarity, humidity, and temperature; this requires extra attention when handling and storing the samples to prevent swelling, shrinkage, and pH change of the samples. All the undesired conditions may cause changes in the mechanical properties of the materials. Furthermore, a large content of water makes the material more susceptible to microbial contamination, requiring care in sterile longer-term storage. Silicone-based polydimethylsiloxane (PDMS) is another material that is commonly used for TFM measurements. Unlike hydrogels, water-free silicone-based PDMS samples are stable and inert, offering long shelf-lives; however, preparing PDMS gels with elastic moduli below 10 kPa has been challenging.[21] The need for softer silicone-based assays motivated me to develop a compliant PDMS-based traction force assay. By using a commercially available silicone kit, I successfully developed a novel elastic stable silicone-based traction force device with physiologically relevant moduli, including moduli lower than 10 kPa. By utilizing a non-hydrogel material as our substrate, I was able to employ a multi-well format on a monolithic substrate. This new format offers not only stability, but also high-throughput measurements, further gaining screening capability. By utilizing this device combined with the TFM technique, physical properties of different biological systems have been studied.

1.1.3 Cell Forces in Diseases

In recent years, significant progress has been made into understanding the physical and mechanical aspects of biological systems. Many studies have demonstrated that changes in these

physical properties such as tissue stiffness, cellular motility and contractile force changes are associated with many diseases and disorders including asthma, kidney failure, and cancer.[22-24] In the following sections, I will briefly describe some of the fields for which I have most closely worked and published on.

1.1.4 Asthma

Asthma is a common, incurable, and yet poorly understood inflammatory disease of the airway. It is characterized by acute narrowing of the airway due to airway hyperresponsiveness. In asthma, airway smooth muscle (ASM) cells contract causing breathing disorders, and in some cases may be triggered by allergens or pollutants, as well as medications.[24-26] Due to this change in contractile response, the airway gets constricted during an asthma attack, making it difficult for patients to breathe. To alleviate the constricted airway, ASM cells need to relax, and inhaled pharmaceuticals, including corticosteroids, are often used.[27] In fact, a smooth muscle relaxant is often used to counteract narrowing of the airway in the current asthma therapy. β2-adrenoceptor agonists, ligands for β2-adrenoceptor, are one of the most commonly used and the most effective bronchodilators for asthma therapy.[28-30] Activation of β2-adrenoceptor, located on the surface of ASM cells, plays an essential role in ASM relaxation, thus making it an ideal target for asthma treatment and management.[31] However, many studies have mainly focused on investigations of immune responses and inflammatory functions instead of the impact of relaxant drugs on the contractility of muscle cells.[32] Given the complexity of asthmatic disorders and desensitization to drugs to relax the airway, there is a need for screening technology to directly measure the contractile response of ASM cells to the relaxation compounds to investigate their efficacy. Using our high-throughput traction assays, we were able to study this change in contractility of the airway of ASM cells and their response to different pharmaceutically relevant relaxation

compounds by directly measuring and quantifying contractile forces of ASM cells *in vitro*. Screening of contractile responses of airway muscle cells with various relaxant agents may be utilized in the development of effective drug therapies for asthma. I will describe these findings along with the PDMS-TFM platform developed for quantifications in Chapter 2. Critically, asthma is only one example of a virtually never-ending list of biomedical challenges with a clear contractile component. Using the same platform, I also extensively studied diverse physical aspects of cancer, focusing on the process of Epithelial to Mesenchymal Transition (EMT) in metastasis from cellular force perspectives. The following sections are primarily focused on cancer and the physical changes in its progression.

1.2 Cancer & Cancer Metastasis

Cancer is a multi-faceted and exceptionally complex disease that has various phases and forms, and many aspects of it are not well known. The nature of its pathology makes generalized diagnostics and treatments difficult, particularly in metastasis, where cancerous cells leave their original tumor site and migrate to new secondary sites, accounting for 90% of cancer-related deaths. There are several genetic and biochemical changes associated with cancer metastasis, and the vast majority of research focuses on these variations. However, research has recently begun to question the role of physical aspects in metastasis, as many cancer cells appear to display similar mechanical changes during metastasis.[33-36]

1.2.1 Cancer Metastasis

During cancer metastasis, typically a sequence of events similar to the following occurs as shown in Figure 1-2.

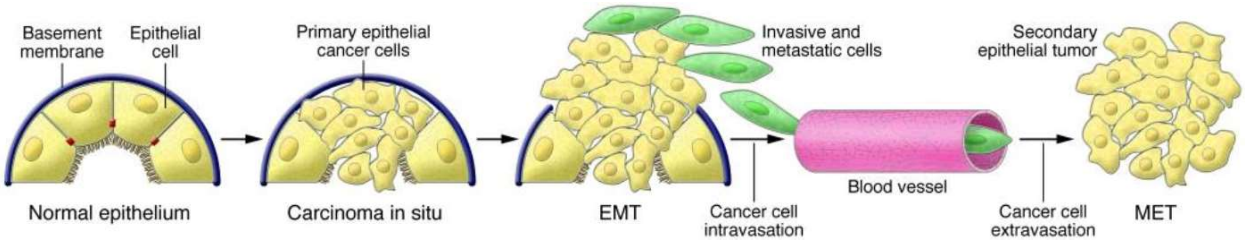

Figure 1-2: A schematic of cancer progression adapted from "The basics of epithelial-mesenchymal transition." by R. Kalluri and R. A. Weinberg, 2009, *The Journal of Clinical Investigation*, *119* (6), 1420-1428. Copyright 2009, with permission from American Society for Clinical Investigation.[37] Epithelial cells with apical-basal polarity detach themselves from the basement membrane. The tumor cells leave their primary site and enter the blood or lymphatic vessels to reach a remote location. The cells exit the vessels and start forming a secondary tumor at their new location.

This process is exceptionally complex in its details, with each step meriting its own review; however, in this work, I will present the general process of metastasis:

1) Detachment: In the first step, tumor cells from the primary site detach themselves from their neighboring cells and invade into the surrounding tissue.
2) Intravasation: Cells enter the blood and lymphatic vessels.
3) Circulation: Once cells enter the vessels, they travel to reach a distant location in the body.
4) Extravasation: The cells leave the vessels and invade the new location.
5) Colonization: Cancer cells grow at their new site, creating a secondary tumor.

   This process in different cases and situations is reviewed in many articles and books; for further reading, an excellent summary of known steps in metastasis can be found in Chitty *et al*.[38]

Considering that the majority of these steps involve cell migration, it is clearly plausible that biophysical changes related to the cell's ability to move, deform, and push its way through the cellular microenvironment are key if not causative to the process. In the following section, I will

describe in greater detail a specific cellular transformation associated with metastatic progression, the Epithelial to Mesenchymal Transition (EMT) and its role in cancer metastasis.

1.2.2 Epithelial to Mesenchymal Transition in Cancer

EMT is a complex biological process where cells undergo changes from a polarized epithelial phenotype to a more migratory elongated mesenchymal phenotype. When cells undergo this transition, epithelial cells lose their cell-cell adhesions and polarity, detach themselves from the epithelial layer, and migrate away, enabling their invasive behavior. EMT is classified into three subtypes based on their biological consequences: Type 1 which is associated with embryonic development, Type 2 which is associated with wound healing, and Type 3 which is associated with cancer metastasis.[39-40] While EMT is related to diverse biological and pathological events, in this thesis, I will focus on Type 3 EMT. During cancer metastasis, these transitions are thought to allow cancer cells to increase their migratory capacity, facilitating the spread of the disease.[37]

Hallmarks of EMT

In the past decades, researchers have characterized EMT, and while EMT itself is a very broad spectrum with indeterminant states between epithelial state and mesenchymal state, there are several factors generally accepted as hallmarks of EMT. Cells undergo several changes during EMT:

(1) Dissolution of cell-cell contacts

Epithelial cells form cell-cell contacts through several types of junctions. These junctions include tight junctions, adherens junctions, gap junctions, and desmosomes. During EMT, these junctions are deconstructed, and cell-cell contacts are weakened. The dissolutions of the cell-cell adhesions are accompanied by relocation or degradation of the proteins present

in these junctions.[41] Changes in the expression levels of particular proteins are essential for separation of the epithelial sheet, and are regarded as hallmarks for EMT; these proteins include claudin[42], E-cadherin[43], and connexin[44].

(2) Loss of apical-basal polarity

Epithelial cells with cell-cell junctions display polar structure with distinct domains: apical, lateral and basal domains. The basal side adheres to the basement membrane (often referred to as cell-Extra Cellular Matrix (ECM) junctions); in the case of *in vitro* studies, cells adhere and spread on the substrate. As junctions between the neighboring cells mature, apical and basal ends are separated, establishing a polar structure.[42] As cells lose cell-cell junctions during EMT, they lose apical-basal polar structure; they form a polar structure with front and rear ends, which facilitates their migration.[41-42]

(3) Re-organization of actin cytoskeletal structure

In epithelial cells, actin filaments are localized in the cortex of the cells as thin bundles (referred to as apical cortex actin).[45] As cells acquire more mesenchymal phenotype during the EMT process, they become more migratory. In order for them to migrate, cells reorganize their actin cytoskeletal structures into thick bundles of parallel actin fibers.[41, 45] These are known as stress-fibers due to their contractile acto-myosin composition and are an essential component of most contractile force generation and motility.

(4) Change in cell morphology

As cells reorganize cytoskeletal actin filaments during the transition, cells change in their morphology. Epithelial cells display more connected structures with a cobblestone-like morphology by forming adhesions with neighboring cells, whereas cells with more

mesenchymal characteristics demonstrate less cell-cell adhesions with more elongated morphologies, having parallel actin bundles.[45]

(5) Change in gene expression

In addition to above-mentioned changes, cells alter various gene expression during EMT such as downregulation of E-cadherin and claudins, upregulation of N-cadherin and vimentin.[37] The changes in the expression of genes vary from cell to cell and tissue to tissue. For example, overexpression of vimentin has been reported in many breast cancer cell lines with more aggressive behaviors, suggesting the role of vimentin in increased migratory and invasive behavior of breast cancer cells.[46-47] Gene expression levels are regulated by different transcription factors, such as SNAIL, ZEB, and TWIST.[41] Changes in gene expression levels and transcription factors associated with these changes are beyond the scope of this thesis; however, I will discuss changes in cadherin expressions and their role in EMT in Section 1.3.1.

Induction & Regulation of EMT

EMT is induced and regulated through various factors and pathways. Transforming growth factor-β (TGF-β) is a cytokine involved in many biological processes, including proliferation, differentiation, and migration.[48-49] In mammals, there are three different forms of TGF-β: TGF-β1, TGF-β2, and TGF-β3, and there are three associated transmembrane receptors: type 1 (TβR-I), type 2 (TβR-II), and type 3 (TβR-III).[40, 49] Both canonical and non-canonical TGF-β pathways contribute to the EMT program.[40] In the canonical pathway, TGF-βs binds to TGF-βR-II receptor, which recruits and activates TGF-βR-I receptor, further activating signaling transducers Smad2 and Smad3, leading to the formation of Smad2/3 complex. This in turn forms additional complexes with Smad4 protein.[49] The interaction of Smad4 with different

transcription factors participates in gene regulation in EMT.[40, 49-50] Non-canonical pathways involve several different pathways, such as the MAP kinase family including JNKs and ERKs and Rho-GTPase family including RhoA and Rac1.[40, 49-50] Although it is widely accepted that cells undergo changes during EMT, the precise role of EMT in cancer metastasis remains unclear.

In this study, by utilizing an EMT-inducible cell line, Normal Murine Mammary Gland (NMuMG) cells, I investigated changes in physical behaviors during EMT. To understand the progression of the transition, I monitored cells treated with TGF-β1 for different incubation times. The physical changes that NMuMG cells undergo with TGF-β1 treatment for various concentrations and different incubation times are presented in Chapter 3.

1.2.3 Breast Cancer

Breast Cancer is the most common cancer among women in Canada apart from non-melanoma skin cancer[51] and is a complex and heterogeneous disease. Based on gene expression patterns, breast cancer is classified into different subtypes: Luminal-A, Luminal-B, HER2-positive, and triple-negative (basal-like and claudin-low), and Normal-like.[52-53] For each subtype, patients' prognosis and clinical outcome are different.[54]

Carcinomas are malignancies which originate from epithelial tissues. The majority of the breast malignancies are of this type.[55] During carcinoma progression, ductal epithelial cells undergo hyperproliferation and develop into ductal carcinoma in situ (DCIS).[56] DCIS is bounded by the basement membrane, thus still contained to the original location.[55] As the disease progresses, the cells invade into the surrounding stroma by penetrating through the basement membrane, evolving into invasive carcinoma.[55-56] In the final stages of the disease, the invasive

carcinoma becomes metastatic and enters vasculature, spreading the disease to the other parts of the body at distant locations.[55-58]

Breast Cancer Therapy

While therapies are not the focus of this work, I would like to discuss some of the current strategies available. There are several different options for treatment of breast cancer. Mastectomy and radiation are applied to locally treat the cancer tissue. For more systemic treatment, medical interventions such as chemotherapy, hormone therapy, and antibody-based therapy are applied.[59-60] These anticancer agents target different biological mechanisms, thus preventing disease progression differently. For example, methotrexate and 5-fluorouracil, commonly used anticancer drug for chemotherapy, both prevent cell proliferation by interfering with DNA synthesis.[60-61] Aromatase inhibitors and hormonal intervention inhibit cell proliferation by preventing the production of estrogen hormones.[60-62] Trastuzumab is an example of antibody-based therapy and directly targets the transmembrane protein HER-2 receptor whose expression is amplified in 30% of breast cancer patients, leading to poor prognosis.[60, 63-64]

Although significant progress has been made in breast cancer therapy, there is still a great need to improve the treatment. My work in studying the mechanics of cancer is strongly motivated by my desire to see breakthrough treatments in this disease. I hope that by having a better understanding of the physical changes in cancer, we may explore new strategies for diagnosing and treating these diseases. In the next section, I will discuss the mechanics and physics of cancer.

1.2.4 Physical Changes in Cancer

The majority of cancer research has focused on genetic and biochemical changes; however, more recently, researchers have started examining roles and impacts of physical and mechanical

changes in this pathology. A significant effort to quantify biomechanical and biophysical changes that occur in cancer has been made in the past decade. As recently discovered during disease progression, tumor cells not only undergo biochemical changes, but also biomechanical changes.[33-34] In fact, cancer is often diagnosed by its increased tissue stiffness.[65] The elevated tissue rigidity in cancer is due to increased ECM stiffness, which arises from modifications in matrix composition and levels of crosslinking matrix fibers.[22, 66-67] Some *in vitro* studies have shown the link between the cell motility and the underlying substrate stiffness, suggesting the altered invasive behavior of cancer cells.[67] Although the tumor tissues are usually found to be stiffer than their surrounding normal tissues, some *in vitro* studies have shown that individual tumor cells are softer than non-cancer counterparts.[68-69] This increased deformability of cancer cells might explain translocation of metastatic cancer cells, squeezing through dense fiber networks and confined small spaces in the body more easily.[70] In addition to alterations in cellular moduli, many *in vitro* studies have shown that cancer cells change contractile forces that they apply on their surroundings: they apply larger contractile forces with increasing malignancy and metastatic potential.[36, 71-73] Critically, these mechanical changes may be a common link between diverse cancers, and studying traction forces and cellular moduli changes may open up new possibilities for cancer screening. Additionally, tuning cancer cells mechanically by targeting physical behaviors, such as increased forces and stiffness of cancer cells at the cellular level, may reveal other possibilities for cancer treatment and management.

1.3 Collective Cell Behaviour

Cells in organisms are rarely isolated, but rather function in concert with each other, generating collective mechanical behavior. In particular, epithelial cells are tightly packed and form cell-cell contacts with neighboring cells, often existing as sheets in our body. During EMT epithelial cells lose their coherent behavior and begin to function as more isolated units; however, the

biochemical and biophysical details of this process are unclear. Although there are many different cell adhesion molecules, I will focus on cadherin, one of the adherins junctions proteins, in the next section as it is believed to play an important role in EMT.

1.3.1 Cadherins in Adherens Junctions

Cadherins are cell-adhesion membrane proteins present in adherens junctions between cells. Adherens junctions link the membrane of neighboring cells. The extracellular domain of cadherins binds to another cell while the cytoplasmic domain binds to adaptor proteins, α- and β-catenins, which anchor to actin filaments. Cadherin proteins mediate cell-cell communication and adhesion, with E- and N-cadherins being the most commonly expressed cadherins.[74] E-cadherin is the primary component of adherens junctions of epithelial cells, providing links to adjacent cells.[43, 74] A cadherin switch is a process in which the expression level of E-cadherin is reduced while the expression level of N-cadherin is increased. This switch is considered as a hallmark of EMT, leading to weakened cell-cell adhesions with neighboring cells and increased migratory and invasive behaviors.[43, 74-76] There has been a growing interest in the collective behaviors of cells, and cadherin switch and its role in cell-cell contacts have been extensively reported in the literature.[77-79] As of yet, many aspects of cell-cell contacts and collective work of cells are still not well-understood. Recent studies have introduced different models to describe the collective behaviors of cells.[80-81] In the following section, I will describe different cell migration modes for both single cells and multi-cellular systems.

1.3.2 Different Modes of Single and Collective Cell Migration

Although cancer cells can travel individually, they can also travel as a collective multi-cellular unit. Single cell migration can be further sub-divided into ameboid and mesenchymal modes. In ameboid mode, cells have a round morphology with high deformability, and coupling between

the cells and underlying ECM is weak, and cells in this mode move quickly.[82-83] In mesenchymal mode, cells form strong adhesion with the underlying substrate and have more spindle-shaped elongated morphology.[82, 84] Mesenchymal cells can also have a chain-like movement where neighboring cells migrate on the track.[84] When cells move collectively, they retain their cell-cell junctions with neighboring cells. Collective migration mode also has several different mechanisms: sheet/cluster migration as in case of tumor cells; a branching morphogenesis migration in case of glandular duct development; and vascular sprout migration in case of blood vessel development.[84-86] It is clear that cells choose the appropriate migration mode to meet their purpose in both physiological and pathological conditions. However, the mechanisms of collective behaviours and cooperativity of neighboring cells in different multi-cellular systems remain unclear. Different modes of cell migration in cancer metastasis are illustrated in Figure 1-3.

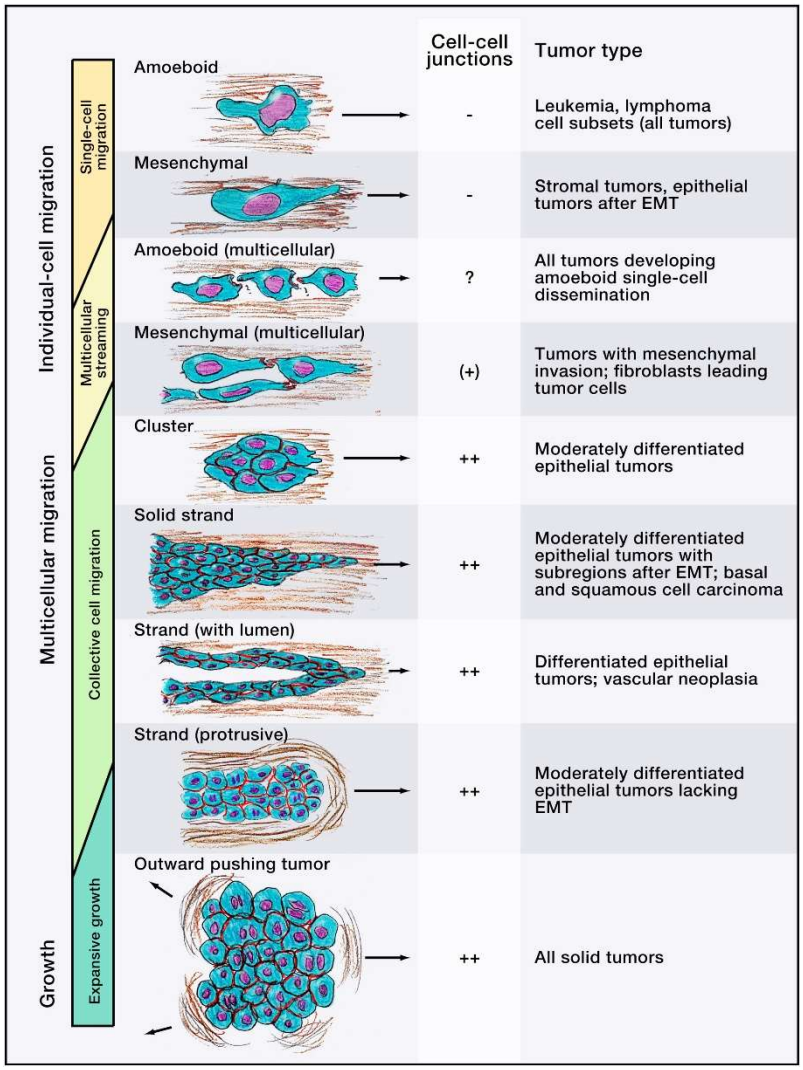

Figure 1-3: Illustration of different modes of cell movement in cancer metastasis. Reprinted from *Cell*, 147 (5), P. Friedl and S. Alexander, Cancer invasion and the microenvironment: plasticity and reciprocity. 992-1009, Copyright (2011), with permission from Elsevier.[80] There are several different modes of cell movement for both single and multi-cellular cell migration. An individual cell can move by amoeboid mode or mesenchymal mode; these modes can also occur in a streaming manner. Multi-cells move collectively as clusters or strands.

In this study, I investigated diverse physical aspects of epithelial cells in monolayer sheets as they undergo EMT. Contractile force changes and moduli changes of monolayer cells were studied based on TFM and Magnetic Twisting Cytometry (MTC), respectively. The changes in cellular and nuclear volumes were also quantified. Additionally, migrations of cells as they undergo EMT were studied by tracking nuclear movements of the cells cultured as monolayer sheets. The goal of Chapter 4 is to give a more comprehensive understanding of EMT from physical perspectives in multi-cellular systems: how cells change physical behaviors as epithelial cells acquire more mesenchymal phenotype, and to give some insights into cooperative behaviors of neighboring cells in monolayer sheets as they go through the transition.

1.3.3 Intercellular Stresses

In order for cells in multi-cellular systems to function as a unit, adjacent cells must form stable adhesions and transmit forces in between. While TFM reveals the contractile stress that the cell applies to the substrate, it does not directly describe the stresses between cells in a monolayer. To fill this need, Tambe *et al.*[87] developed Monolayer Stress Microscopy (MSM), a technique to measure local stress at the cell-cell junctions within the monolayer sheet of the cells. In MSM, intercellular stresses are calculated from the unbalanced tractions between cells and substrate.[88] Detailed analysis of intercellular forces would give a better understanding of how neighboring cells communicate and work together in cancer. The understanding of this communication is critical in the treatment of these diseases as it can give researchers new therapeutic targets.

Chapter 2 : Traction force screening enabled by compliant PDMS elastomers

Haruka Yoshie[1], Newsha Koushki[1], Rosa Kaviani[1], Mohammad Tabatabaei [1,5], Kavitha Rajendran[2], Quynh Dang[2], Amjad Husain[2], Sean Yao[2], Chuck Li[3], John K Sullivan[3], Magali Saint-Geniez[4], Ramaswamy Krishnan[2*], Allen J. Ehrlicher[1*,#].

[1]Department of Bioengineering, McGill University, Montreal, Quebec, Canada;

[2]Department of Biomedical Engineering, Amirkabir University of Technology, Tehran, Iran

[3]Beth Israel Deaconess Medical Center, Boston, Massachusetts

[4]Amgen Inc., Thousand Oaks, California

[5]Schepens Eye Research Institute, Harvard Medical School, Boston, Massachusetts

* contributed equally

Corresponding author

2.1 Abstract

Acto-myosin contractility is an essential element of many aspects of cellular biology, and manifests as traction forces that cells exert on their surroundings. The central role of these forces makes them a novel principal therapeutic target in diverse diseases. This requires accurate and higher capacity measurements of traction forces; however, existing methods are largely low throughput, limiting their utility in broader applications. To address this need, we employ Fourier-transform traction force microscopy in a parallelized 96-well format, which we refer to as contractile force screening (CFS). Critically, rather than the frequently employed hydrogel polyacrylamide (PAA), we fabricate these plates using polydimethylsiloxane (PDMS) rubber. Key to this approach is that the PDMS used is very compliant, with a lower-bound Young's

modulus of approximately 0.4 kPa. We subdivide these monolithic substrates spatially into biochemically independent wells, creating a uniform multiwell platform for traction force screening. We demonstrate the utility and versatility of this platform by quantifying the compound and dose-dependent contractility responses of human airway smooth muscle cells and retinal pigment epithelial cells. By directly quantifying the end-point of therapeutic intent, ASM contractile force, fills an important methodological void in current screening approaches for bronchodilator drug discovery, and more generally, in measuring contractile response for a broad range of cell types and pathologies.

2.2 Introduction

Many adherent cells employ acto-myosin contractility to exert traction forces on their surroundings. These forces are an essential part of cellular deformation[89-91], adhesion[92-94], spreading[95], and migration[23, 88, 96], as well as growth[97], homeostasis[98-99], gene expression[100], and apoptosis [101]. The significant role of traction force makes it a novel principal therapeutic target in diverse diseases, however, accurate measurements of traction forces are essential for this approach.

To quantify cell traction forces, researchers have employed a variety of techniques and tools. From the first wrinkling thin silicone sheets[102] to complex 3D multicellular contractility[103], a multitude of biomechanical methods have been developed collectively referred to as Traction Force Microscopy (TFM), as reviewed here[104]. While these approaches have enabled the discovery of valuable mechano-biological connections, these methods are generally inherently slow and restricted to low-throughput implementation, limiting their utility as tools in broader pharmacological applications.

To address this need, we employ Fourier-transform traction force microscopy in a parallelized 96-well format, an approach we refer to as contractile force screening (CFS). Critically, rather than using the frequently employed hydrogel polyacrylamide (PAA), we fabricate these plates using polydimethylsiloxane (PDMS) rubber. Key to this approach is that the PDMS used is very compliant, with a lower-bound Young's modulus of approximately 0.4kPa, unlike commonly used Sylgard 184 formulations (additional detailed mechanical characterization is presented in the online material). Like PAA, soft PDMS elastomers possess several material-favorable properties: their stiffness is tunable over a large physiological range (Figure 2-1), and they are non-toxic, non-degrading, and biologically inert. In addition to these aspects, this compliant PDMS has numerous advantages over PAA: 1) it is optically transparent with a refractive index of ~ 1.4 which is comparable to glass, 2) it is indefinitely stable after production without special storage considerations, 3) it is amenable to spin coating providing a simple means of creating a uniform and flat surface, 4) it is a uniformly non-porous surface, unlike PAA whose porosity can vary strongly with cross-linking concentration[105]. Critically, the monolithic impermeable nature of these silicone substrates makes them easy and ideal to subdivide spatially into biochemically independent wells, creating a uniform multi-well platform for traction force microscopy. Taken together, our compliant PDMS presents numerous advantages in becoming a new standard in soft substrates for TFM; these advantages are particularly important for a standardized higher-throughput technology and will enable widespread adoption of CFS from our previous approach using PAA[106].

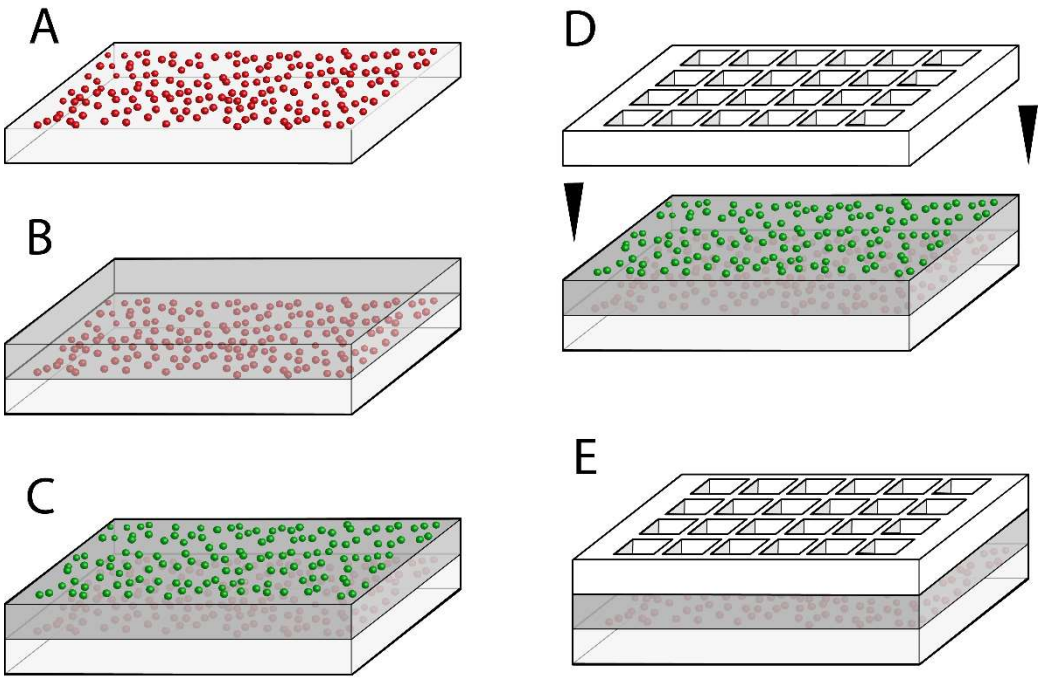

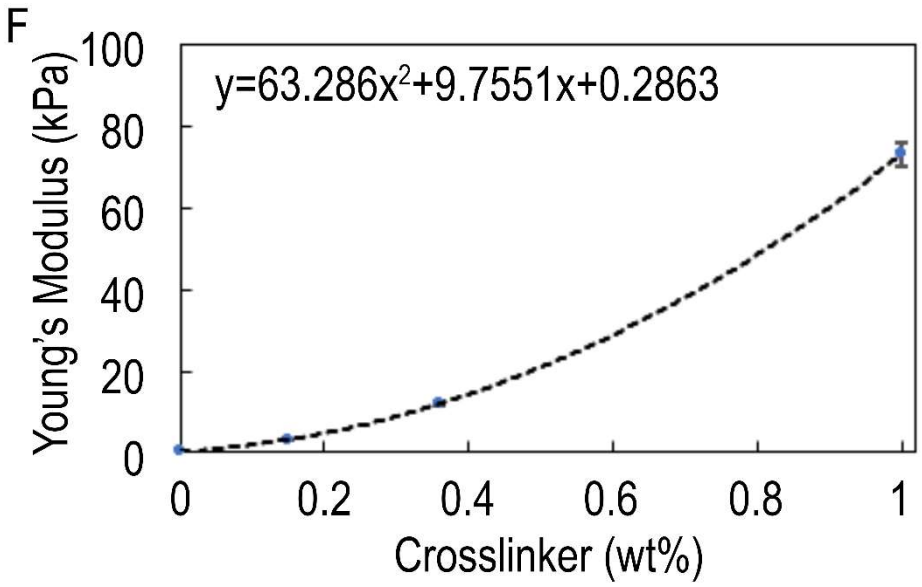

Additional Crosslinker Concentration (wt%)	G'(kPa)	Young's Modulus (kPa)
0	0.135 ± 0.014	0.358 ± 0.043
0.15	1.0096 ± 0.102	3.0288 ± 0.035
0.36	4.027 ± 0.245	12.08 ± 0.73
1	24.443 ± 0.989	73.32 ± 2.96

Figure 2-1: **Fabrication of multi-well substrates and mechanical characterization of tunable PDMS elastomer.** Multi-well PDMS devices for TFM are fabricated by A) optionally coating a layer of fluorescent microspheres (for de-drifting images) on the custom glass slide, B) spin coating a ~100μm thick layer of compliant PDMS, C) spin coating a ~1μm thick layer of compliant PDMS mixed with custom-synthesized beads with different fluorescence emission for measuring cell induced deformation of the PDMS, D) bonding a multiwell partitioning strip to the top, and E) ligating and culturing cells. F) Graph of PDMS moduli as determined by shear rheology (n=4 independent preparations per data point). G) Table of same mean PDMS moduli +/- standard deviation.

2.3 Methods

Cell culture: Primary human airway smooth muscle (ASM) cells were obtained from the Gift of Hope Organ and Tissue Donor Network. These cells have been well-characterized previously, e.g. [107]. All measurements were performed using cells at passage 5-8 from two non-asthmatic donors. ARPE-19 (retinal pigment epithelium) cells were obtained from American Type Culture Collection. All culture media formulations are provided in the supplemental material.

Preparation of silicone substrates in custom 96-well plates: We fabricate our multiwell TFM dishes by applying very compliant and tunable modulus PDMS onto custom cut glass slides and then partitioning the wells with a plastic subdivider. In brief, very compliant commercial PDMS (NuSil® 8100, NuSil Silicone Technologies, Carpinteria, CA) is mixed with a small percentage by weight of Sylgard 184 crosslinking agent to make a tunable (E= 0.4 to 73 kPa) substrate, which is impregnated with a ~1μm thick layer of fiduciary particles to reveal cell-induced deformations. This approach differs from existing PDMS TFM strategies, as this substrate is comparably compliant to polyacrylamide and linearly elastic, yet not a hydrogel. Full details of plate preparation, including detailed substrate functionalization and mechanical characterization, are provided in the supplemental materials.

Mechanical characterization of PDMS substrates: We measured the frequency dependent storage and loss shear moduli for PDMS with different additional crosslinker formulations using shear rheology (Anton Paar MCR 302, 25mm parallel plate tool). Samples of approximately 0.6ml were loaded and cured at 100 C for 2-3 hours, the normal force was reset, and the shear modulus was measured at 1 Hz and 0.5% percent strain. Young's moduli, E, were calculated from shear moduli, G, as $E=2*G(1+v)$ by assuming the PDMS is incompressible with a Poisson ratio, v, of 0.5. Further mechanical characterization is described in the online supplement.

Measurements of cell traction forces: The 96-well plate was mounted within a heated chamber (37°C) upon an automated computer-controlled motorized stage and imaged at 10x magnification using a monochrome camera (Leica DFC365 FX) affixed to an inverted microscope (DMI 6000B, Leica Inc., Germany). We acquired fluorescent images of microspheres embedded in the elastic substrate immediately underneath the cells at (i) *baseline* with no treatment, (ii) after *treatment*, and (iii) after cell detachment with trypsin (*reference null-force image*). By comparing the fluorescent images at reference with the corresponding images at baseline and after treatment, we obtain a time series of bead-displacement, and hence substrate deformation fields (resolution = ~15μm). Using the measured substrate deformation, the pre-defined substrate modulus, and thickness, traction force maps and the root-mean squared value were calculated over a 732μm by 732μm area, on a well-by-well basis, using the approach of Fourier-transform traction cytometry[17] modified to the case of cell monolayers[108].

Drugs: Histamine, Isoproterenol, Salbutamol, Salmeterol, Formoterol, Thrombin, and H_20_2 were purchased from Sigma-Aldrich. Y27632 was purchased from EMD Millipore. Human VEGF-A^{165} and Bevacizumab were purchased from R&D systems and Genentech, respectively.

Statistics: Statistical comparisons for traction differences were performed using the non-parametric Wilcoxon matched-pairs signed rank test. Differences were considered significant when $p<0.05$.

2.4 Results and Discussion

CFS entails quantifying the cell-generated forces by measuring fluorescent bead positions in each well of the 96-well plate: 1) without cells, 2) with cells adhered at baseline contractility, and 3) after treatment with the compound(s) of interest. For example, for a representative well of a 96-well plate (Figure 2-2A), shown are ASM traction force maps and the root-mean squared

value (inset) at baseline (Figure 2-2D, 93Pa), following treatment with the contractant, the H1 agonist, histamine (Figure 2-2E, 112Pa), and after additional treatment with the relaxant, the β2 adrenergic receptor agonist, isoproterenol (Figure 2-2F, 52Pa).

First, we tested the suitability of our approach for higher-capacity measurements. We evaluated common factors associated with ASM contraction including constituents of the culture medium and properties of the cellular substrate. While serum deprivation only marginally affected the scope of ASM relaxation (contraction with 10μM histamine –relaxation with additional 1μM isoproterenol), substrate stiffness had a profound impact, with an optimal response on 12kPa stiff substrates. Given these findings, we focused subsequent studies on 12kPa stiff substrates prepared in 96-well plates. Individual wells of a representative plate were either assigned to a *positive* or *negative control* group. In the positive control group, cells were pre-stimulated with 10 μM histamine to induce maximal contractility followed by post-stimulation with the relaxant, 10μM Y27632 for 30 minutes. In the negative control group, cells were pre-stimulated with vehicle (PBS) followed by post-stimulation with vehicle (PBS) for 30 minutes. In both groups, traction force measured post-stimulation was normalized to the corresponding pre-stimulation value on a well-by-well basis. From these measurements of normalized changes, we determined that the groups were statistically different ($p<0.05$), as ascertained by an unpaired student t-test.

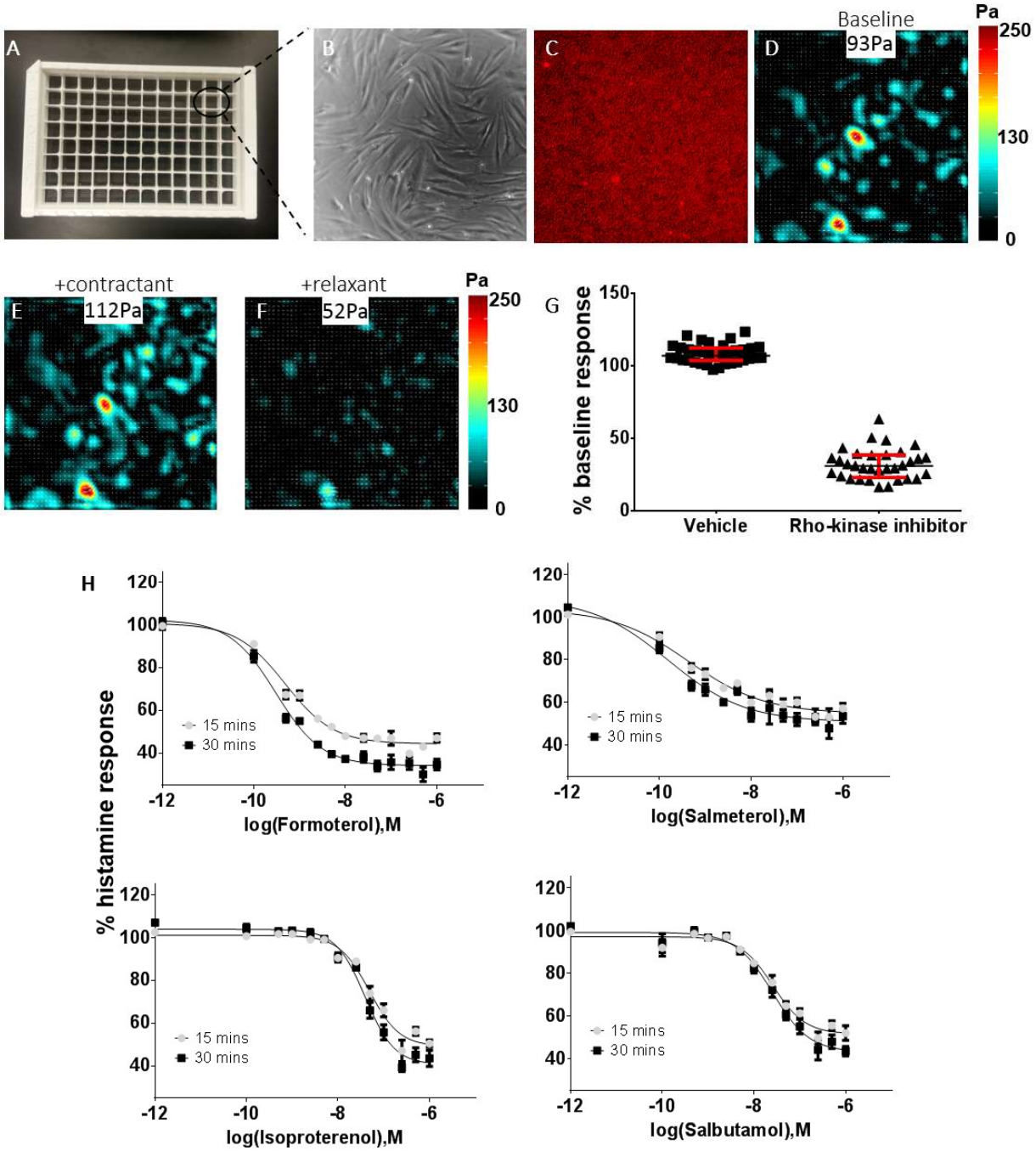
A
B
C
D
Baseline
93Pa
Pa
250
130
0
+contractant
E
112Pa
+relaxant
F
52Pa
Pa
250
130
0
G
% baseline response
150
100
50
0
Vehicle
Rho-kinase inhibitor
H
% histamine response
120
100
80
60
40
15 mins
30 mins
-12
-10
-8
-6
log(Formoterol),M
log(Salmeterol),M
log(Isoproterenol),M
log(Salbutamol),M

Figure 2-2: **CFS using soft elastomeric substrates recapitulates known ASM pharmacological responses.** Human ASM cells were cultured to confluence upon Young's Modulus = 12kPa (0.36% crosslinker) collagen-coated 96-well silicone substrates. A-D) For a representative well of a 96-well plate, shown are images of cells, fluorescent beads, traction force maps and average magnitude (inset) at baseline. E-F) For the same well, shown are traction force maps and average magnitude (inset) with the contractant compound, histamine (10μM, 30 minutes), and after additional treatment with the relaxant compound, Isoproterenol (0.5μM, 30 minutes). G) Over the 96-well plate, the force measurements are statistically different (p<0.05) between positive and negative controls, as ascertained by an unpaired t-test. H) Force measurements confirmed known differences in potency amongst a panel of functionally diverse ASM relaxation compounds (Formoterol > Salmeterol > Salbutamol > Isoproterenol). Plotted are the mean±SEM calculated from 3-8 wells per dose per ASM relaxation compound. Data were pooled from 2-4 96 well plates tested on different days but under identical experimental conditions.

Next, we verified the utility of our approach in pharmacology by examining traction force changes induced by a diverse set of well-known and clinically relevant airway smooth muscle (ASM) relaxation compounds[109]. Each compound was evaluated in a 10-point dose response manner, across adjacent rows of the 96 well-plate. Data were pooled from multiple plates and reported as a percentage of histamine response. The extent of ASM relaxation confirmed the known differences in potency of the β2 adrenergic receptor agonists (Salmeterol > Formoterol > Salbutamol > Isoproterenol)[109], and the full agonist, Formoterol, provided a greater scope of relaxation than the partial agonist, Salmeterol, as expected[110] (Figure 2-2H, Table S 2-1). Notably, as supported by negligible standard errors and the small coefficients of variation, the data were highly reproducible.

Here we have focused on ASM response; yet this approach is applicable in pharmacology to any adherent contractile cell type and is therefore expected to be of broad utility. In ASM this need is particularly exigent, as current efforts to screen new ASM relaxation drugs employ indirect assay methods that are poorly predictive of functional response. Commonplace examples include the dissociation of intracellular calcium regulation from the effects of bradykinin, bitter tastants[111], and proton-sensing receptor ligands[112] on ASM contraction, a similar dissociation of cAMP regulation from bronchorelaxant effect (pro-contractile receptor antagonists, and again bitter tastants), and the limited predictive utility of membrane potential for almost all drugs whether they target receptors or other contractile effectors or signaling elements. A more relevant screen that directly quantifies the target output of ASM relaxation, as does CFS, is required to efficiently test the pending generations of ASM relaxation drugs. To this end, CFS fills an important methodological void in ASM biology, and more generally, in measuring contractile response for a broad range of cell types and pathologies.

To demonstrate the versatility of CFS, we examined a key pathogenic mechanism common to many ocular pathologies – dysfunction of the retinal pigmented epithelium (RPE)[113]. We discovered that the RPE barrier-disruptive agent, thrombin[114], the pro-angiogenic cytokine, VEGF-A[115], and the oxidative stressor, H_2O_2[116], each caused an increase in RPE traction forces (Figure 2-3). Conversely, the Rho Kinase inhibitor, Y27632, or the VEGF-A inhibitor, Bevacizumab, ablated these forces. Taken together, these data reveal a novel role for traction force increase in RPE dysfunction and advocate for new discovery efforts targeted at reducing these forces. This might be especially pertinent to offset RPE dysfunction in the commonly occurring dry form of macular degeneration[117], wherein no therapeutic intervention currently exists.

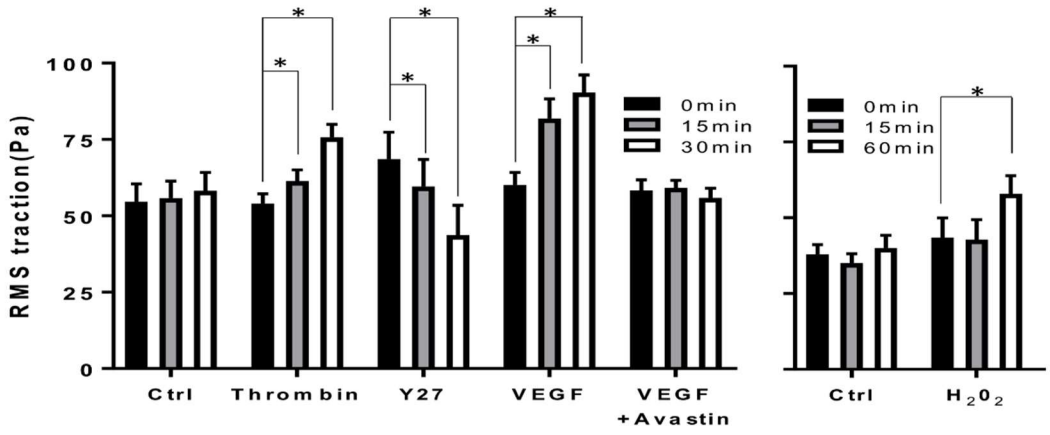

Figure 2-3: **Mediators of retinal epithelial dysfunction increase cell traction forces.** Human ARPE-19 cells were cultured to confluence upon Young's Modulus = 12kPa (0.36% crosslinker) collagen-coated 96-well silicone substrates, and cell-contractile forces were measured at baseline (0 min) and after treatment (15, 30/60 min). While thrombin (1unit/ml) VEGF (100ng/ml), and H_2O_2 (100nM) increased baseline forces in a time-dependent manner, the rho-kinase inhibitor, Y27632 (10μM) ablated them. Bevacizumab (0.05mg/ml) prevented the VEGF-induced force increase. Plotted are the mean±SEM pooled from 8-24 well per time point per treatment. * indicates significant difference compared to baseline.

2.5 Conclusion

We have demonstrated utility for a 96-well silicone-based substrate for CFS. This approach is advantageous over CFS using PAA[106] as the material itself is more robust and uniform, and the fabrication of multiwell-silicone substrates eliminates time-consuming production steps, utilizes standard micro-fabrication procedures, and obviates the need for surface-bound fluorescent beads by embedding them as a monolayer by spin-coating. Moreover, silicone elastomers possess many material-favorable properties over PAA. Specifically, they are predominantly elastic in the stiffness range that encompasses most physiological microenvironments, are non-porous and impermeable, thus obviating common concerns associated with PAA[105], and possess superior optical properties.

Mechanical malfunction appears be an integral component of many diverse diseases including asthma, ocular pathologies, acute lung injury, bladder dysfunction, vascular diseases, fibrosis, and cancer, wherein cell contractile forces play a pivotal role. CFS using elastic silicone substrates is expected to enable mechanistic studies for both quantitatively describing the aberrant contractile forces, as well to mechanically rectify the responses by directly evaluating potential therapeutic compounds.

Author Contributions

HY, NK, RK (Kaviani), and MT fabricated and measured PDMS TFM surfaces; KR, SY, and QD performed TFM in ASM cells; CL, and JKS optimized TFM in ASM cells; AH performed TFM in RPE cells; MSG, RK (Krishnan) and AJE devised study, contributed reagents, and wrote the manuscript.

2.6 Acknowledgements

The authors thank Cynthia Crespo, Erin Hannen, and Luc Mongeau for technical assistance. AJE acknowledges NSERC RGPIN/05843-2014 & EQPEQ/472339-2015, CIHR Grant # 143327, and CCS Grant #703930. R. Krishnan acknowledges NIH R21HL123522 and Amgen Inc. HY was supported by FRQS. MSG acknowledges NIH DP2-OD006649.

2.7 References

Balaban, N. Q., Schwarz, U. S., Riveline, D., Goichberg, P., Tzur, G., Sabanay, I., . . . Geiger, B. (2001). Force and focal adhesion assembly: a close relationship studied using elastic micropatterned substrates. *Nat Cell Biol, 3*(5), 466-472.

Battram, C., Charlton, S. J., Cuenoud, B., Dowling, M. R., Fairhurst, R. A., Farr, D., . . . Trifilieff, A. (2006). In vitro and in vivo pharmacological characterization of 5-[(R)-2-(5,6-diethyl-indan-2-ylamino)-1-hydroxy-ethyl]-8-hydroxy-1H-quinolin-2-o ne (indacaterol), a novel inhaled beta(2) adrenoceptor agonist with a 24-h duration of action. *J Pharmacol Exp Ther, 317*(2), 762-770.

Butler, J. P., Tolic-Norrelykke, I. M., Fabry, B., & Fredberg, J. J. (2002). Traction fields, moments, and strain energy that cells exert on their surroundings. *Am J Physiol Cell Physiol, 282*(3), C595-605.

Chen, C., Krishnan, R., Zhou, E., Ramachandran, A., Tambe, D., Rajendran, K., . . . Fredberg, J. J. (2010). Fluidization and resolidification of the human bladder smooth muscle cell in response to transient stretch. *PLoS One, 5*(8), e12035.

Chen, C. S., Alonso, J. L., Ostuni, E., Whitesides, G. M., & Ingber, D. E. (2003). Cell shape provides global control of focal adhesion assembly. *Biochem Biophys Res Commun, 307*(2), 355-361.

Chen, C. S., Mrksich, M., Huang, S., Whitesides, G. M., & Ingber, D. E. (1997). Geometric control of cell life and death. *Science, 276*(5317), 1425-1428.

Comer, B. S., Camoretti-Mercado, B., Kogut, P. C., Halayko, A. J., Solway, J., & Gerthoffer, W. T. (2014). MicroRNA-146a and microRNA-146b expression and anti-inflammatory function in human airway smooth muscle. *Am J Physiol Lung Cell Mol Physiol, 307*(9), L727-734.

Deshpande, D. A., Wang, W. C., Mcilmoyle, E. L., Robinett, K. S., Schillinger, R. M., An, S. S., . . . Liggett, S. B. (2010). Bitter taste receptors on airway smooth muscle bronchodilate by localized calcium signaling and reverse obstruction. *Nat Med, 16*(11), 1299-1304.

Ehrlicher, A. J., Krishnan, R., Guo, M., Bidan, C. M., Weitz, D. A., & Pollak, M. R. (2015). Alpha-actinin binding kinetics modulate cellular dynamics and force generation. *Proc Natl Acad Sci U S A, 112*(21), 6619-6624.

Ghosh, K., Thodeti, C. K., Dudley, A. C., Mammoto, A., Klagsbrun, M., & Ingber, D. E. (2008). Tumor-derived endothelial cells exhibit aberrant Rho-mediated mechanosensing and abnormal angiogenesis in vitro. *Proc Natl Acad Sci U S A, 105*(32), 11305-11310.

Hanus, J., Zhang, H., Wang, Z., Liu, Q., Zhou, Q., & Wang, S. (2013). Induction of necrotic cell death by oxidative stress in retinal pigment epithelial cells. *Cell Death Dis, 4*, e965.

Harris, A. K., Wild, P., & Stopak, D. (1980). Silicone rubber substrata: a new wrinkle in the study of cell locomotion. *Science, 208*(4440), 177-179.

Jager, R. D., Mieler, W. F., & Miller, J. W. (2008). Age-related macular degeneration. *N Engl J Med, 358*(24), 2606-2617.

Kim, J. H., Serra-Picamal, X., Tambe, D. T., Zhou, E. H., Park, C. Y., Sadati, M., . . . Fredberg, J. J. (2013). Propulsion and navigation within the advancing monolayer sheet. *Nature Materials, 12*(9), 856-863.

Klettner, A., Kaya, L., Flach, J., Lassen, J., Treumer, F., & Roider, J. (2015). Basal and apical regulation of VEGF-A and placenta growth factor in the RPE/choroid and primary RPE. *Mol Vis, 21*, 736-748.

Krishnan, R., Park, C. Y., Lin, Y. C., Mead, J., Jaspers, R. T., Trepat, X., . . . Fredberg, J. J. (2009). Reinforcement versus fluidization in cytoskeletal mechanoresponsiveness. *PLOS ONE, 4*(5), e5486.

Krishnan, R., Tambe, D., Steward, R., Hardin, C., & Butler, J. (2015). Traction Microscopy. In *Cells, Forces, and the Microenvironment* (pp. 75-96): Pan Stanford.

Lele, T. P., Pendse, J., Kumar, S., Salanga, M., Karavitis, J., & Ingber, D. E. (2006). Mechanical forces alter zyxin unbinding kinetics within focal adhesions of living cells. *J Cell Physiol, 207*(1), 187-194.

Park, C. Y., Zhou, E. H., Tambe, D., Chen, B., Lavoie, T., Dowell, M., . . . Krishnan, R. (2015). High-throughput screening for modulators of cellular contractile force. *Integr Biol (Camb), 7*(10), 1318-1324.

Penn, J. S., Madan, A., Caldwell, R. B., Bartoli, M., Caldwell, R. W., & Hartnett, M. E. (2008). Vascular endothelial growth factor in eye disease. *Prog Retin Eye Res, 27*(4), 331-371.

Pourati, J., Maniotis, A., Spiegel, D., Schaffer, J. L., Butler, J. P., Fredberg, J. J., . . . Wang, N. (1998). Is cytoskeletal tension a major determinant of cell deformability in adherent endothelial cells? *Am J Physiol, 274*(5 Pt 1), C1283-1289.

Prager-Khoutorsky, M., Lichtenstein, A., Krishnan, R., Rajendran, K., Mayo, A., Kam, Z., . . . Bershadsky, A. D. (2011). Fibroblast polarization is a matrix-rigidity-dependent process controlled by focal adhesion mechanosensing. *Nat Cell Biol, 13*(12), 1457-1465.

Saxena, H., Deshpande, D. A., Tiegs, B. C., Yan, H., Battafarano, R. J., Burrows, W. M., . . . Penn, R. B. (2012). The GPCR OGR1 (GPR68) mediates diverse signalling and contraction of airway smooth muscle in response to small reductions in extracellular pH. *Br J Pharmacol, 166*(3), 981-990.

Sparrow, J. R., Hicks, D., & Hamel, C. P. (2010). The retinal pigment epithelium in health and disease. *Curr Mol Med, 10*(9), 802-823.

Stamenovic, D., Suki, B., Fabry, B., Wang, N., & Fredberg, J. J. (2004). Rheology of airway smooth muscle cells is associated with cytoskeletal contractile stress. *J Appl Physiol, 96*(5), 1600-1605.

Steinwachs, J., Metzner, C., Skodzek, K., Lang, N., Thievessen, I., Mark, C., . . . Fabry, B. (2016). Three-dimensional force microscopy of cells in biopolymer networks. *Nat Methods, 13*(2), 171-176.

Sturton, R. G., Trifilieff, A., Nicholson, A. G., & Barnes, P. J. (2008). Pharmacological characterization of indacaterol, a novel once daily inhaled 2 adrenoceptor agonist, on small airways in human and rat precision-cut lung slices. *J Pharmacol Exp Ther, 324*(1), 270-275.

Tambe, D. T., Hardin, C. C., Angelini, T. E., Rajendran, K., Park, C. Y., Serra-Picamal, X., . . . Trepat, X. (2011). Collective cell guidance by cooperative intercellular forces. *Nat Mater, 10*(6), 469-475.

Tan, J. L., Tien, J., Pirone, D. M., Gray, D. S., Bhadriraju, K., & Chen, C. S. (2003). Cells lying on a bed of microneedles: an approach to isolate mechanical force. *Proc Natl Acad Sci U S A, 100*(4), 1484-1489.

Trappmann, B., Gautrot, J. E., Connelly, J. T., Strange, D. G., Li, Y., Oyen, M. L., . . . Huck, W. T. (2012). Extracellular-matrix tethering regulates stem-cell fate. *Nat Mater, 11*(7), 642-649.

Trepat, X., Wasserman, M. R., Angelini, T. E., Millet, E., Weitz, D. A., Butler, J. P., & Fredberg, J. J. (2009). Physical forces during collective cell migration. *Nat Phys, 5*(6), 426-430.

Wang, N., Tolic-Norrelykke, I. M., Chen, J., Mijailovich, S. M., Butler, J. P., Fredberg, J. J., & Stamenovic, D. (2002). Cell prestress. I. Stiffness and prestress are closely associated in adherent contractile cells. *Am J Physiol Cell Physiol, 282*(3), C606-616.

2.8 Supplemental Materials

Table S 2-1: **Potency of a panel of beta-agonist compounds measured by Traction Force Screening.** The potency value is the concentration of the drug where the force response is reduced by half. This is also called the relative IC50 value. It was calculated from a least squares curve fit of a log(inhibitor) versus response using variable slope (four parameters). The calculation of potency was performed using Prism 6.03 software.

Condition	Potency(M), 15min	Potency(M), 30min
Formoterol	$4.8*10^{-10}$	$3*10^{-10}$
Salmeterol	$4.3*10^{-10}$	$1.6*10^{-10}$
Isoproterenol	$4.8*10^{-8}$	$3.9*10^{-8}$
Salbutamol	$2.6*10^{-8}$	$2.5*10^{-8}$

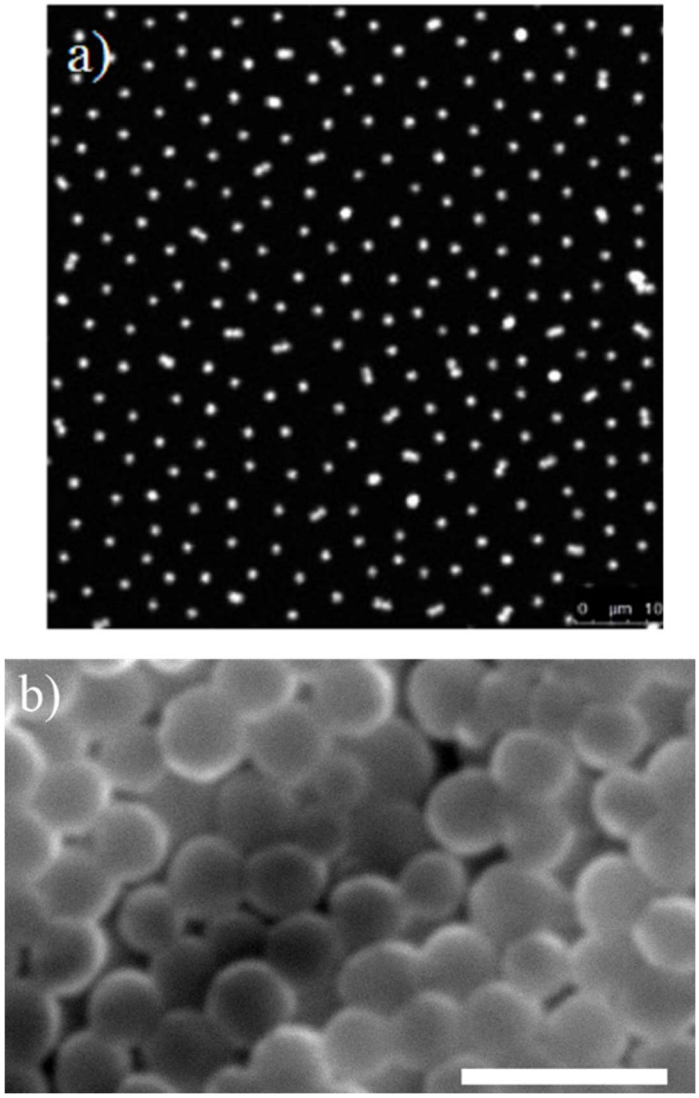

Figure S 2-1: Bead synthesis & characterization. a) The fluorescent image confirms that the particles were fluorescent and well dispersed in PDMS media (scale bar 10 μm). b) Additionally, particles were sputter-coated with gold and imaged with SEM (Hitachi Scanning Electron Microscope SU3500). The SEM image demonstrates the particle size and shape consistency (scale bar 1 μm).

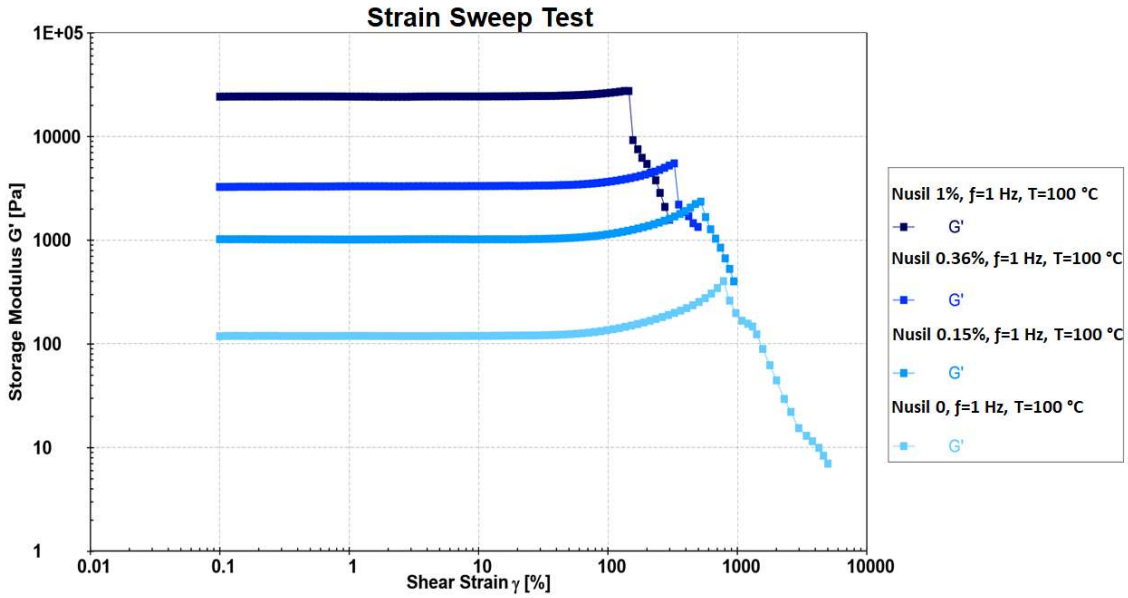

Figure S 2-2: **PDMS samples exhibit linear elasticity.** Different formulations of PDMS were tested for nonlinear behavior such as strain-stiffening. Only at deformations approaching 100% strain did samples exhibit any change in the measured storage moduli.

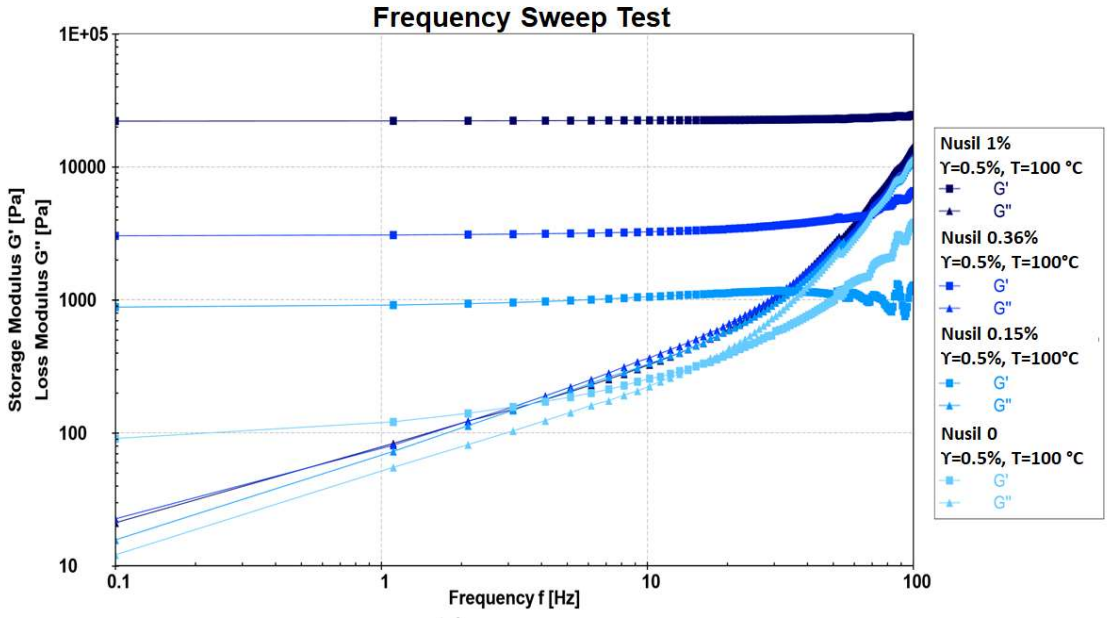

Figure S 2-3: **Frequency dependent response of PDMS samples.** Frequency sweep of PDMS formulations at 0.5% strain shows a relatively flat response in the storage modulus of all samples, with 0% crosslinker increasing above 2Hz, and other formulations remaining flat even at higher frequencies.

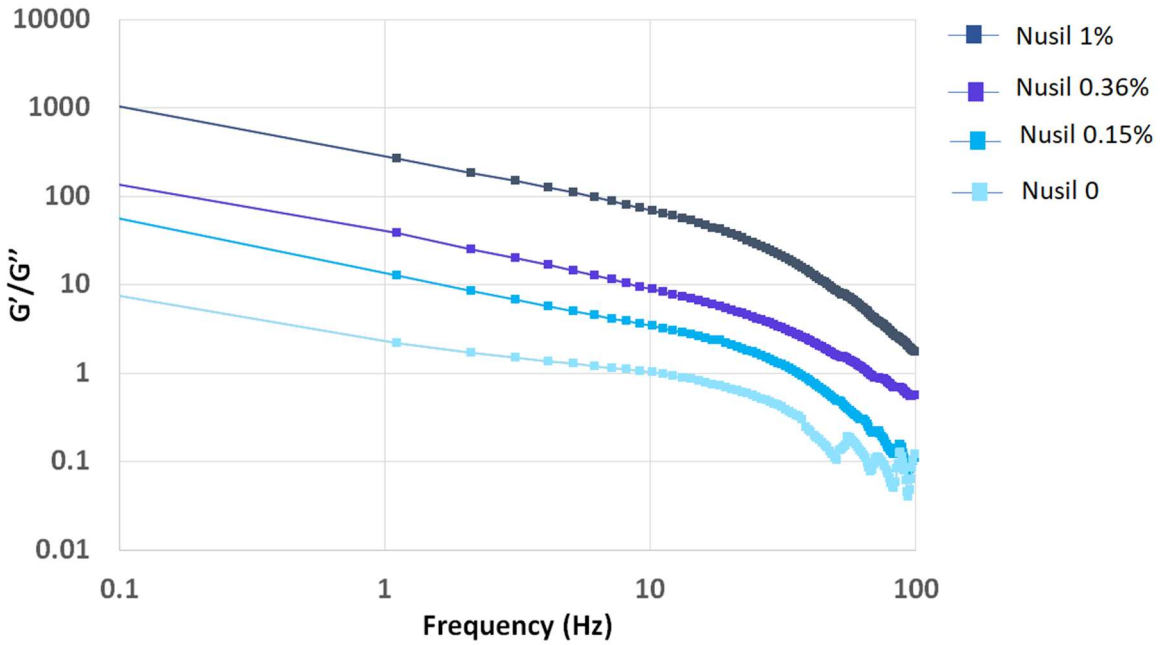

Figure S 2-4: **Inverse Loss Tangent (ILT) of PDMS samples.** The ILT quantifies G'/G", and is a measure of the relative solid-like to fluid-like response of the material, and a material with an ILT of 1 would be highly viscoelastic. All formulations of PDMS are predominantly elastic, with the lowest being approximately 9 for 0% additional crosslinker, and approximately 1000 for 1% additional crosslinker. These data suggest that the PDMS formulations may be treated as elastic solids for the purposes of TFM calculations.

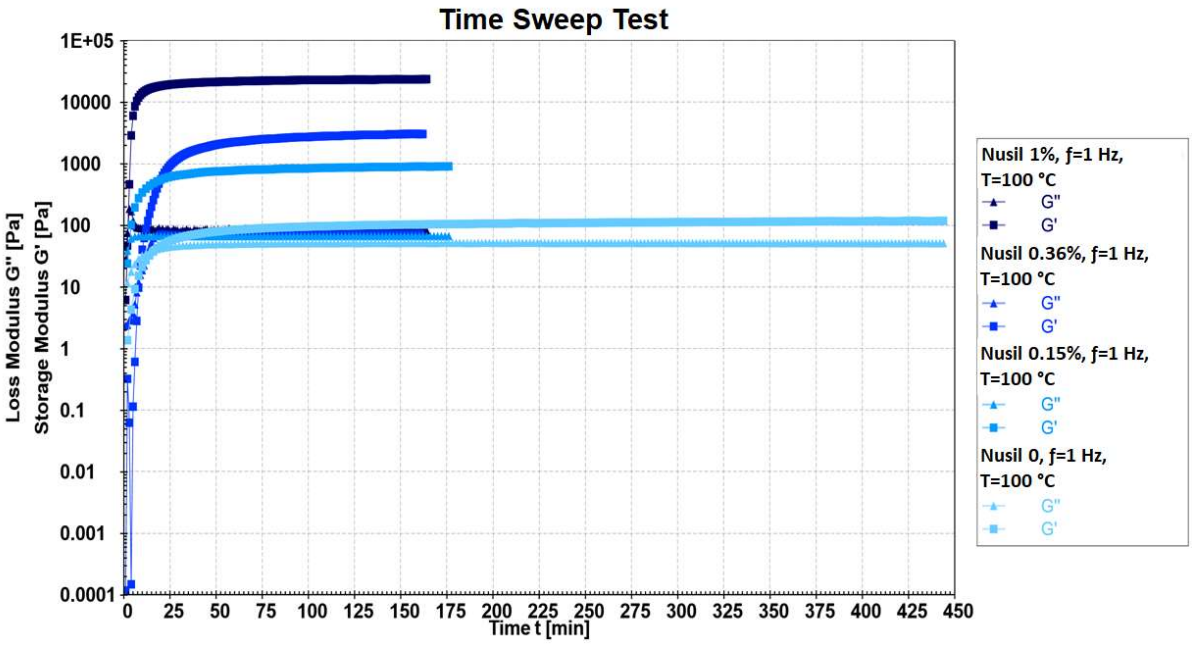

Figure S 2-5: **Gelation curves for curing PDMS samples.** Uncured PDMS samples were mixed and loaded onto the rheometer, and shear rheology was performed during the curing process at 100^0C. These data reveal that the samples have largely cured after 25 minutes, and are completely cured within three hours.

Table S 2-2: **Spatial heterogeneity of modulus as measured with AFM.** To examine the uniformity of modulus on PDMS substrates, we created TFM substrates with several different formulations, and then used an AFM (JPK Nanowizard 3, JPK Berlin Germany) to measure 10 independent positions, spaced at least 100 µm from each other. These data demonstrate that the substrates display little variability and are uniform. Deviation in absolute moduli values reported here from those measured in shear rheology are attributed to challenges in contact mechanics modeling[118-119].

additional crosslinker %	Average Young's Modulus (kPa)	Standard Deviation (kPa)	n (number of points)
0%	0.9894	0.0797	10
0.15%	2.106	0.4768	10
0.36%	4.934	0.1133	10
0.72%	19.22	0.6206	10

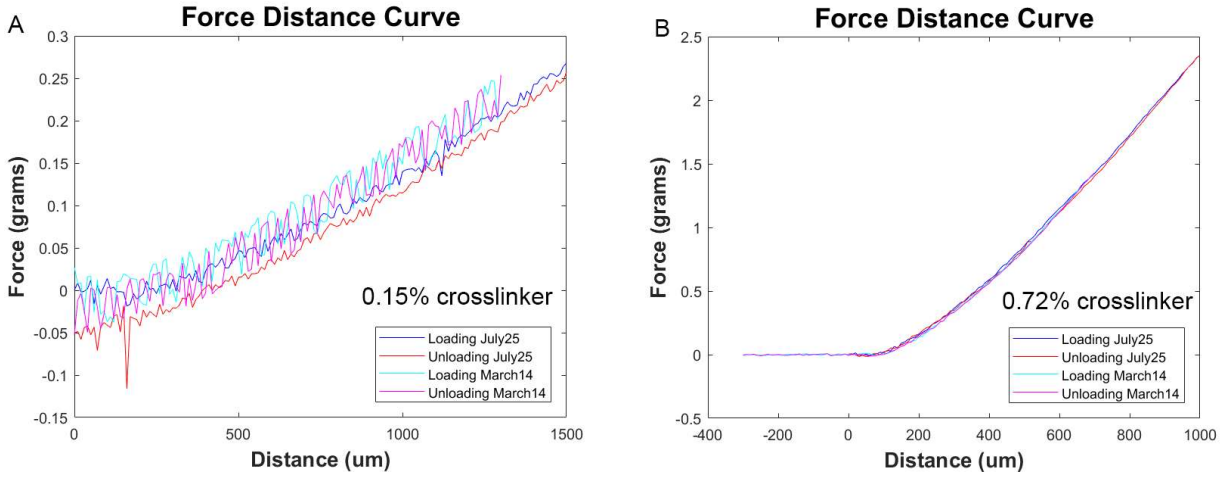

Figure S 2-6: **Long-term elastic measurements of PDMS substrates.** To assess any long-term changes in the elastic modulus of prepared PDMS samples, we used a custom-built microindenter as described previously[120]. In brief, the instrument uses a load cell (S256, Strain Measurement Devices, CT USA) which is moved by a 3-axis micromanipulator (Sutter MP285, Olympus ON Canada). The movement of the micromanipulator and the load-cell data collection are run by custom Matlab software, and the load/strain curve is calibrated using an analytical balance.

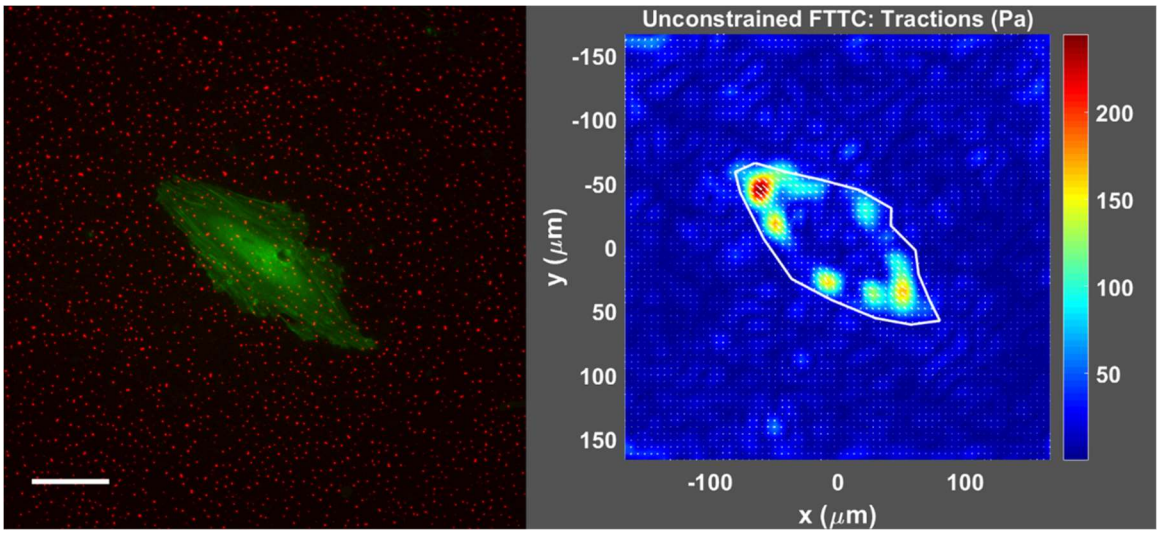

Figure S 2-7: **Single cell TFM PDMS substrates.** To provide an example for comparison with other single-cell traction force studies, we examined HEK293 cells on a 3.6 kPa PDMS substrate. The left panel depicts a HEK293 cell transfected with EGFP-LifeAct (Michael Davidson, Addgene plasmid #54610) on a PDMS substrate with red fiduciary beads. The right panel shows the calculated unconstrained traction stresses generated by the cell. This reveals that single cells display traction stress profiles similar to those previously shown in PAA studies, and the maximum traction stress is observed to be approximately 200 Pa. Scale bar in left panel is 50 μm.

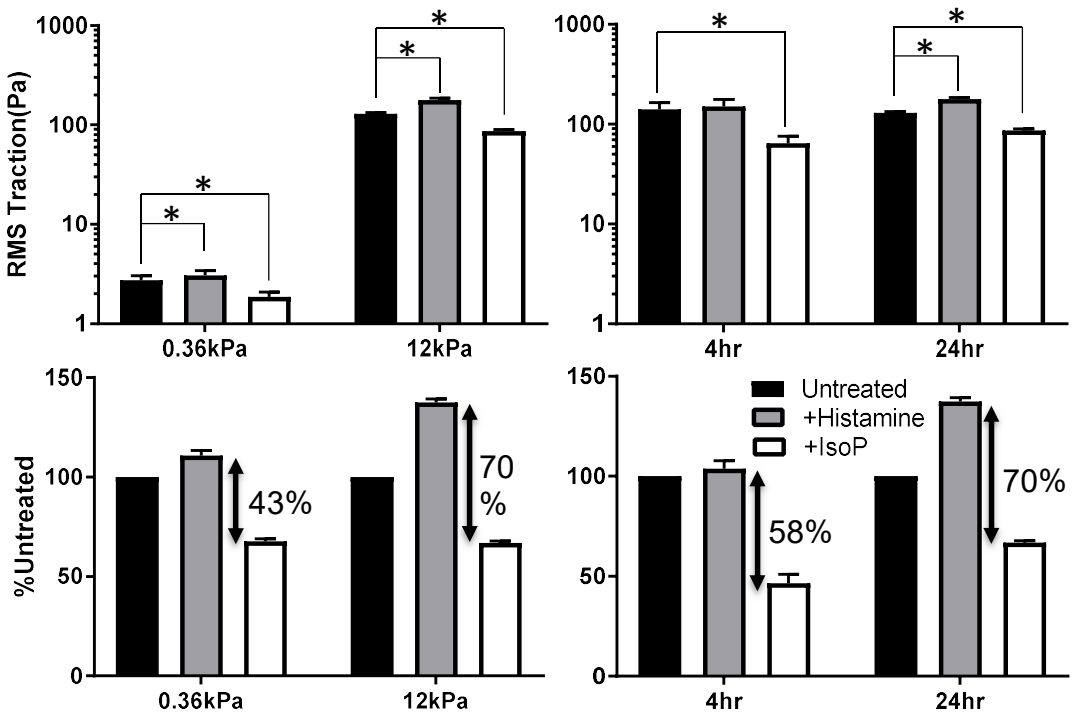

Figure S 2-8: **The scope of ASM relaxation.** Bar graphs reflect the difference in contractility, as reported by RMS traction in Pa (top) and % of untreated (bottom) in untreated, with histamine, or with isoproterenol, with the left panel depicting changes on two different substrate moduli, and the right panel quantifying changes with two different serum deprivation times. In the bottom panels, also shown is the difference between contraction with 10μM histamine (gray bar) and relaxation with additional 1μM isoproterenol (white bar). This difference is greater on 12 kPa than 0.4kPa stiff substrate (n=22-24 separate wells per stiffness group), and, only marginally affected by serum deprivation (n=8 and 24 wells for 4 hr and 24 hr deprivation, respectively). Plotted data are mean±std.error. Data sets were compared using the Wilcoxon matched-pairs signed rank test and differences are reported as * for $p<0.05$.

Detailed methods:

Mechanical testing of PDMS mixtures:

Shear Rheology: Measurements of PDMS moduli as functions of formulation, curing time, frequency, and strain were performed with a stress-controlled shear rheometer using a 25mm parallel plate geometry (Anton Paar, MCR 302, Montreal Canada).

Microindentation measurements: To assess any long-term changes in the elastic modulus of prepared PDMS samples, we used a custom-built microindenter as described previously [120]. In brief, the instrument uses a load cell (S256, Strain Measurement Devices, CT USA) which is moved by a 3-axis micromanipulator (Sutter MP285, Olympus ON Canada). The movement of the micromanipulator and the load-cell data collection are run by custom Matlab software, and the load/strain curve is calibrated using an analytical balance.

Cell culture media:

Primary human airway smooth muscle cell culture and measurements were performed either in serum containing medium comprising DMEM/F12 supplemented with 10% FBS (35-010-CV, Corning Life Sciences, Tewksbury, MA) and 1% penicillin-streptomycin (P0781; Sigma-Aldrich, St. Louis, MO), 1% L-glutamine (25030149; Thermo-Fisher Scientific, Waltham, MA), 1% amphotericin B (15290018; Thermo-Fisher Scientific, Waltham, MA), 0.17% 1M CaCl2*2H20, and 1.2% 1M NaOH or in serum deprived medium comprising F12 with the above supplements except for replacement of FBS with 1% insulin-transferrin-selenium supplement (25-800-CR; Corning Life Sciences, Tewksbury, MA).

ARPE-19 (retinal pigment epithelium) cells were obtained from American Type Culture Collection and cultured in DMEM/F12 medium supplemented with 1% penicillin-streptomycin, 1% L-glutamine and 10% FBS. For monolayer preparation, ARPE-19 (1.7×10^5 cells/cm^2) were

seeded on collagen-coated soft PDMS substrates in low serum media for 2-12 hours before the experiment.

Preparation of NuSil substrates in custom 96-well plates.

As a material for our substrates, we used a very compliant commercial PDMS (NuSil® 8100, NuSil Silicone Technologies, Carpinteria, CA). When prepared as per manufacturer instructions, i.e. 1:1 component mixing, we measured these silicone substrates to have Young's moduli of approximately of 0.36 +/- 0.043 kPa, as determined with shear rheology (Anton Paar MCR302, Montreal Canada). From this baseline, we increased the modulus of the PDMS by including a small amount of additional crosslinker (Sylgard 184 curing agent, Dow Corning, Midland, MI), allowing us to create substrates with higher Young's moduli as desired, and we tested up to 73.32+/-2.96 kPa with 1% additional crosslinker (Figure 2-1F&G), spanning two orders of magnitude in compliance.

To prepare the multiwell plates, we selected custom cut glass slides (109.6 mm x 78mm x 1mm, Hausser Scientific, Horsham PA) so that our plates are compatible with existing multiwell tools (Figure 2-1A-E). Optionally, the glass surface can be coated with fluorescent bead markers for de-drifting images during an experiment (Figure 2-1A). To create the deformable layer with a particular modulus, PDMS was mixed to the by combining mixing NuSil 8100 or as per manufacturer instructions, and then adding additional Sylgard 184 crosslinking agent and slowly mixing on a rotator for approximately 30 minutes to achieve the desired elastic modulus (Figure 2-1F&G).

Next, we spin coat the uncured PDMS mixture, prepared as described above, on the glass slide (Figure 2-1B). To ease loading and centering the glass slides onto the spin coater, we mark the XY center of the glass slide with a solvent resistant marker, and align that mark with the vacuum

chuck on the spin coater (Laurell WS-650Mz-23, Laurell Technologies, USA). We then add 3-4 ml of uncured PDMS to cover the substrate, and use a pipette tip to coarsely spread it from the center to the edges. The slide is then spun with the following protocol: 1) 200 rpm 1min, acceleration 50rpm/s; 2) 300 rpm for 1 min, acceleration 200 rpm/s; 3) deceleration to stop 50 rpm/s. This protocol produces a layer approximately 100 microns thick. The slide with uncured PDMS is then removed from the chuck and placed on a solid surface (i.e. not a wire rack) in a preheated 100^0C oven for 90 minutes. While it may be cured longer, it should not be done hotter than 100^0C as this may cause a degradation and reduction in stiffness. Care should be taken that the oven surface is precisely level to ensure that the PDMS layer has a uniform thickness.

To form the fiduciary bead layer, ~2ml of uncured PDMS mixture from the previous step is mixed with a stock bead solution. Our fluorescent beads are synthesized with a PMMA core and a PDMS shell based on work published previously [121] (Figure S 2-1) and had a final diameter of ~300nm. Their complete synthesis is described in detail below. Beads are stored in hexane, and prior to addition to the uncured PDMS, they are mixed for 30 minutes at approximately 20% volume fraction to the uncured PDMS. The actual bead concentration depends on the desired final bead density, which for our experiments is ~0.05- 0.2 beads 1 μm^2, and the stock bead concentrations, which is approximately $9.2x10^{11}$ beads per ml. To produce a thin layer of bead-embedded PDMS, the uncured mixture is spun on the slide with the following protocol: 1) 500 rpm for 1 minute, acceleration 100 rpm/s; 2) 5000 rpm for 20 sec, acceleration 200 rpm/s; 3) Deceleration to stop at 100 rpm/s. The slide is then placed back in the 100^0C oven for 1 hour to cure the top bead layer. This protocol produces a bead layer approximately 1 micron thick, with an approximate density of 0.05-0.2 beads per 1 μm^2. The elastic substrate and bead layers are now complete (Figure 2-1C).

To create a multiwell dish from the single piece of PDMS-coated glass, we then bonded a 96-well insert (2572; Corning, Tewksbury, MA) on top of the bead layer, allowing each compartment from the insert to function as an individual well on the compliant PDMS substrate, forming the complete multiwell dish (Figure 2-1D).

To facilitate attachment, we apply a thin coat of uncured PDMS (Sylgard 184, Dow Corning, USA) mixed per manufacturer instructions of 10:1 polymer base to crosslinking agent to the insert bottom, invert, lay the slide and deformable PDMS substrate upside-down onto the insert, and incubate the insert together with the substrate at 65°C for one hour. Inversion is important as it prevents uncured PDMS from flowing down and covering the substrate surface.

Substrate functionalization and ligand binding

The wells are washed and surface-activated using the cross-linker, Sulfo-SANPAH (Proteochem, Hurricane, UT). Briefly, Sulfo-SANPAH is dissolved in 0.1M HEPES buffer at a final concentration of 0.4mM and exposed to UV (Wavelength=254nm, Power=40W, Philips, USA) for 6 minutes. Upon activation, the SANPAH will visibly darken. The SANPAH is then removed from the wells by washing twice with phosphate-buffered saline (PBS). Finally, the wells are ligated with 0.05 mg/ml of collagen type 1 solution in PBS (5005; Advanced Biomatrix, Carlsbad, CA) overnight at 4°C in preparation for measurements, and sterilized by UV exposure in a Biosafety cabinet in preparation for measurements. While our experiments have used collagen, this process should also be successful with other ligands such as fibronectin.

Fluorescent Bead Synthesis

Commonly available fluorescent polystyrene spheres do not readily disperse in non-polar fluids such as uncured PDMS, requiring in house synthesis of compatible spheres.

The following procedure for fluorescent particle synthesis is based on the method described by Klein et. al.[121]

Table S 2-3:Materials used for PDMS-coated fluorescent bead synthsis

1,1'-Dioctadecyl-3,3,3',3'-Tetramethylindocarbocyanine Perchlorate (DiI)	1-5 mg	Sigma-Aldrich 468495-100MG
Methyl methacrylate, 99%, contains ≤30 ppm MEHQ as inhibitor	15 mL	Sigma-Aldrich M55909-500ML
Inhibitor Remover		Sigma-Aldrich 306312-1EA
Polydimethylsiloxane stabilizer (25,000g/mol) *Methacryloxypropyl-terminated	0.5 g	Gelest DMS-R31 (25,000g/mol)
2,2'-azobisisobutyronitrile (AIBN 98%) (=2,2'-Azobis(2-methylpropionitrile)	0.15g	Sigma-Aldrich 441090-25G
Hexane Anhydrous (for reaction)	100 mL	Sigma-Aldrich 296989-1L
Hexane, mixture of isomers	~ 200 mL	Sigma-Aldrich 227064-1L

0.5 g of PDMS stabilizer and 5 mg of fluorophore were dissolved in 100 mL of anhydrous hexane in 250 mL two-neck flask. The necks were prepared with a water cooled reflux condenser, a rubber septum with a nitrogen inlet needle and an outlet needle, and a rubber septum for adding monomer solution via a syringe, respectively. The flask was placed in the mineral oil bath at 75 °C and purged with nitrogen gas for 1 hour. To ensure uniform heating, a small magnetic stir bar was placed in the reaction flask. 0.100g of AIBN was dissolved in 6 g of methyl methacrylate and purged with nitrogen for 1 hour. *Methyl methacrylate was flushed through prepacked column to remove inhibitors before use. After purging both hexanes and the initiator with monomers, the reaction was initiated by adding a monomer and initiator mix

solution to the three-neck flask. The initially transparent solution became cloudy as nuclei for the particle growth were formed and tuned milky as they continue to grow. After 3 hours, the reaction flask was placed in an ice water bath after 3 hours to terminate the reaction. The solution was vacuum-filtered through a coarse filter paper. The filtrate was then centrifuged to remove unreacted stabilizer, and re-suspended in fresh hexane. To facilitate the redispersion, the particles in hexane were placed in an ultrasonic bath - the final hexane volume to be added depends on the product yield and desired bead concentration.

Synthesized beads were found to be 300-400 nm in diameter as measured by SEM (Figure S 2-1 b).

Bead Addition to Uncured PDMS

Prior to mixing, the bead solution was sonicated for 15-30 minutes and vortexed for ~60 seconds to prevent beads from aggregating. Each corresponding PDMS mixtures left from the previous step (NuSil GEL-8100 mixtures) was mixed with fluorescent beads (suspended in hexane) in 10:1 (equal PDMS mix : bead solution) ratio (the amount of bead solution to be added depends on the concentration of the bead solution) by weight, and the whole mixture was vortexed for 1-2 minutes. *Beads can be filtered through 5 μm pores using syringe filters right before adding to PDMS mixture to further avoid bead clumping – this is especially important when using beads in high density.

References for Supplemental Materials

Klein, S. M., Manoharan, V. N., Pine, D. J., & Lange, F. F. (2003). Preparation of monodisperse PMMA microspheres in nonpolar solvents by dispersion polymerization with a macromonomeric stabilizer. *Colloid Polym Sci Colloid and Polymer Science : Kolloid-Zeitschrift und Zeitschrift für Polymere., 282*(1), 7-13.

Notbohm, J., Poon, B., & Ravichandran, G. (2012). Analysis of nanoindentation of soft materials with an atomic force microscope. *Journal of Materials Research, 27*(1), 229-237.

Pham, J. T., Schellenberger, F., Kappl, M., & Butt, H.-J. (2017). From elasticity to capillarity in soft materials indentation. *Physical Review Materials, 1*(1), 015602.

Zhang, W., Dong, X., Cruz, S. S., Heris, H. K., Mongeau, L. G., Ehrlicher, A. J., & Liu, X. (2015, 2-5 Aug. 2015). *A cost-effective microindentation system for soft material characterization.* Paper presented at the 2015 IEEE International Conference on Mechatronics and Automation (ICMA).

Preface to Chapter 3

In Chapter 2, I introduced a novel TFM assay utilizing soft elastic silicone materials. Silicone-based PDMS assays can offer more stable and reproducible results than commonly used hydrogel-based approaches. Utilizing PDMS materials, we were able to assemble a multi-well device, allowing us to perform high-throughput measurements. This new device was utilized for force screening assay to study contractile responses of airway smooth muscle cells with the treatment of pharmaceutical compounds.

Chapter 3 examines changes in contractility of cancer cells during EMT with an EMT-inducible cell line, NMuMG cells, with TGF-β treatment. In this study, using a 96-well format, I was able to investigate 17 different combinations of TGF-β concentrations and incubation times. I measured force and work to increase as cells go through the transition. This chapter also describes very detailed protocols for the fabrication of our soft silicone-based multi-well TFM assays.

Chapter 3 : High Throughput Traction Force Microscopy using PDMS Reveals Dose-Dependent Effects of Transforming Growth Factor-β on the Epithelial-to-Mesenchymal Transition.

Authors and Affiliations

Haruka Yoshie[1], Newsha Koushki[1], Clayton Molter[1], Peter M. Siegel[2,3], Ramaswamy Krishnan[4], Allen J. Ehrlicher[1,2,#]

[1]Department of Bioengineering, McGill University, Montreal, QC, Canada

[2]Goodman Cancer Research Centre, McGill University, Montreal, QC, Canada

[3]Department of Medicine, McGill University, Montreal, QC, Canada

[4] Department of Emergency Medicine, Beth Israel Deaconess Medical Center, Boston, MA, USA

Corresponding author

Keywords

- PDMS (Polydimethylsiloxane)
- Traction Force Microscopy
- High throughput
- Contractile Force Screening
- Epithelial-to-Mesenchymal Transition
- Mechanobiology
- Cancer

3.1 Summary

We present a high throughput traction force assay fabricated with silicone rubber (PDMS). This novel assay is suitable for studying physical changes in cell contractility during various biological and biomedical processes and diseases. We demonstrate this method's utility by measuring a TGF-β dependent increase in contractility during the epithelial-to-mesenchymal transition.

3.2 Abstract

Cellular contractility is essential in diverse aspects of biology, driving processes that range from motility and division, to tissue contraction and mechanical stability, and represents a core element of multi-cellular animal life. In adherent cells, acto-myosin contraction is seen in traction forces that cells exert on their substrate. Dysregulation of cellular contractility appears in a myriad of pathologies, making contractility a promising target in diverse diagnostic approaches using biophysics as a metric. Moreover, novel therapeutic strategies can be based on correcting the apparent malfunction of cell contractility. These applications; however, require direct quantification of these forces.

We have developed silicone elastomer-based traction force microscopy (TFM) in a parallelized multiwell format. Our use of a silicone rubber, specifically polydimethylsiloxane (PDMS), rather than the commonly employed hydrogel polyacrylamide (PAA) enables us to make robust and inert substrates with indefinite shelf-lives requiring no specialized storage conditions. Unlike pillar-PDMS based approaches that have a modulus in the GPa range, the PDMS used here is very compliant, ranging from approximately 0.4 kPa to 100 kPa. We create a high-throughput platform for TFM by partitioning these large monolithic substrates spatially into

biochemically independent wells, creating a multiwell platform for traction force screening that is compatible with existing multiwell systems.

In this manuscript, we use this multiwell traction force system to examine the Epithelial to Mesenchymal Transition (EMT); we induce EMT in NMuMG cells by exposing them to TGF-β, and to quantify the biophysical changes during EMT, we measure the contractility as a function of concentration and duration of TGF-β exposure. Our findings here demonstrate the utility of parallelized TFM in the context of disease biophysics.

3.3 Introduction

Acto-myosin contractility is an essential element of active cell mechanics, impacting cell behaviors from motility and proliferation to stem cell differentiation. In tissues, contractility drives activity from polar separation in embryogenesis, to airway constriction and cardiac activity. Critically, to generate tension, cells must first adhere to their extracellular environment. In doing so, this contractility generates traction forces on their surroundings. Traction Force Microscopy (TFM) has emerged in a multitude of forms as a way to quantify these forces from diverse cells under different conditions.

The field of TFM has seen an exceptional breadth of innovation and application, and the results have paved the way for new perspectives in biology, which incorporate mechanics and physical forces. Starting with wrinkling silicone substrates[14], researchers applied various techniques to measure cell traction forces. These approaches have been continuously improved and have now reached a level of resolution on the order of several microns[122]. However, one principal problem has emerged, which is the difficulty in creating substrates of suitably low moduli using the available silicones. To circumvent this problem, polyacrylamide was adopted as a replacement due to the ease of creating substrates on the order of 1-20 kPa[18]. We recently

implemented very compliant silicones in TFM[123], allowing us to fabricate the same range of moduli as polyacrylamide, but with the advantages of inert and robust silicone.

TFM approaches have enabled valuable mechano-biological discoveries, however, a persistent shortcoming is their complexity, often restricting their use to researchers in the engineering or physical sciences disciplines. This is due, in large part, to the detailed calibrations and challenging calculations that are required to quantify contractility. Another significant challenge is that TFM methods are largely low-throughput and therefore ill-suited to study many different conditions or populations simultaneously[106]. This has presented a bottleneck, which has hampered transfer of TFM from a specialist biophysics setting into broader biological sciences and pharmacology applications.

We have recently developed a multi-well format TFM plate, which allows researchers to parallelize their TFM measurements for faster quantification of contractility metrics, while exploring the impact of different compounds and also using less reagents[4]. This methodology has broad utility in diverse mechanobiology studies, from evaluating the effects of compounds on cellular activity, to quantifying the contractile changes in differentiation or disease.

One area of biomedical research that will benefit greatly from TFM is the study of how physical cues impact the malignant phenotypes of cancer cells. Metastasis, responsible for 90% of cancer-related deaths, is characterized by cancerous cells leaving their original tumor site and colonizing a secondary site. For cells to migrate through tissue and pass in and out of the vascular system, they must radically change their shapes to squeeze through these physical barriers while generating substantial forces to pull their way along extracellular matrix or move between other cells. These forces are transmitted to the substrate through focal adhesion interactions[6, 104], and can be quantified using TFM. While cancers are biochemically

exceptionally diverse, with an expanding repertoire of known mutations and protein changes, some common physical changes have been observed; in a variety of cancers, including breast, prostate, and lung cancers, metastatic cells have been shown to exert 2-3 times the traction forces of non-metastatic cells [124-126]. These results suggest that there may be a strong correlation between metastatic progression and the traction forces exerted by cells; however, the detailed time-dependent changes in contractility are difficult to examine.

The epithelial-to-mesenchymal transition (EMT) is a process whereby cells reduce adherens- and tight-junction mediated cell-cell adhesion, becoming more migratory and invasive. In addition to physiological functions that include wound healing and developmental processes, EMT is also a process exploited during metastasis, making it a useful model system to study this process. Using TGF-β, we can induce the EMT in ErbB2-transformed murine mammary epithelial cells (NMuMG-derived)[127] to directly quantify the physical changes during this transformation, and characterize the time and dose-dependent effects of TGF-β on EMT and cell contractility. In this article, we demonstrate the utility of this approach by measuring the changes in contractility during an induced EMT.

3.4 Protocol

The following protocol will guide researchers in fabricating and using the multi-well TFM dish shown in Figure 3-1.

1. Preparation of PDMS Silicone Substrates

1.1. Preparation of PDMS silicone rubber mixture based on a composite mixture of two commercially available kits.

1.1.1. Add Part A and Part B of PDMS kit (NuSil GEL-8100) in a 1:1 weight ratio into the 50 mL tube.

Note: The mixture is mixed on a rotator at a speed slow enough for the mixture to flow back and forth during revolution to ensure complete mixing.

1.1.2. Add the required amount of Curing Agent (Sylgard 184) for the desired modulus of the substrate.

Note: The amount of Curing Agent to be added to the mixture depends on the desired modulus of the substrate and may typically range from 0.1% to 1.8%. Refer to Table 3-1 and Figure 3-3 for a guide to specific crosslinker concentrations and resulting moduli.

1.1.3.Mix the formulation on the rotator for 30-45 min; ensure the rotation is slow enough for thorough mixing.

1.2. Bottom Layer - Coating PDMS Substrates on the Glass Slide

1.2.1. Place the custom-built chuck illustrated in Figure 3-2 on the spin-coater. Clean the glass with ethanol or isopropanol, and dry with lint-free wipe. Place the glass slide in the chuck and turn on the vacuum to hold the slide in place.

1.2.2. Apply uncured PDMS approximately 1 cm from the edges and work in towards the center. Apply enough (3-4 mL) PDMS to ensure the whole surface will be covered.

Note: To ensure that the PDMS is evenly spread on the surface of the glass, a pipette tip may be helpful to spread the PDMS mixture from the center to the edges.

1.2.3. Spin the glass with the PDMS mixture on a spin-coater with the following protocol:

1.2.3.1. To spread the uncured PDMS on the slide, accelerate at 50 rpm/s from 0 to 200 rpm; hold at 200 rpm for 1 min.

1.2.3.2. To achieve a 100 μm PDMS thickness, accelerate at 50 rpm/s to 300 rpm and hold for 1 min at 300 rpm. Different desired thicknesses other than 100 μm will require specific rpm values.

1.2.3.3. To remove, decelerate 50 rpm/s to 0 rpm. Disable vacuum and remove coated slide, taking care not to touch the coated surface.

Note: It is important to include the acceleration and deceleration steps to ensure a smooth continuous surface.

CAUTION: To ensure that the sample does not fly off the chuck, the custom-made holder should be used to hold the slide, and not rely simply on vacuum and the existing flat chuck. The details and specifications of this holder are given in Figure 3-2.

1.2.4. Place the spin-coated sample in the oven at the manufacturer recommended temperature (100 °C) for 2 h.

Note: The surface of the oven where the sample is placed should be solid (*i.e.* not a wire rack) and level surface to ensure the uniform heating and thickness of the sample. A ceramic or steel plate makes an ideal surface.

1.3. Top Bead Layer

1.3.1. Add bead solution in the appropriate ratio to the remaining PDMS mixture.

Note: This ratio depends on the concentration of the stock bead solution and the desired bead density on the sample. Typical final values are 9.2×10^{11} beads/mL and 0.05-0.2 beads/μm^2, and an excess of beads is generally preferable to an inadequate amount.

1.3.2. Mix the bead solution with the uncured PDMS. This may be accomplished by placing the tube on a rotator for approximately 30 minutes, vortexing for 1-2 minutes, or sonication for 30 minutes. These methods may be combined. In our application, we find sonication is effective in breaking bead aggregates, and rotation is effective in mixing.

Note: Synthesized fiduciary beads may aggregate in storage. Prior to use, they may be resuspended in hexane and sonicated. If there are significant large aggregates, one can filter the

bead suspension through a 5 μm syringe filter. This filtration step is optional; it helps to coat the sample with monodispersed beads, but a significant fraction of beads may be lost in the filter.

1.3.3. Take out the slide from the oven, allow to cool to room temperature, and place it on the spin-coater.

1.3.4. Add 3-4 mL of the bead & uncured PDMS mixture onto the surface of the coated sample.

Note: The mixture with beads added is less viscous due to the hexane. Make sure not to touch the surface of the substrate as it may damage the already-coated PDMS substrate. Additionally, the bead mixture may initially not wet the surface; take care that the mixture does not immediately flow off the cured PDMS surface.

1.3.5. Spin the sample with the following protocol.

1.3.5.1. To spread the bead & uncured PDMS mixture, accelerate at 100 rpm/s from 0 to 500 rpm; hold at 500 rpm for 1 min.

1.3.5.2. To achieve a thin layer of bead-embedded PDMS (~1 μm), accelerate at 200 rpm/s from 500 to 5000 rpm; hold at 5000 rpm for 10 s.

1.3.5.3. To remove, decelerate at 100 rpm/s to 0 rpm. Disable vacuum and remove coated slide, taking care not to touch the coated surface.

1.3.6. Place the spin-coated sample in the oven at 100 °C for 1 h.

Note: Temperatures above 100°C or durations longer than 1 hour can reduce the bead fluorescence. Make sure that the oven temperature is set to 100 °C and not higher.

Note: The protocol can be paused here. To store the sample, cover the surface to avoid dust and light exposure. Make sure nothing touches the surface. The sample is shelf-stable at room temperature indefinitely.

1.4. Assembling the Plate

1.4.1. Add Part A (Base) and Part B (Curing Agent) of PDMS Elastomer kit in 1:1 weight ratio into the 50 mL tube.

1.4.2. Mix the mixture on the rotator for 30-45 min.

Note: For one plate, mix 5 mL of Base with 0.5 mL of Curing Agent. Up to 1 mL of hexane can be added to reduce the viscosity of the mixture.

1.4.3. Apply the mixture to the bottom of the divider and spread the mixture.

Note: The divider should be placed upside-down.

1.4.4. Lay the substrate onto the divider upside-down.

1.4.5. Place the sample upside-down in the oven at 65 °C for 2 h.

1.4.6. Take out samples from the oven and clean the bottom of the glass with 70% ethanol or isopropanol to remove any PDMS residue.

Note: The protocol can be paused here. To store the sample, place a lid on the substrate and wrap the device in aluminum foil to avoid exposure to the light. The sample is shelf-stable at room temperature indefinitely.

Note: The divider utilized in this method is 96-well format; however, researchers may employ other formats (384 well, 2-well, 4-wells, 8-wells, etc…) depending on desired experiment set-ups and availability of dividing structures. Some further optimization may be required.

2. Surface Functionalization

2.1 Dissolve 80 µL of a Sulfo-SANPAH aliquot in 40 mL of 0.1 M HEPES buffer (pH 7-9).

Note: Prepare Sulfo-SANPAH aliquots by dissolving 100 mg of Sulfo-SANPAH powder in 2 mL of sterile DMSO.

Note: Prepare 0.1 M HEPES buffer by diluting 50 mL of HEPES in 450 mL of sterile deionized water and filter through 0.22 µm pores.

2.2. Add 200 μL of diluted Sulfo-SANPAH solution to each well of the 96-well plate.

2.3. Expose the plate to UV (300-460nm) at appropriate distance and duration.

Note: After UV exposure, the color of the solution should be darker. UV exposure distance and duration depend on the UV lamp power. In our application, we expose for 10-15 minutes at a distance of 5 cm.

2.4. Remove the Sulfo-SANPAH solution from the wells and add 200 μL of 5 μg/mL of fibronectin solution to each well.

Note: Researcher specified protein can be used for surface coating. Some commonly used proteins are collagen, fibronectin, and laminin. We have found Sulfo-SANPAH to be the most effective method, and plasma cleaning while sometimes employed in PDMS is discouraged as it creates a silicon dioxide layer and visibly damages the surface.

2.5. Incubate the plate at 4 °C overnight.

Note: Different incubation methods can be applied depending on the protein used for coating.

2.6. Remove the fibronectin solution and wash each well with PBS twice.

2.7. Place a lid on the sample.

2.8. Add 200 μL of PBS to each well.

Note: The protocol can be paused here. (The fibronectin-coated samples can be stored at 4 °C for up to 2 weeks.)

3. UV Sterilization

3.1. Sterilize the sample under UV in a biological safety cabinet for 30 min.

Note: Longer UV exposure times may negatively impact the bead fluorescence. All subsequent steps must be performed under sterile conditions.

4. Cell Culture

4.1. Remove PBS from each well and add 200 μL of cells suspended in culture media to each well.

Note: Plate the cells at the desired cell density. Cell density depends on the desired experiment. For single cell studies, cells should be minimum of 50 μm apart and cells near the edges of the imaging window should be not be included in the TFM measurement. For monolayer cells, the imaging window should have the viewing field covered with a confluent layer of cells.

Note: Prepare the complete growth culture media for NMuMG cells by supplementing DMEM with 5% FBS, 10 mM HEPES, 10 μg/mL insulin, 1% penicillin-streptomycin, 1 mM L-glutamine, and amphotericin B 0.5 ug/mL.

Note: Preparation of insulin stock

Reconstitute in acidified water (2.5 mL of glacial acetic acid in 130 mL of deionized water) to a concentration of 10 mg/mL. Store the stock solution at 4 °C. Wait until the solution is clear, and then filter through 0.22 μm pores

4.2. TGF-β Addition

4.2.1. Add 1.5 μL of TGF-β stock solution to 10 mL of the complete cell culture media to constitute the cell culture media with the final TGF-β concentration of 3 ng/mL.

Note: Preparation of TGF-β stock

Dissolve 2 μg of TGF-β in 100 μL of 10 mM citric acid (pH 3.0) and filter sterilize with 0.22 μm pores. Vortex the tube and aliquot into the desired volumes. Store the aliquots at -80 °C.

Note: To make 10 mM pH 3.0 citric acid, dilute the acid in water and adjust pH to 3.0 by adding HCl

5. Data Acquisition

5.1. For each position, acquire at least one image of fiduciary particles and cells. Focus on the bead layer.

Note: Pixel size should be optimized based on size of the fiduciary particles and image processing method being used. In this application, the authors use a 10x 0.4 NA objective, and images are acquired with 1024x1024 resolution, with 455 nm/pixel. In general, it is helpful to retain a resolution of at least approximately 1-5 pixels per bead; here, beads are polydisperse and have an individual size of 300-500 nm.

Note: It is critical that the fluorescent fiduciary beads be in focus for images to be used for TFM calculations. The focus and imaging quality of the beads should be prioritized over imaging the cells themselves. There should be no cross-talk between different channels, particularly any fluorescence not from the fiduciary beads which appears in the imaging spectra of the beads.

5.2. Once all the positions of interest have been recorded, add detachment solution to each well to acquire force-free reference images of the fiduciary particles.

Note: Preparation of cell detachment solution

Mix an aqueous solution containing 2% TritonX-100, 50 mM sodium azide, and 500 mM potassium hydroxide.

Note: The above is provided as an example of an effective detachment solution. Different detachment solutions at researchers' discretion may be used to detach the cells off the substrate surface.

6. Image Analysis

6.1. Analysis software was developed in-house. Image analysis may be done with custom-made software or software available online.

7. Bead Synthesis

The following protocol is based on the synthesis method described by Klein *et al.*[121].

7.1. Under a fume hood, prepare the three-neck flask with a water-cooled reflux condenser.

CAUTION: Set up a synthesis in a well ventilated chemical fume hood.

7.2. Add 0.5 mL of PDMS stabilizer and fluorophore to the flask.

7.3. Equip one neck with a rubber septum with a nitrogen inlet needle and an outlet needle and equip the other neck with a rubber septum for adding reagent with a syringe.

7.4. Add 100 mL of anhydrous hexane in 250 mL to the flask and add a small magnetic stir bar.

7.5. Place the flask in the mineral oil bath at 75 °C and purge it with nitrogen gas for 1 h.

7.6. Add 6 mL of methylmethacrylate to 25 mL of round bottom flask.

7.7. Add 0.100 g of 2,2'-azobisisobutyronitrile (AIBN) to the round bottom flask and purge the mixture with nitrogen gas for 1 h.

Note: Flush methylamethacrylate through prepacked column to remove inhibitors before use.

Add methylamethacrylate and AIBN mixture to the three-neck flask

7.8. The solution initially becomes cloudy and turns milky. Let the reaction run for 3 h after the solution becomes cloudy.

7.9. After 3 h, place the flask in an ice water bath.

7.10. Vacuum-filter the solution with coarse filter paper.

7.11. Centrifuge the filtrate and re-suspend the particles in hexane.

Note: The volume of the hexane to be added depends on the desired concentration of the bead solution.

Note: Sonication facilitates re-dispersion of the bead particles in hexane solution. Beads produced by the authors have polydisperse diameters of approximately 300-500nm. Due to the

use of cross-correlation pattern tracking to determine displacements, monodisperse beads are not required.

8. Rheology Measurement Protocol

Rheology is not required for every researcher or experiment, but is necessary to quantify the moduli for new formulations of PDMS. In this protocol, we employ a shear rheometer to measure the effects of crosslinker, frequency, and strain on moduli of PDMS samples. Depending on the available tools and expertise, moduli may also be measured using many other mechanical analysis approaches. Additionally, researchers using this protocol may elect to use our published moduli presented in Table 3-1 and Figure 3-3 & Figure 3-4.

8.1. Use a rheometer with a 25 mm diameter parallel plate geometry. Other geometries may be used.

8.2. Initialize the system and calibrate the device and measuring system (parallel plate, d=25 mm). After measuring the zero gap, begin loading the PDMS sample.

8.3. As soon as the PDMS elastomer and crosslinking agent has been mixed, pipet it onto the bottom plate of rheometer.

8.3.1. Move the spindle down to completely contact the top of the PDMS sample.

8.3.2. Carefully trim the loaded sample excess from the bottom plate.

8.4. In a strain sweep test, apply increasing strains for each composition with different crosslinking density to ensure the polymer structure remains in the linear viscoelastic regime during all shear measurements.

Note: Strain values relevant for cell studies are typically in the range of .1-10%. We have found PDMS to be linear up to approximately 100% strain.

8.5. Measure the dynamic shear storage modulus (G'), and loss modulus (G″) of the PDMS network in a time sweep test with frequency of 1 Hz and oscillatory shear strain of 0.5 % at 100 °C.

8.6. To determine the viscoelasticity and time dependency of the final PDMS network, apply a frequency sweep test with frequency ranging from 0.1-100 Hz and oscillatory shear strain of 0.5 %.

3.5 Representative Results

Before addition of TGF-β, a confluent monolayer of cells has a cobblestone like shape and is tightly packed. Upon TGF-β treatment, cells become more elongated in morphology, enlarging the cell area and acquiring a more mesenchymal phenotype. Utilizing the multi-well device fabricated with soft PDMS elastomers, the physical properties of cells in a total 17 different conditions were studied. The cells were treated with 4 different TGF-β concentrations (0.5, 1, 2, and 4 ng/mL) and 4 different incubation times (12, 24, 48, 96 h), and these results are summarized in Figure 3-5. The cells treated with TGF-β applied larger traction stresses and strain energies than the cells cultured without TGF-β. Cells incubated with TGF-β for 96 hours showed the largest traction stresses and strain energies. The cells applied larger stresses and strain energies when treated with higher concentration of TGF-β. The difference in tractions and strain energies were more distinct at longer incubation times.

The surface of the substrate needs to be smooth and uniformly coated with ligands, such as fibronectin or collagen. With scratched surface and/or non-uniform coating of ligands may lead to improper cell attachment, resulting in inaccurate traction measurement. Figure 3-6 shows the localized traction stresses due to the non-uniform substrate surface.

3.6 Figures and Tables

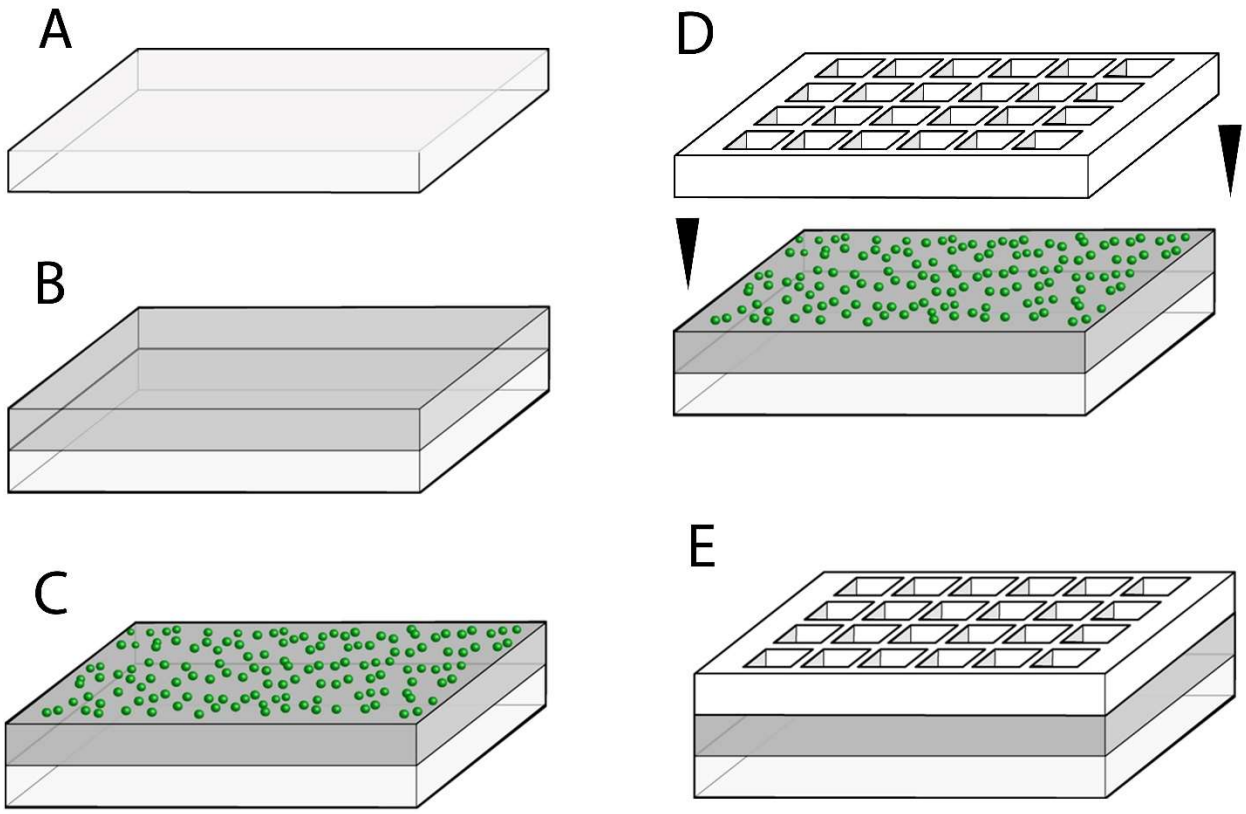

Figure 3-1: **Overview of multi-well plate fabrication**. **A.** A custom-cut glass slide is the starting point. **B.** The glass slide is coated with a thick (~100µm layer of PDMS). **C.** A layer of fiduciary beads (shown in green) are then spin-coated in a ~1µm thick layer on top of the previous layer. **D.** The multi-well divider is carefully placed on top of the fiduciary bead layer. **E.** The complete multi-well plate is assembled and ready for use or storage.

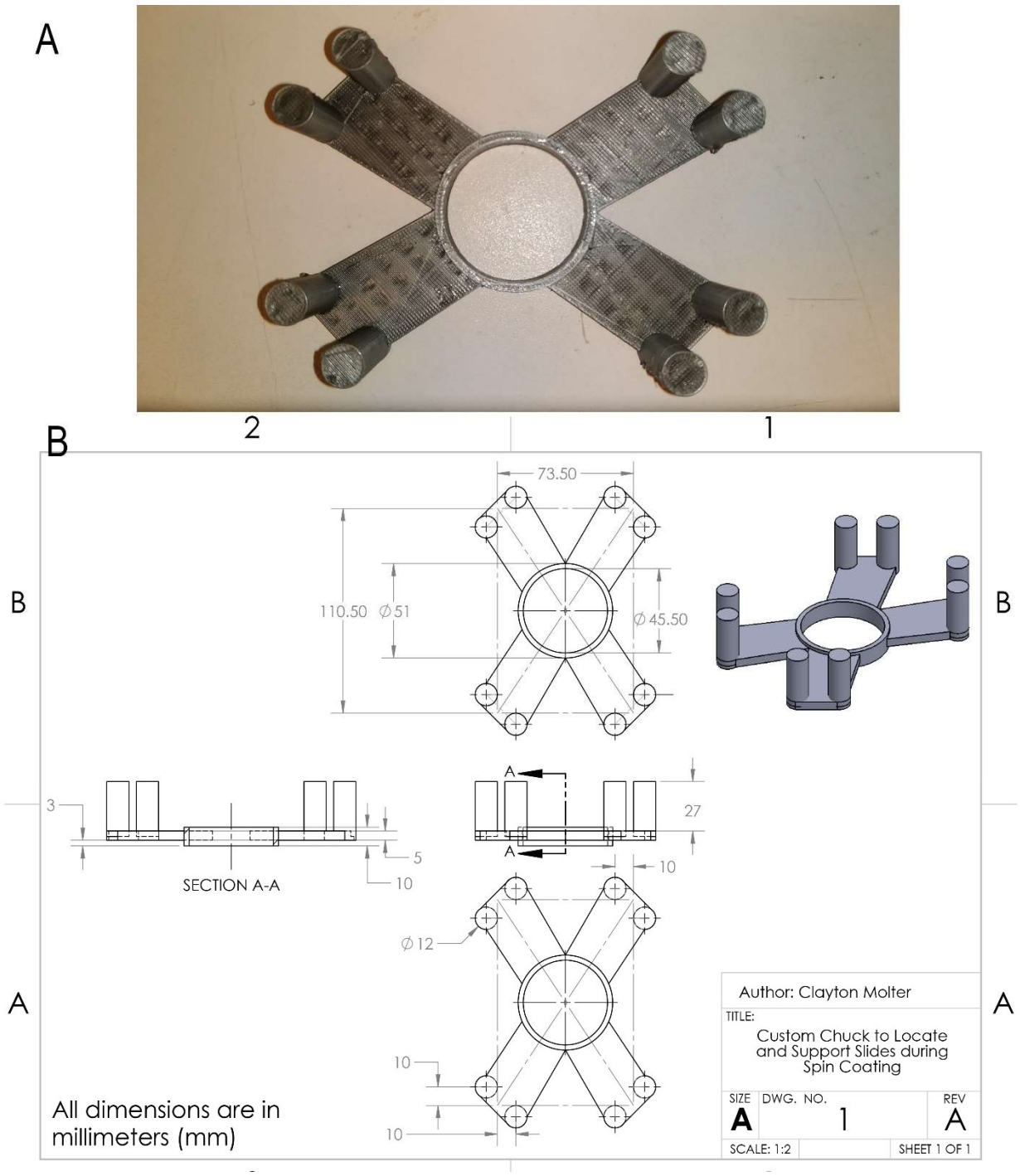

Figure 3-2: **Custom chuck for spin-coater.** To prevent the bottom glass (where PDMS is coated) from flying off of the standard spincoater chuck, a custom-made holder is placed onto the chuck. **A.** A custom-made holder for the spincoater chuck. **B.** Engineering drawing of the holder with all the dimensions.

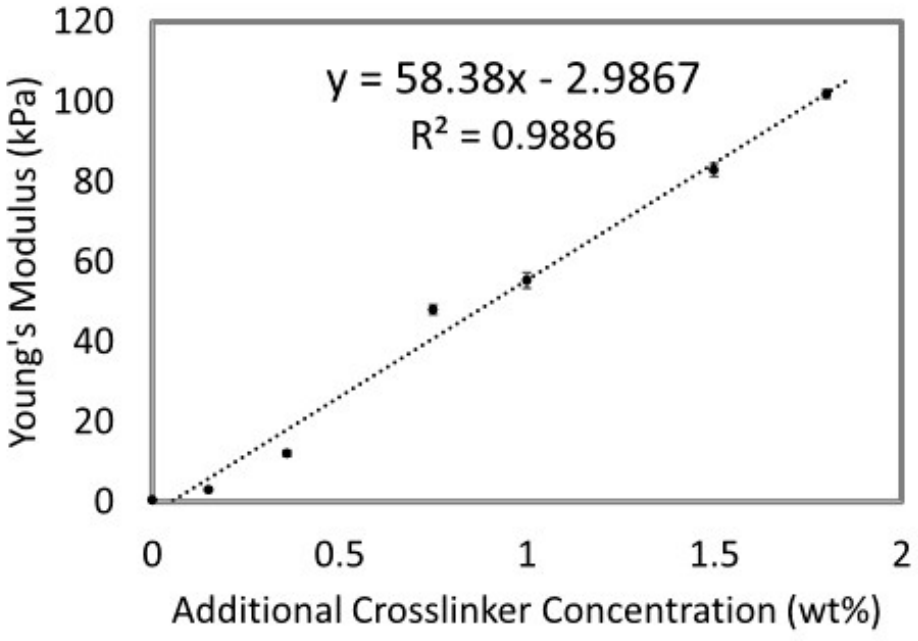

Figure 3-3: **Substrate stiffness with changing crosslinker concentration (wt%).** PDMS mixtures are prepared as described, with the additional crosslinker percentage increasing the elastic modulus until a max of 100 kPa at 1.8 weight percent crosslinker. As a guide, the modulus as a function of crosslinker is fit linearly, which can be used by researchers to formulate their own mixture at a particular desired modulus within this range.

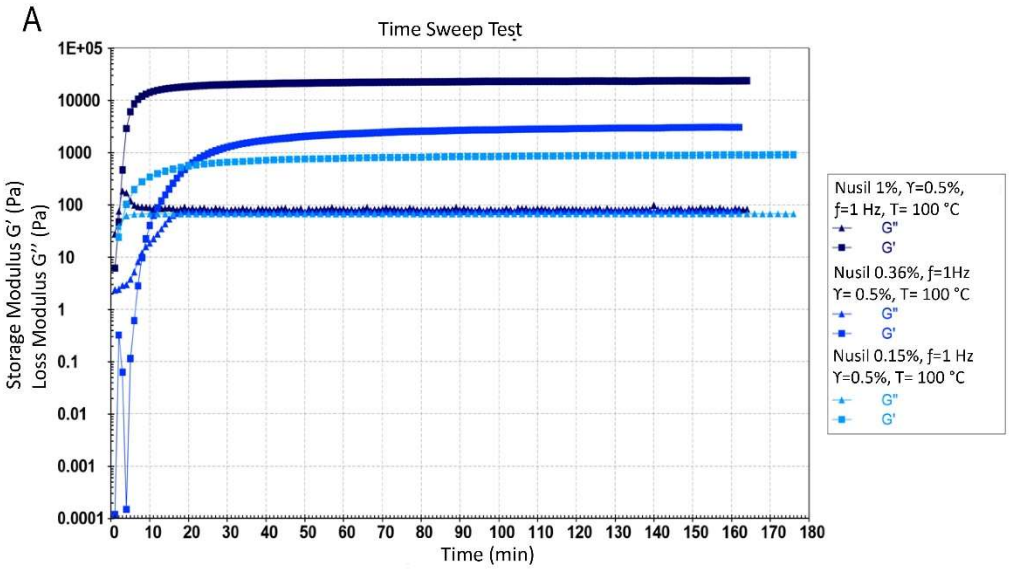
A
Time Sweep Test
Storage Modulus G' (Pa)
Loss Modulus G'' (Pa)
1E+05
10000
1000
100
10
1
0.1
0.01
0.001
0.0001
0 10 20 30 40 50 60 70 80 90 100 110 120 130 140 150 160 170 180
Time (min)
Nusil 1%, Y=0.5%, f=1 Hz, T= 100 °C
G"
G'
Nusil 0.36%, f=1Hz Y= 0.5%, T= 100 °C
G"
G'
Nusil 0.15%, f=1 Hz Y=0.5%, T= 100 °C
G"
G'

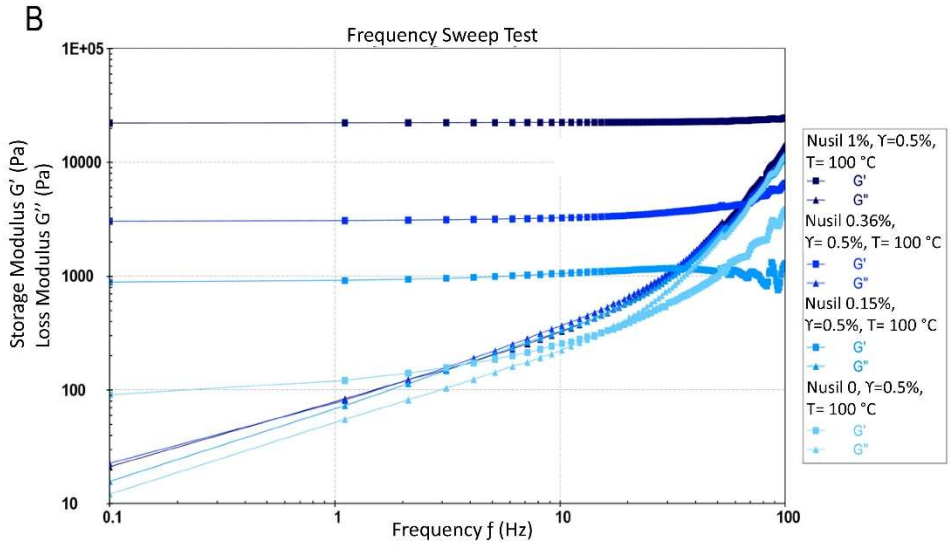
B
Frequency Sweep Test
Storage Modulus G' (Pa)
Loss Modulus G'' (Pa)
1E+05
10000
1000
100
10
0.1
1
10
100
Frequency f (Hz)
Nusil 1%, Y=0.5%, T= 100 °C
G'
G"
Nusil 0.36%, Y= 0.5%, T= 100 °C
G'
G"
Nusil 0.15%, Y=0.5%, T= 100 °C
G'
G"
Nusil 0, Y=0.5%, T= 100 °C
G'
G"

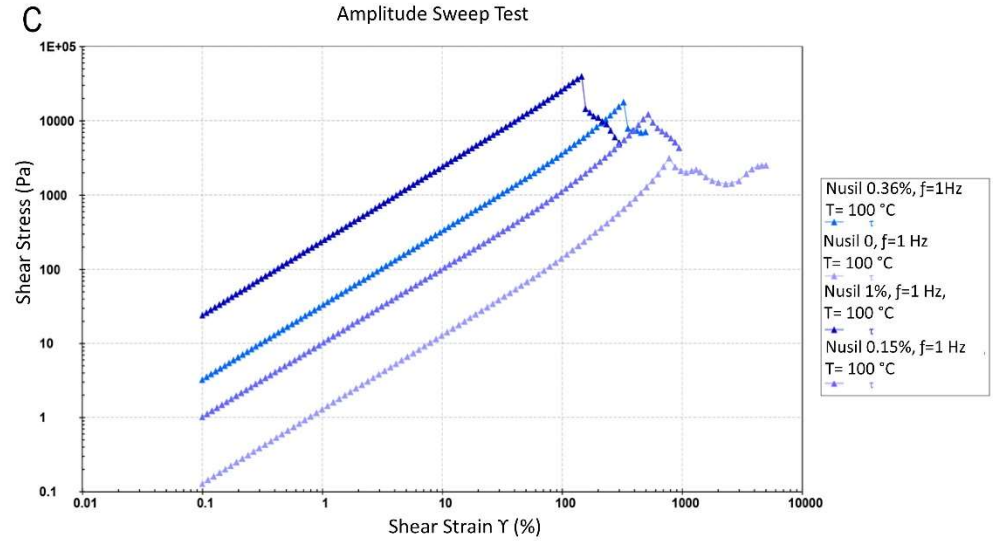
C
Amplitude Sweep Test
Shear Stress (Pa)
1E+05
10000
1000
100
10
1
0.1
0.01
0.1
1
10
100
1000
10000
Shear Strain ϒ (%)
Nusil 0.36%, f=1Hz T= 100 °C
τ
Nusil 0, f=1 Hz T= 100 °C
τ
Nusil 1%, f=1 Hz, T= 100 °C
τ
Nusil 0.15%, f=1 Hz T= 100 °C
τ

Figure 3-4: **Rheology of PDMS elastomer containing 0, 0.15, 0.36 and 1 wt% of crosslink agents (Sylgard 184 curing agent) at a temperature of 100 °C. Triangle symbols indicate loss modulus (G'') and square symbols indicate storage modulus (G'). A.** Oscillatory Time sweep at frequency of 1 Hz and shear strain of 0.5 % during gelation. **B.** Oscillatory frequency sweep of PDMS network at shear strain of 0.5 %. **C.** Strain sweep of PDMS network at frequency of 1 Hz. All data points were acquired in triplicate.

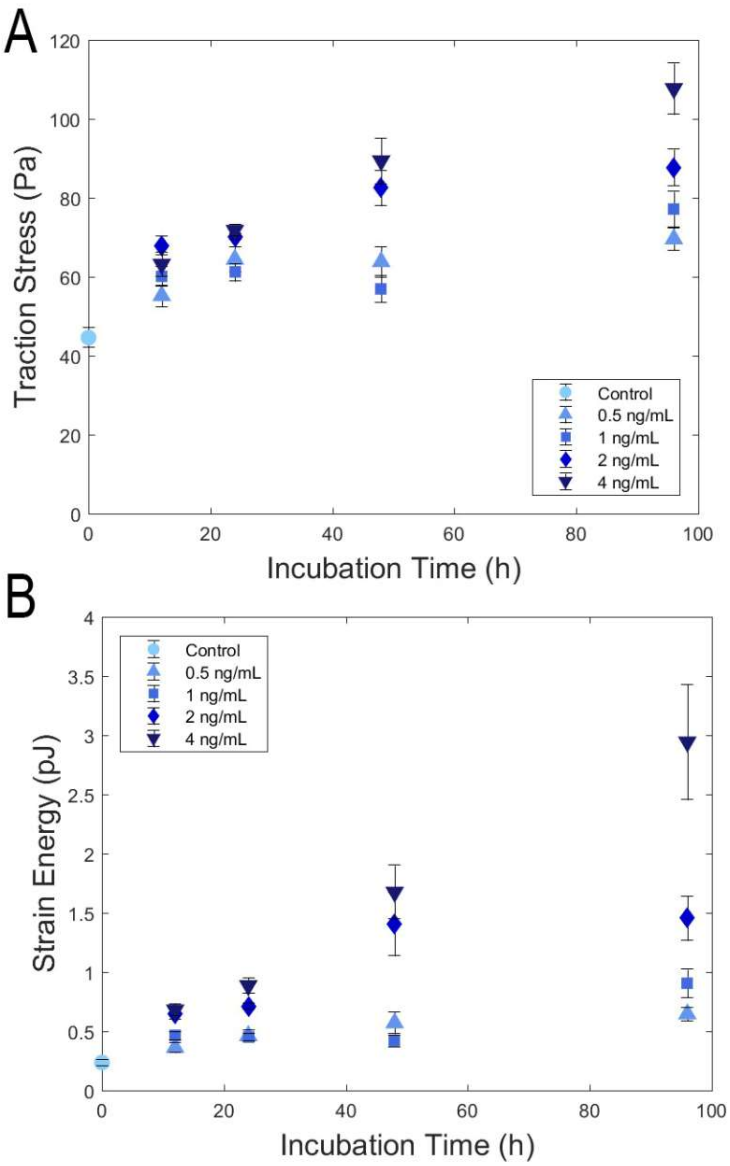

Figure 3-5: **Representative results utilizing traction stress device with multiwell format. Monolayer of cells in different conditions were cultured in multi-well device to measure contractility and strain energy. A.** Graph of traction stresses with increasing TGF-β incubation time for different TGF-β concentrations. Traction stresses increased with increasing TGF- β concentrations and incubation time. All data are statistically significant with respect to control (i.e. no TGF- β) except the following: 12h-0.5ng, 12h-1ng, 48h-1ng **B.** Graph of strain energy with increasing TGF-β incubation time for different TGF-β concentrations. Strain Energies increased with increasing TGF- β concentrations and incubation time. Sample sizes range from n=7 to n=15. All data are statistically significant with respect to control (i.e. no TGF- β) except the following: 12h-0.5ng, 12h-1ng, 24h-0.5ng, 24h-1ng, 48h-1ng. Statistical significance was determined using the Kruskal Wallis test, which does not assume a normal distribution.

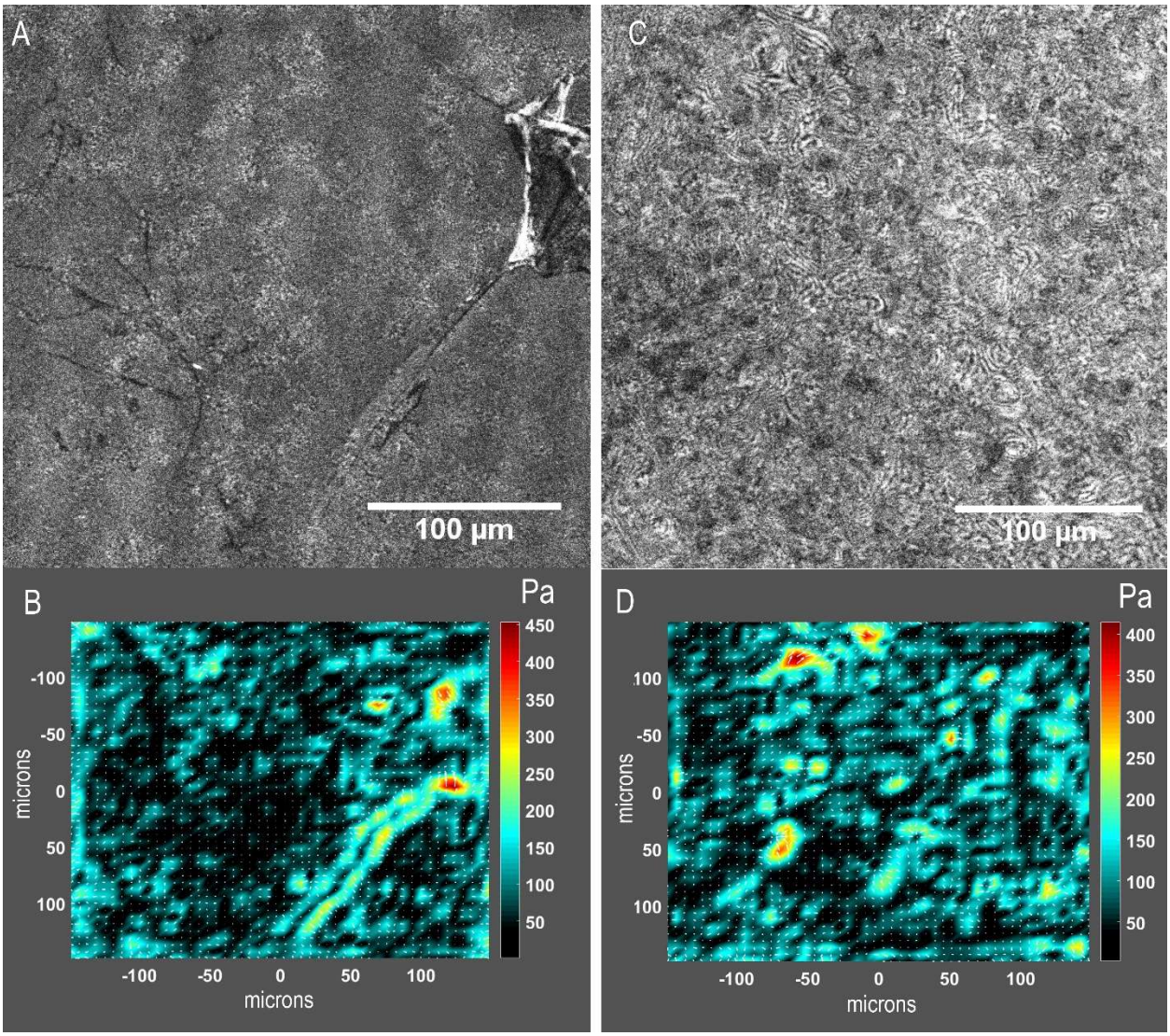

Figure 3-6: **Representative results from sub-optimal (A&B) and satisfactory (C&D) experiment. A.** Reflection image of the substrate surface. Undesired contaminants, which can include dust or fibers, or material defects such as scratches are present on the surface substrate. **B.** Stress map of cell contractility: Due to the non-uniform surface, irregular and inaccurate traction stresses are observed around the objects. **C.** Reflection image of the substrate surface. No apparent contaminants are visible. **D.** Stress map of cell contractility: no artifact discontinuities are visible.

Table 3-1: **Substrate stiffness with changing crosslinker concentration (wt%).** By changing additional crosslinker concentrations, PDMS substrates of the desired Young's moduli are fabricated. PDMS shear moduli were measured with a rheometer and Young's moduli were determined. For each data point, 3 independent preparations were done and the standard deviation is given

Crosslinker concentration (wt%)	G' (Pa)	Standard Deviation	E (kPa)	Standard Deviation
0	0.135	0.014	0.405	0.043
0.15	1	0.1	3	0.35
0.36	4.027	0.245	12.081	0.73
0.75	16.01	0.49	48.03	1.2
1	18.44	0.989	55.32	1.94
1.5	27.638	0.93	82.91	1.64
1.8	33.986	0.88	101.94	1.088
2	33.36	0.67	100.08	1.1

3.7 Discussion

Critical Steps in the protocol

It is critical to have a uniformly coated sample with a constant thickness of approximately 100 μm. The modulus should be carefully chosen to examine the physical significance of the biological system of interest. When fabricating a top layer, the concentration of the fiducial fluorescent particles should be optimized for accurate analysis of displacement and traction stress. Analyzing isolated single cells requires a denser fiduciary layer than measuring confluent monolayers. Additionally, the surface of the substrate should have stable and uniform coating of adhesion molecules such as collagen, fibronectin, and laminin to ensure proper attachment of the cells to the substrate surface. Particular care must be taken when attaching the multiwell divider; it should be placed without sliding to prevent sealing PDMS glue from being smeared on the culture surface, and the outer edge must be carefully aligned with the glass dimensions to prevent any leaks on the border wells.

Modifications and troubleshooting of the method

To prevent wells from being leaky, an adequate amount of PDMS glue needs to be applied to the well-divider to hold it in place. However, use of excessive amounts will cover cell culture surface.

Sufficient volume of PDMS needs to be added during the spin-coating procedure. When curing, the oven and racks need to be level. Inadequate PDMS or an unleveled oven may lead to uneven PDMS thickness.

Bead density needs to be optimized for proper analysis. When the bead density is not adequate, concentration of the beads in fiduciary PDMS mixture needs to be increased. Additionally, an adequate amount of the mixture needs to be added for spin coating.

To ensure proper fluorescent signals of the fiduciary bead particles, curing condition should be carefully monitored. Longer times and higher temperatures than the ones specified in this protocol may degrade the fluorescence.

Improper protein coating on the surface of the sample may lead to poor cell adhesion. To prevent this, the surface needs to be cleaned and the expiration of reagents such as Sulfo-SANPAH and ligands needs to be checked. UV exposure time and strength should be optimized. Immunofluorescence or other fluorescent protein construct may be tested to ensure uniform ligand coating.

Limitations of the method

The device fabricated with this method and set of PDMS formulations is only applicable to substrates with Young's moduli ranging from 0.4 kPa to 100 kPa. Other moduli may be possible using alternative formulations, however, the current range spans a large set of physiologically relevant values. While this method is specifically for mutliwell fabrication, it may also be used to prepare individual slides or other slide geometries, and in these instances further user troubleshooting may be necessary. In this embodiment, a relatively thick (1mm) glass slide is employed, precluding common high numerical aperture (NA) objectives on an inverted microscope. While it is technically feasible to construct these multi-well TFM dishes using thinner glass, the fragility of these in processing and assembly may result in a large rate of breakage, and can run contrary to the higher-throughput approach.

Furthermore, surface coating may be investigated further for wider applications of the device.

The significance of the method with respect to existing/alternative methods

Multiwell advantage: Utilizing a multiwell format, high-throughput experiments are possible. Multiwell format enabled us to examine the physical changes of NMuMG cells during EMT with

TGF-β treatment with combinations of different concentrations and different incubation times in a single dish.

PDMS Advantage: Fabrication of traction stress devices with hydrogels such as polyacrylamide gel have several limitations. Dominant ingredient being water, hydrogels are sensitive to salt concentrations (osmolarity), temperature, humidity, and pH changes. Changes in any of these properties can lead to the change in mechanical properties of the material, requiring extra care in using samples and interpreting results.

Furthermore, having water, hydrogels are more susceptible to infections, requiring extra cautions. In contrast to water-based hydrogels, silicone-based PDMS is stable and inert. Once fabricated, it can be stored at room temperature indefinitely without requiring any special handling and storing condition.

The impermeable nature of PDMS allows us to fabricate a monolithic substrate, ensuring that all wells are truly identical in substrate thickness and composition, while allowing unique biochemistry to be applied in the media, or different cells to be utilized in each well. A hydrogel based surface allows diffusive factors to permeate and travel through it, necessitating adding the hydrogel to wells that are otherwise partitioned to prevent cross-contamination.

Future applications or directions of the method

This method allows researchers to study cell contractility, a basic and ubiquitous aspect of cell biology, in a high-throughput manner, enabling more efficient and reproducible data acquisition. This helps to translate Traction Force Microscopy into Contractile Force Screening, allowing researchers to truly use contractility as a metric for cell activity, or efficacy of a compound. As a methodology, this has broad applications across biophysical and biomedical sciences, from understanding the physics of cells, to characterizing and testing pharmaceutical compounds

against standardized cell types, or perhaps highly specialized individual cells for personalized medicine.

3.8 Acknowledgments

The authors thank Tom Kodger, Michael Landry, and Christopher J. Barrett for assistance with bead synthesis. A.J.E. acknowledges Natural Sciences and Engineering Research Council grants RGPIN/05843-2014 and EQPEQ/472339-2015, Canadian Institutes of Health Research grant no. 143327, Canadian Cancer Society grant no. 703930, and Canadian Foundation for Innovation Project #32749. R. Krishnan acknowledges National Institutes of Health grant no. R21HL123522 and R01HL136209. H.Y. was supported by Fonds de recherche Santé Québec, and Fonds de recherche Nature et Technologies Québec. The authors thank Johanan Idicula and Zixin He for assistance in preparing the video component of this manuscript.

Disclosures

AJE and RK have interest in Live Cell Technologies, a company which fabricates materials described in this article.

3.9 References

Dembo, M., & Wang, Y.-L. (1999). Stresses at the Cell-to-Substrate Interface during Locomotion of Fibroblasts. *Biophysical Journal, 76*(4), 2307-2316.

Guo, M., Ehrlicher, A. J., Jensen, M. H., Renz, M., Moore, J. R., Goldman, R. D., . . . Weitz, D. A. (2014). Probing the stochastic, motor-driven properties of the cytoplasm using force spectrum microscopy. *Cell, 158*(4), 822-832.

Harris, A., Wild, P., & Stopak, D. (1980). Silicone rubber substrata: a new wrinkle in the study of cell locomotion. *Science, 208*(4440), 177-179.

Klein, S. M., Manoharan, V. N., Pine, D. J., & Lange, F. F. (2003). Preparation of monodisperse PMMA microspheres in nonpolar solvents by dispersion polymerization with a macromonomeric stabilizer. *Colloid Polym Sci Colloid and Polymer Science : Kolloid-Zeitschrift und Zeitschrift für Polymere., 282*(1), 7-13.

Kraning-Rush, C. M., Califano, J. P., & Reinhart-King, C. A. (2012). Cellular Traction Stresses Increase with Increasing Metastatic Potential. *PLOS ONE, 7*(2), e32572.

Krishnan, R., Tambe, D., Steward, R., Hardin, C., & Butler, J. (2015). Traction Microscopy. In *Cells, Forces, and the Microenvironment* (pp. 75-96): Pan Stanford.

Ngan, E., Northey, J. J., Brown, C. M., Ursini-Siegel, J., & Siegel, P. M. (2013). A complex containing LPP and α-actinin mediates TGFβ-induced migration and invasion of ErbB2-expressing breast cancer cells. *Journal of Cell Science, 126*(9), 1981-1991.

Oliver, T., Jacobson, K., & Dembo, M. (1995). Traction forces in locomoting cells. *Cell Motility, 31*(3), 225-240.

Park, C. Y., Zhou, E. H., Tambe, D., Chen, B., Lavoie, T., Dowell, M., . . . Krishnan, R. (2015). High-throughput screening for modulators of cellular contractile force. *Integr Biol (Camb), 7*(10), 1318-1324.

Yoshie, H., Koushki, N., Kaviani, R., Tabatabaei, M., Rajendran, K., Dang, Q., . . . Ehrlicher, A. J. (2018). Traction Force Screening Enabled by Compliant PDMS Elastomers. *Biophysical Journal, 114*(9), 2194-2199.

Preface to Chapter 4

In Chapter 3, I studied changes in contractile forces and strain energies by treating NMuMG cells with TGF-β for various concentrations and incubation times to examine physical changes during EMT. Both of these physical parameters increased with increasing concentrations and TGF-β, finding that epithelial cells apply larger forces and do more work on their environment as they go through the transition to become mesenchymal cells.

To determine the mediators for the changes in forces and work observed during EMT in Chapter 3 and the influence of these changes in cancer metastasis, I investigated other mechanical properties during EMT. I observed changes in actin architectures and shear moduli. Furthermore, the movement of the cells in the multi-cellular system was quantified by tracking the nucleus of individual cells in a confluent monolayer sheet. Collectively, these results help us to better understand EMT mechanisms from physical perspectives and collective behaviors of cells in monolayer sheets as they go through the transition.

Chapter 4 : Mechanical and Migratory Changes during the Metastatic Epithelial to Mesenchymal Transition

Authors & Affiliations

Yoshie, H.[1]; Ghagre, A.[1]; Tirgar, P.[1]; Tao, Y.[1]; Ou, J.[1]; Huang, Y.[1]; Mochulska, V.[1]; Hayer, A.L.[2]; Siegel, P. M.[3,4]; Ehrlicher, A. J.[1,3,#]

[1]Department of Bioengineering, McGill University, Montreal, QC, Canada

[2]Department of Biology, McGill University, Montreal, QC, Canada

[3]Goodman Cancer Research Centre, McGill University, Montreal, QC, Canada

[4]Department of Biochemistry, McGill University, Montreal, QC, Canada

Corresponding author

4.1 Abstract

The Epithelial-to-Mesenchymal Transition (EMT) is a key transformation in many physiological and pathological processes. During EMT, tightly packed epithelial cells become more invasive and motile mesenchymal cells. This biophysical change is believed to contribute to the increased tumor cell motility in cancer metastasis. Cancer cells are known to undergo various biomechanical changes during this transition, yet a comprehensive and cohesive quantification of these changes is lacking. Here we quantified diverse biophysical and mechanical changes of isolated and confluent NMuMG cells during EMT. We observe that cells reorganize their internal cytoskeleton, forming pronounced stress-fibers (F-actin length increased from 2.54 ± 0.09 to 10.4 ± 0.7 μm), which compress and flatten the cell and nuclei (volume decreased from 5741 ± 170 to 1974 ± 76 μm^3 and 1591 ± 460 to 507 ± 55 μm^3, respectively). We find that contractility and work increase (from 44 ± 3 to 108 ± 6 Pa and from 0.22 ± 0.03 to 2.9 ± 0.5 pJ,

respectively), and cellular shear moduli also increase (from 306 ± 11 to 798 ± 24 Pa) as cells go from epithelial to mesenchymal states. To examine how the changes influence migratory behaviour of cells, we studied cell motility by tracking individual nuclei in monolayer sheets, discovering that during EMT cells transition from slow diffusive movement to faster persistent motion. These results demonstrate the importance of biophysical and biomechanical aspects in EMT, which illustrate their interconnected nature during this transformation.

4.2 Significance

In this study, we quantified diverse biophysical parameters to understand mechanical changes in cells as they transition from non-motile epithelial cells forming sheets to more migratory mesenchymal cells during EMT. Our lab and others have previously shown that as epithelial cells acquire more migratory and invasive mesenchymal characteristics, they apply more forces on their surroundings and do more work.[128-129] How this increased contractility functions in concert with other mechanical changes during EMT to promote migration is not well understood. Our results here show that remodeling of actin leads to a highly elongated, flattened morphology, a stiffer cell, larger displacements, and persistence of motion. These results suggest that increased cell migratory invasiveness in tissues may be critically dependent on contractility but not reliant on cell softening.

4.3 Introduction

The Epithelial to Mesenchymal Transition (EMT) is a complex process whereby the epithelial cell sheet transforms from a single cohesive unit into a collection of more mechanically autonomous cells. This basic change from collective to single cell behavior is a crucial element of multi-cellular life and plays a central role in many physiological multi-cellular events such as embryonic development, wound healing, and organ fibrosis.[37] For example, during gastrulation,

EMT allows epithelial cells to separate from the initial layer to form different layers.[130] In addition to driving normal physiology, EMT also contributes to pathologies such as tissue fibrosis. Previous research has shown that cells that have undergone EMT produce excessive amount of collagen and that crosslinking of fibrous networks is also altered; these changes may leads to malfunctioning organs in organ fibrosis.[130-131]

EMT is also thought to contribute to metastasis in some epithelial cancers.[37, 132] During cancer metastasis, cells leave their primary site, migrate in the body, and develop tumors at a distant secondary site, spreading the disease. This metastatic behavior of cancer cells accounts for 90% of cancer-related mortality. During the progression of the disease, EMT is believed to allow tumor cells to migrate through the Extra Cellular Matrix (ECM) and tissues more easily, promoting metastasis.[37] When cells undergo EMT, epithelial cells lose apical-basal polarity and cell-cell adhesions, becoming more migratory and invasive mesenchymal cells with elongated structure.[37] This change in migratory behavior is partly due to remodeling of ECM. During EMT, ECM is remodeled by matrix metalloproteinases. This remodeling of ECM alters cell-matrix interactions and cell-cell interactions, contributing to their increased motility and invasiveness.[133-135] Cells also alter expression levels of certain genes as they go through the transition, and these changes in gene expressions are frequently utilized as markers for EMT, often referred to as hallmarks of EMT. The hallmarks of EMT include decreased expression of claudins and E-cadherins, and increased vimentin and N-cadherins, each of them playing specific role in EMT.[46-47] While many of these biological changes are relatively well characterized, one can also expect there to be significant changes in the mechanics and forces of cells during this transformation.[45, 128, 136] Work over the last decades has revealed that EMT may indeed be characterized as a physical and mechanical transformation. A previous *in vitro* study has shown

that head and neck cancer cells become softer during EMT[136], and that traction stresses increase during EMT[128-129]. The dynamic remodeling of actin filaments from thin fibers primarily concentrated in cell cortex in epithelial cells to pronounced aligned contractile bundles in mesenchymal cells was previously observed.[45] Nevertheless, these biophysical measurements have typically characterized only a few aspects of mechanical changes involved in EMT, leading to a fragmented and sometimes inconsistent picture of this process, leading to an inability to compare the relative roles of these mechanical changes in migration. Moreover, the majority of studies to date have focused on isolated cells, which are unlikely to capture the multi-cellular interactions that contribute to this transformation.

Here, to understand how the time-dependent physical changes function in concert to facilitate this motile transformation, we approached EMT from a comprehensive physical perspective: we quantified changes in contractility, cellular moduli, and motility. Additionally, we observed changes in structure of the whole cell, actin stress-fibers, and nuclei. By viewing EMT through these sets of measurements, we formulate a perspective of how these interlinked processes function together to transform cell function and behavior.

To examine the cohesive nature of epithelial cells, we performed all measurements on monolayer sheets. To focus on the changes during the transition rather than the stable epithelial and mesenchymal states, we used a model cell line derived from Normal Murine Mammary Gland (NMuMG) cells that can undergo EMT with TGF-β1 treatment. TGF-β is a growth factor whose signaling cascade involves many physiological processes such as cell growth and differentiation, cell proliferation, and immune regulations.[137] Upon binding to transmembrane receptors, TGF-β activates canonical and non-canonical pathways. Canonical pathways involves

signaling through Smad proteins, leading to interactions with several transcription factors, which in turn alter gene expressions of EMT-associated proteins.[49]

When treated with TGF-β, NMuMG cells transition from epithelial cells to mesenchymal cells as described previously[138]. By inducing EMT in cells cultured in monolayers, we measure that epithelial NMuMG cells increase contractility and stiffness by approximately 2.5 folds. Cells treated with TGF-β1 for 96 hours have a 4-fold increase in actin length, and this has striking effects on both cell and nuclear volume. Both nuclei and volume get compressed, leading to approximately 70% reduction of volume in both cases. These changes in cellular architectures, mechanical properties and contractility have a profound influence on cell motility, making cells displace in a higher rate and processive motion. These results suggest that epithelial cells acquire a more migratory phenotype by changing their biomechanical properties through sequential processes. The cells undergo structural changes of their actin network influenced by the EMT signaling cascade, which in turn influences the cellular moduli, and the transmission of contractile forces. These processes together act to modify the migratory behaviour of the cells during EMT.

4.4 Results

Mesenchymal Cells Apply Larger Contractile Forces and Do More Work than Epithelial Cells.

To compare the contractile forces of cells in epithelial state and mesenchymal state, we performed Traction Force Microscopy (TFM) on an EMT-inducible cell line NMuMG +/- TGF-β1 for both single cells and confluent monolayer sheets. The experimental process consisted of culturing isolated cells and confluent monolayers on soft elastic PDMS substrates, and measuring cell-induced deformations of the substrate using TFM described previously[129].

To establish a baseline behavior, we examined isolated single NMuMG cells. We found that traction stresses increase from the epithelial state to the mesenchymal phenotype, consistent with previous findings[128-129]. When cultured on 1 kPa substrates, TGF-β1-treated single NMuMG cells (96h) exerted larger traction stresses than non-treated single NMuMG cells (31 ± 2, and 58 ± 3 Pa, respectively), as shown in Figure 4-1. TGF-β1-treated cells also did approximately 9 times higher work than non-treated cells (from 0.0062 ± 0.0008 to 0.054 ± 0.006 pJ) cultured on the substrate of the same stiffness (Figure 4-1).

While this characterization of individual cells is the simplest possible, epithelial cells in animals rarely exist as single isolated cells, but rather as sheets of interacting cells. To examine the collective response rather than just that of individual cells during EMT, we quantified the traction stresses of confluent monolayers of NMuMG cells as a function of TGF-β1 exposure time; this allows us to capture the transition between the epithelial and mesenchymal states. Similar to isolated cells, when monolayers were cultured on 9.2 kPa substrates, TGF-β1-treated NMuMG cells (96h) increased the Root Mean Squared (RMS) average traction stresses 2.5-fold (from 44 ± 3 to 108 ± 6 Pa), as shown in Figure 4-1. Additionally, we observed that cells with TGF-β1 (96h) had 13 times higher strain energy than non-treated counterpart (from 0.22 ± 0.03 to 2.9 ± 0.5 pJ) (Figure 4-1).

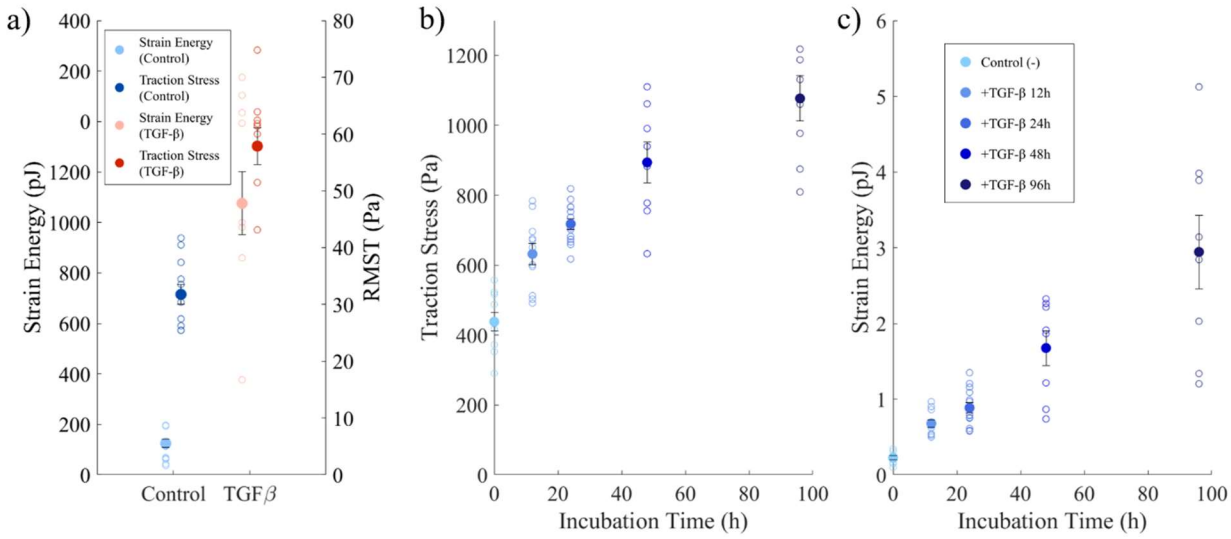

Figure 4-1: **Mesenchymal cells apply larger contractile forces and total work than epithelial cells. (a)** Root mean squared traction stresses (RMST) and strain energies of NMuMG cells +/- 4ng/mL TGF-β1 for single cell TFM (n=15 & n=10 for non-treated & TGF-β1-treated, respectively) cultured on 1 kPa PDMS substrate. (**b** & **c**) Traction stresses (**b**) and strain energies (**c**) of NMuMG cells +/- 4ng/mL TGF-β1 (12h, 24h, 48h, & 96h) for monolayer TFM (n=8-14) cultured on 9.2 kPa PDMS substrate. Each open circle represents an independent cell (for single cell measurements) or position (for monolayer measurements), and each filled circle represents the average of these separate circles. Bars indicate standard errors.

Cell moduli increase during EMT.

Numerous previous studies have shown that as cancerous cells become more metastatic, their mechanical moduli decrease, leading to more compliant phenotypes.[126, 136, 139-141] Conversely, other studies reported an increase in moduli.[142-143] To examine how cells change their mechanical properties during EMT, we used Magnetic Twisting Cytometry (MTC) to measure complex shear moduli of cells as described previously[144]. We find that during time-dependent EMT progression, we see an increase in shear moduli. Monolayers of TGF-β1-treated cells (96h) monotonically increased their complex shear moduli roughly 2.5 times relative to the control without TGF-β1 (306 ± 11 to 798 ± 24 Pa) (Figure 4-2), demonstrating that the cells are continuously becoming stiffer during EMT. In all studies related to measurements of mechanical

properties of the cells, moduli measured may be influenced by various factors such as methodology, whole-cell architecture, cytoskeletal actin structures, and water efflux[145]. These differences lead to the observed variable trends in cellular moduli during metastasis and EMT.

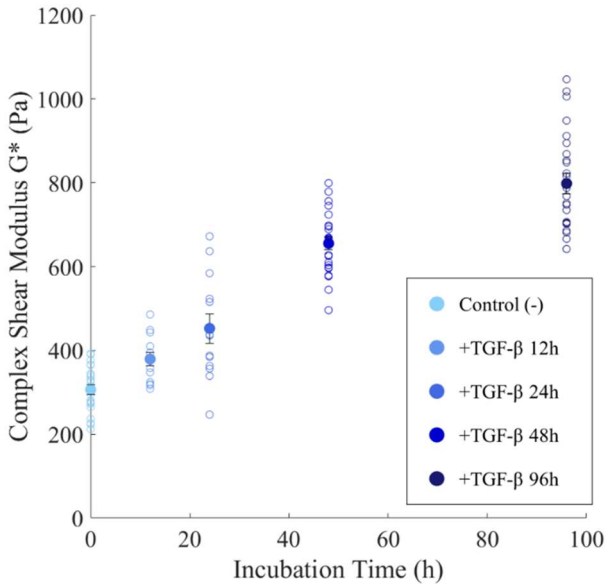

Figure 4-2: **During EMT, epithelial cells increase their complex shear moduli.** RDG-coated 4.5 μm microbeads were used to apply shear stress on NMuMG cells cultured on 9.2 kPa PDMS substrate, and magnetic twisting cytometry measurements were performed at 1 Hz. Extended exposure to TGF-β1 increased cell's cortex shear moduli (n=13 to 25). Each open circle represents an independent position, and each filled circle represents the average of these separate circles. Bars indicate standard errors.

Cell morphology changes during EMT, resulting in cell flattening.

To examine the changes in overall cell structure within the monolayer, we first captured bright-field images of NMuMG cells as a function of TGF-β1 exposure time. In Figure 4-3, cells with prolonged TGF- β1 exposure can be seen to significantly narrow, elongate and align. To quantify the morphological changes, we measured the spread area of the cells. We see an increase in cell spread area during EMT progression; monolayers of TGF-β1-treated cells (96h)

increased their spread area roughly 6 times relative to the control without TGF-β1 (187 ± 15 to 1144 ± 240 μm^2) (Figure 4-3), indicating that the cells become more spread during EMT. To examine the effect of cell spreading on the overall cell structures, cell volume was measured by acquiring z-stack images of cells with a confocal microscope (details can be found in Materials and Methods). We find that cell volume decreases with increasing TGF-β1 incubation times. We measured that cell volume of epithelial cells on average decreases approximately 70% after 96h of TGF-β1 incubation (5741 ± 170 to 1974 ± 76 μm^3) (Figure 4-3).

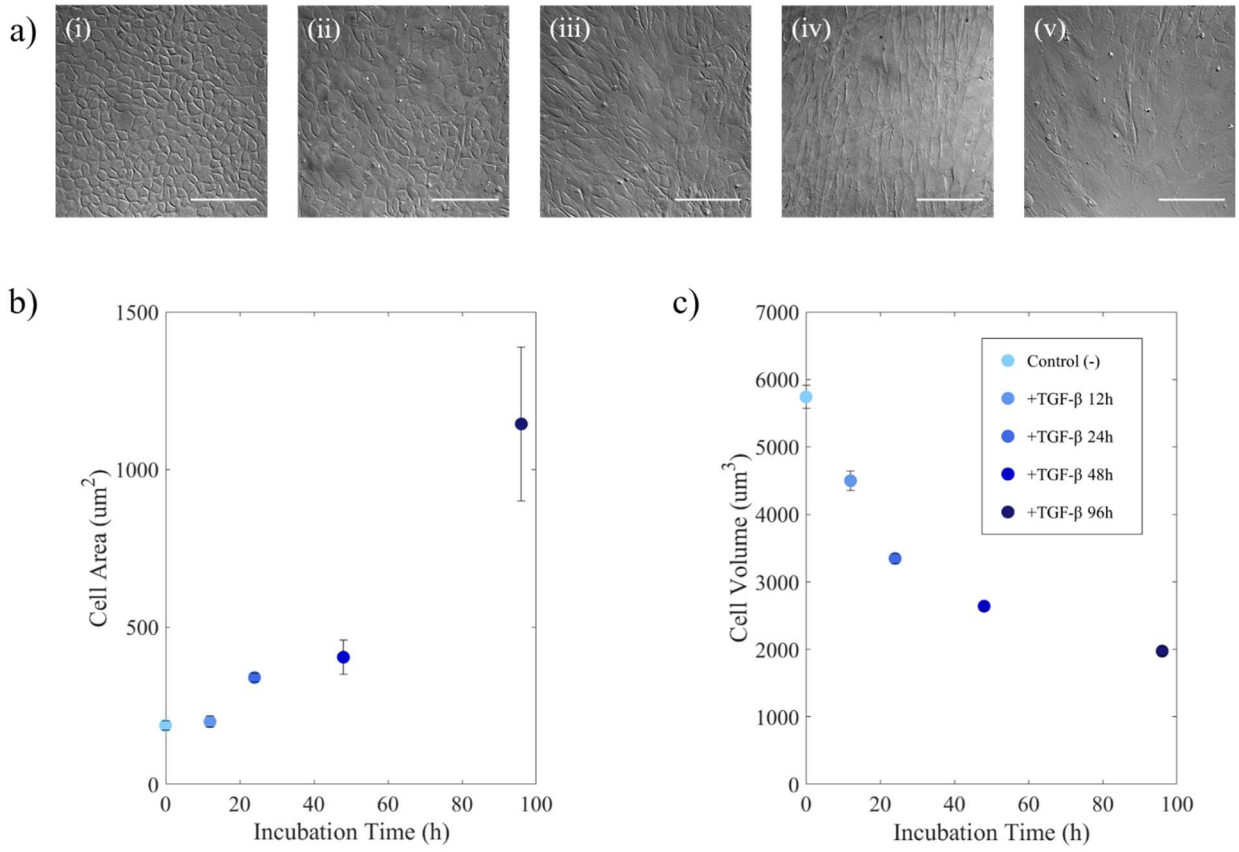

Figure 4-3: **As epithelial cells acquire more mesenchymal phenotype, cells elongate their morphologies and flatten. (a)** DIC images of NMuMG cells treated (i) without , or with 4ng/mL TGF-β1 for (ii) 12h, (iii) 24h, (iv) 48h, and (v) 96h. Scale bar, 100 μm. **(b & c)** Cell spread area (n=22-157) **(b)** and volume (n=9-14) **(c)** of individual NMuMG cells cultured in monolayers +/- 4ng/mL TGF-β1 (12h, 24h, 48h, & 96h).

Nuclei flatten as cells acquire more mesenchymal phenotype.

Previous work has shown that there is a tight relationships between cell moduli and cell and nuclear volumes.[145] To examine how nuclear mechanics change, we measured changes in nuclear volume during EMT. We observed that nuclei flatten with increasing exposure times to TGF-β1 (0h, 12h, 24h, 48h, and 96h). Nuclear volume decreased approximately 70% as they go through the transition (1591 ± 460 for non-TGF-β1-treated to 507 ± 55 μm^3 for 96h of TGF-β1-treatment) (Figure 4-4).

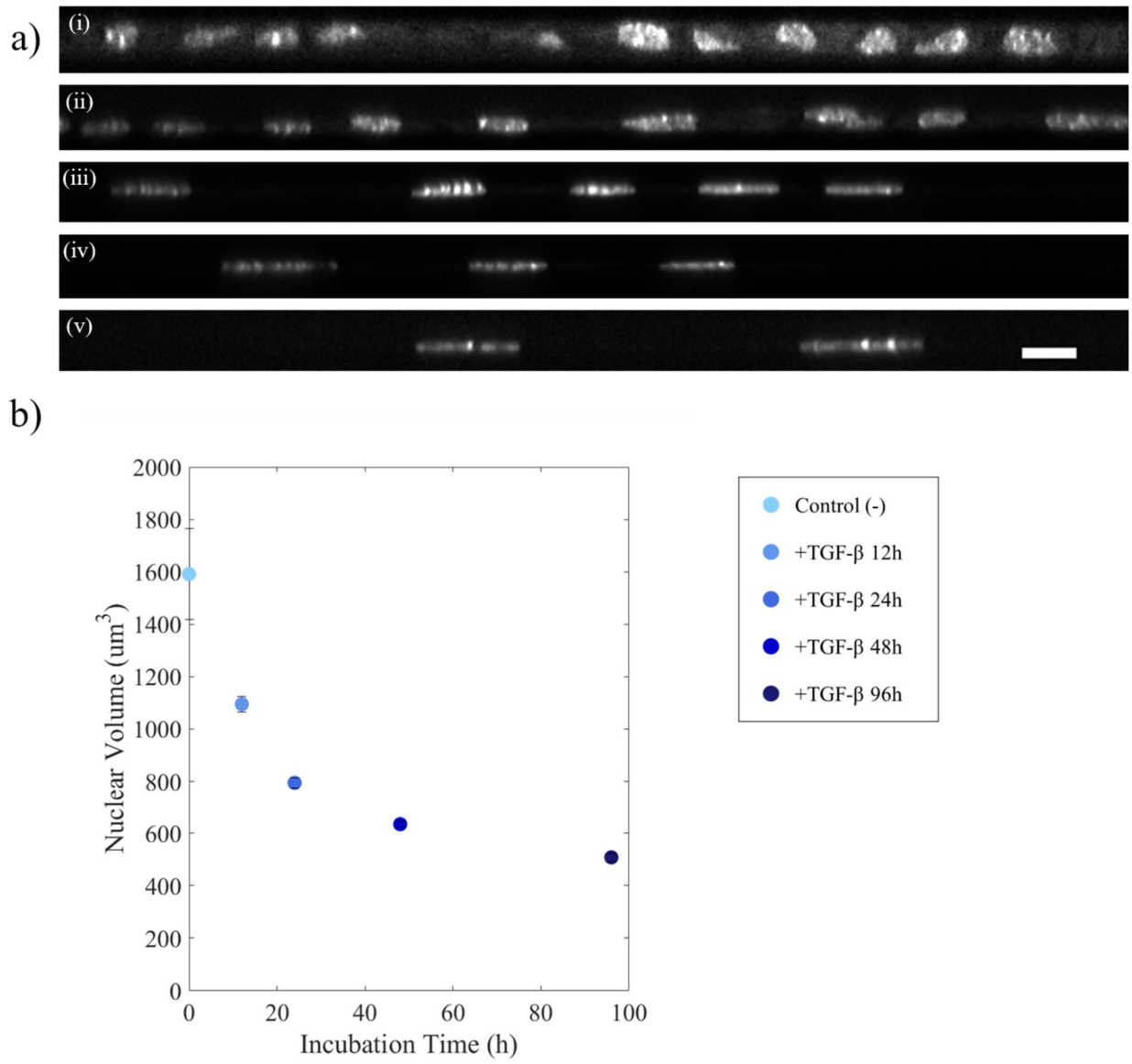

Figure 4-4: **Nuclei get compressed during EMT. (a)** Side views of DAPI-stained nuclei of fixed NMuMG cells treated (i) without, or with 4ng/mL TGF-β1 for (ii) 12h, (iii) 24h, (iv) 48h, and (v) 96h. Scale bar, 10 μm. **(b)** nuclear volume (n=9-14) of NMuMG cells of individual cells cultured in monolayers +/- 4ng/mL TGF-β1 (12h, 24h, 48h, & 96h) (n=9-14).

Epithelial cells elongate actin fibers as they become more mesenchymal cells.

Cellular traction forces are primarily generated by acto-myosin contractility, as such it has been observed that actin structures significantly reorganize to localize contractility along a particular axis and increase total contractile force.[146] Studying the properties of actin fibers in

fixed cells under different EMT states (i.e. TGF-β1 exposure times), we found that actin remodels into longer stress-fibers (Figure 4-5). Briefly, cells were fixed and F-actin was stained with fluorescently-conjugated phalloidin. Labelled fluorescent F-actin was detected using an open source software (details can be found in Materials and Methods). As discussed previously, during EMT actin fibers within a given cell elongate as cells become more uniaxial and polarized. On average, actin length increased roughly 4 times (2.54 ± 0.09 for non-TGF-β1-treated to 10.4 ± 0.7 μm for 96h of TGF-β1-treatment) (Figure 4-5).

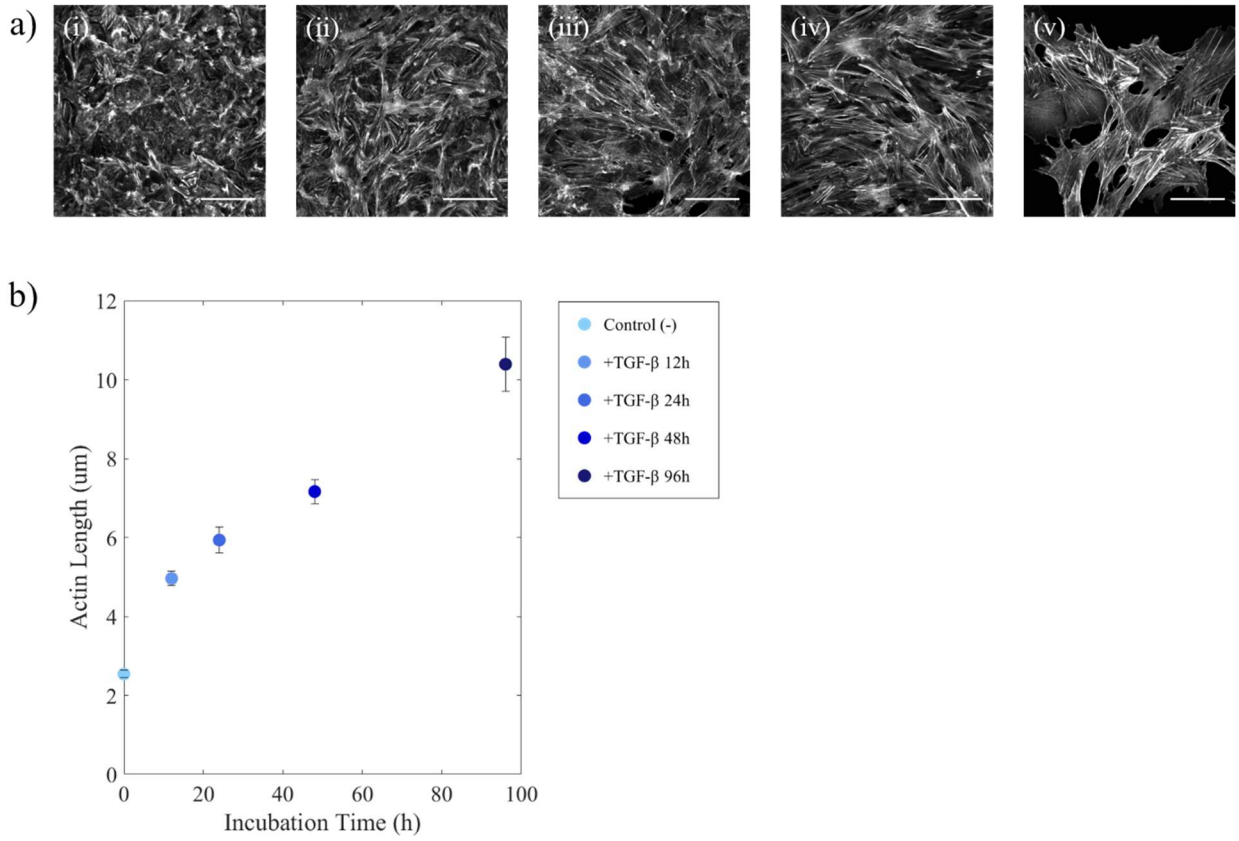

Figure 4-5: **As epithelial cells acquire more mesenchymal phenotype, cells reorganize actin cytoskeleton forming and elongating stress-fibers, applying larger stresses on the underlying substrates. (a)** Representative images of actin fibers of NMuMG cells without (i) or with TGF-β1 treatment for (ii) 12h, (iii) 24h, (iv) 48h, and (v) 96h stained with fluorescently labeled phalloidin. Scale bar, 50 μm. **(b)** F-actin length of NMuMG cells cultured in monolayers +/- 4ng/mL TGF-β1 (12h, 24h, 48h, & 96h) (n=656-4747).

Cells transition from slow diffusive movement to directed faster migration during EMT.

In principle, all the metrics discussed eventually impact the migratory changes during EMT. To capture these changes in motility, we tracked nuclei of NMuMG, which were stably transfected with H2B-mTurquoise. We quantified the mean squared displacement (MSD) of cells at these discrete stages, revealing changes in the motility of cells. In general, the MSD plot describes both the instantaneous speed (vertical position) at each time-lag, Tau, and the slope of the MSD describes the nature of the movement, where a slope of unity reflects diffusive random movement, and less or more than unity is sub-diffusive or directed movement. Examining the MSD during EMT, we see a pronounced increase in the motile speed as demonstrated by the vertical shift of the MSD as a function of TGF-β1 exposure time, shown in Figure 4-6. In later exposure times, we also see a transition from diffusive to a more directed ballistic movement as reflected by the increase in the MSD slope (1.13 for non-TGF-β1-treated to 1.50 for 96h TGF-β1-treatment).

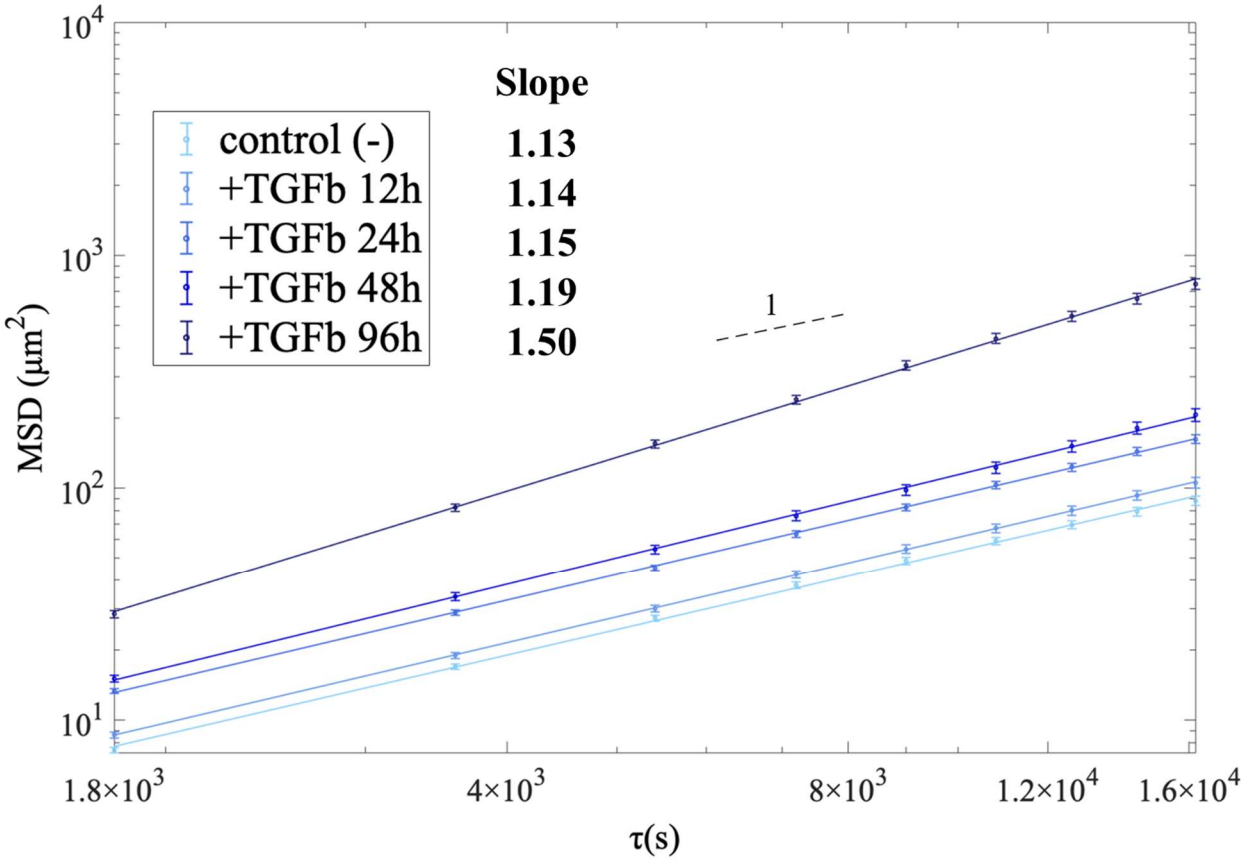

Figure 4-6: **Cell migration becomes faster and more directed during EMT.** MSD of individual nuclei of H2B-mTurquoise-transfected NMuMG cells in a monolayer sheet. Movement of cells -/+ TGF-β1 (12h, 24h, 48h, & 96h) are tracked every ~30 mins for ~4.5 hours. Linear slope of each curve is shown next to the legend. Dashed lines indicate a purely-diffusive line with a slope of 1. Bar indicates standard errors (n=214 to 903).

Cells change physical behaviours in an organized and coordinated manner.

To examine how all the observed changes influence each other, normalized values for each measured physical parameter were plotted together as shown in Figure 4-7. F-actin length increases significantly in the first 12-hours as shown in Figure 4-7, demonstrating that remodeling of actin into stress-fibers occurs initially as cells undergo EMT. As cells reorganize their actin fibers during EMT, cells also increase in forces and work. They apply larger forces and do more work on the substrate as longer actin fibers are being formed. Actin remodeling,

along with force and work changes, have several effects on the cells: cells increase in spread area and decrease in volume. This flattening of cells is accompanied by nuclear flattening. The compression of the nuclei is interconnected with the overall compression mechanics of the cell as a whole as shown in Figure 4-7 (cell and nuclear volumes are shown in pink square and diamond, respectively). This compression also occurs at earlier times in EMT; as cells get compressed, their moduli increase, ultimately becoming stiffer. Finally, all the observed biophysical changes lead to motility change, making cells move faster and in a more directed manner. These results suggest that all the physical parameters are highly regulated, and changes of these parameters occur in a highly organized manner. Interestingly, cell area is the slowest changing parameter; hence, it may not be the suitable parameter to be considered when biophysically quantifying EMT.

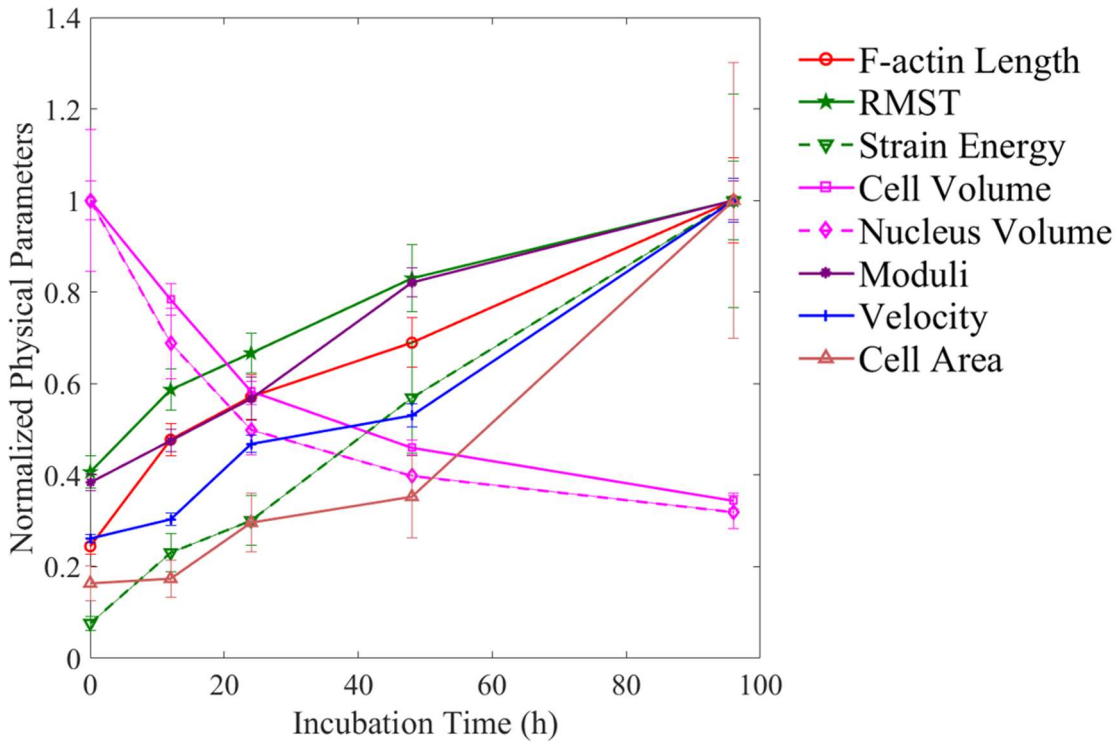

Figure 4-7: **Physical parameters are regulated during EMT.** Each quantified biomechanical parameter is normalized and plotted together in one plot. Individual parameters were measured using monolayer sheets of NMuMG cells +/- TGF-β1 (12h, 24h, 48h, & 96h) as described in previous sections. F-actin length, RMST, strain energy, moduli, and cell area are inversely proportional to the cell volume and nucleus volume. Bar indicates standard errors.

4.5 Materials and Methods

Preparation of PDMS Substrate.

Polydimethyl siloxane (PDMS) substrates for TFM were fabricated as described previously[123, 129]. In brief, PDMS components (Nusil 8100, Sylgard 184 curing agent) were mixed together at a given ratio to produce substrates with desired elastic moduli ranging from 0.3 kPa to 100 kPa. They were cured at 100°C, spin-coated with a monolayer of fiduciary fluorescent beads in the same PDMS mixture, cured again, functionalized with Sulfo-SANPAH (ProteoChem) and ligated with fibronectin (Sigma-Aldrich).

Cell Culture.

NMuMG cells (ATCC) were cultured in DMEM media supplemented with 5% FBS, 10 mM HEPES, 10 mg/ml insulin, 200mM L-glutamine, and 250ug/ml amphotericin B. For NMuMG expressing H2B-mTurquoise, 1 μg/ml of puromycin was added additionally.

NMuMG cells stably expressing the nuclear marker H2B-mTurquoise were generated using lentiviral transduction. To generate lentivirus, pLV-EF1a-H2B-mTurquoise-IRES-Puro[147] was transfected into 293FT cells using Lipofectamine 2000, along with the packaging plasmids pMDLg/pRRE, pRSV-rev, pCMV-VSVG, as described previously[148]. 48h later, the supernatant was collected, 0.22μm filtered, and virus concentrated using centrifugal filter units (100 kDa cutoff, Millipore, UFC910024). NMuMG cells, plated at 50% confluence, were infected with the concentrated virus in the presence of 4μg/ml Polybrene, and transduced were cells selected using 1μg/ml Puromycin (InvivoGen), starting 24h post infection. For EMT induction, NMuMG cells were incubated with TGF-β1 (4 ng/ml) for 12h, 24h, 48h, and 96h.

Immunofluorescence.

Cells were fixed with 4% paraformaldehyde in PBS and then blocked and permeabilized with a blocking buffer, PBS containing 10% FBS, 1% BSA, 0.1% Triton-X-100, and 0.01% sodium azide before being incubated for 30 mins with fluorophore-conjugated phalloidin (Acti-stain 670 phalloidin, Cytoskeleton) and DAPI (Sigma-Aldrich). At the end of staining, cells were mounted on the glass slide with mounting media, Prolong Diamond (ThermoFisher).

Traction Force Microscopy.

Contractile forces of single cells and monolayer cells on PDMS substrates were calculated as previously described[17, 149]. Briefly, cells were cultured on compliant PDMS substrates with

known Young's moduli, a thin PDMS top layer of embedded fiduciary fluorescent particles. Cells and fluorescent particles were imaged with a Leica TCS SP8 confocal microscope with 10x 0.4 NA air objective at a resolution of 0.28μm/pixel. The reference images of the particles were acquired at the end of the experiment by detaching the cells from the substrate surface.

Calculating Cellular Traction Stress and Strain Energy.

Cell-substrate traction stresses and strain energies were calculated as described previously for single cells[17] and monolayer cells[149]. Briefly, local displacements of the fiduciary particles were calculated by comparing the particle positions with cells on the substrate and reference particle positions without cells. From the particle displacement and known Young's moduli of the PDMS substrate, cellular contractile stresses were calculated. The strain energies were calculated by the previously described approach[17].

Imaging.

All imaging for TFM, F-actin staining, and nucleus tracking was performed either with a Leica TCS SP8 confocal microscope with 10x air objective (NA=0.4) and 63x oil objective (NA=1.4) or a Nikon A1 confocal microscope with 10x, 20x air objectives, and 60x oil objective (NA=0.45, 0.75, & 1.24 for 10x, 20x, & 60x respectively).

Cell Motility Imaging. Nuclei of H2B-mTurquoise-transfected cells were imaged with a Nikon A1 confocal microscope with 10x air objective (NA=0.45) at 0.50 μm/pixel resolution.

F-actin Imaging. To investigate how cells reorganize cytoskeletal structures during EMT, we imaged F-actin structures of fixed cells stained with fluorescently conjugated phalloidin. NMuMG cells were incubated with TGF-β1 for different durations (0h (-), 12h, 24h, 48h, and 96h) prior to staining; then cells were fixed and stained. Actin filament images were taken with a Nikon A1 confocal microscope with a 20x air objective at 0.19 μm/pixel resolution.

Cell Volume Imaging. Cells were stained with Cell Tracker CMFDA (ThermoFisher) and imaged with Leica SP8 confocal microscope with x63 oil objective (NA 1.4). z-stack images were taken with a slice size of 0.5 μm.

Nuclei Volume Imaging. Nuclei of NMuMG cells transfected with nucleus marker (see details in Cell Culture) were imaged using Leica SP8 confocal microscope with x63 oil objective (NA 1.4). z-stack images were recorded at 0.5 μm.

Fixed Nuclei Imaging. DAPI-stained nuclei of fixed cells were imaged with a Nikon confocal microscope with a 60x (NA 1.24) oil objective. z- stack imaging was performed. Each slice for z-stack was 0.27 μm thick.

Actin Filament Length and Cell Area Analysis. To analyze cell spread area and actin length, an open-access software and tool were used. Spread areas of the cells were quantified with cell profiler[150], an open source image analysis software developed by the Carpenter Lab[151]. To extract actin length, all the images were processed using Filament Sensor, a tool developed by Eltzner *et al*.[152]

Cell and Nuclei Volume.

Before volume calculations, the images were deconvolved using Iterative deconvolve 3D plug in in ImageJ[153]. After thresholding z-stack, using Voxel Counter plugin in Image J[153] the number of voxels for z-stack are extracted. By multiplying the number of voxels by the known voxel size, volumes were calculated.

Complex Shear Moduli of the cells. To quantify the mechanical change in EMT, we performed MTC on cells with various exposure times to TGF-β1 (0h, 12h, 24h, 48h, and 96h). MTC measurements were performed as described previously[144]. In brief, 4.5 μm diameter ferromagnetic beads (obtained from Jeff Fredberg, Harvard School for Public Health) were

coated with RGD peptide and attached to the cell. Magnetized beads were twisted, and bead motion was recorded with a confocal microscope (Leica, TCS SP8) at 1Hz. The complex shear moduli (G*) were calculated as described previously[144].

Cell Motility and Migration. To study collective behaviors of neighboring epithelial cells in monolayer sheet, we tracked nuclei of the cells undergoing EMT. NMuMG cells transfected with nuclear marker H2B-mTurquoise were cultured on 8.1 kPa PDMS substrate and fluorescent images of nuclei were imaged with a Nikon A1 confocal microscope. To quantify the motility at different time-points of EMT, nuclei of cells which have been incubated with TGF-β1 for different exposure times were imaged for ~4.5 hours at every ~30mins. The vector displacements of each nucleus between each time frame were calculated by in-house developed MATLAB code, and mean-squared displacements (MSD) of individual nuclei were generated.

4.6 Discussion

EMT is a biological process by which epithelial cells acquire migratory and invasive characteristics of mesenchymal cells. This acquisition of more mesenchymal characteristics is believed to promote translocation of cancer cells during metastatic progression of the disease. Many efforts have been made to characterize EMT biochemically and genetically such as molecular mechanisms, signalling pathways and changes in expressions levels of certain genes during EMT.[40-41, 132] In addition to the biological characterization of EMT, recent studies have measured changes in physical parameters to understand the underlying biophysical mechanism of EMT.[128-129, 136, 141] Although significant advancement has been made in studying EMT from biophysical perspectives, comparisons between the different biophysical parameters and overall understanding of biophysical changes during EMT are still missing. In this manuscript, we have broadly quantified diverse physical properties of the cells during EMT in the context of cancer

metastasis, focusing on changes in these physical parameters using an EMT-inducible cell line, NMuMG. While it is not possible for all data to be collected simultaneously, we are able to compare their average properties between different experiments using the robustness of the inducible transition, and mapping between experiments using time post TGF-β1 exposure, ultimately creating a composite picture of the mechanics of EMT.

To examine the physical response of EMT, we measured the contractility of NMuMG cells by increasing TGF-β1 exposure time. We find that cells in monolayers exert larger stresses and produce more work than isolated cells, demonstrating the essential cooperative nature of contractility in the monolayer. Cells undergo morphological changes during EMT; during this transition, cobblestone-shaped cells become more spread on the substrate. These morphological changes are accompanied by the rearrangement of cytoskeletal structures observed here by cells forming and elongating stress-fibers. These fibers allow them to pull and work harder on their underlying substrates and this reorganization appears to be an early event during EMT.

Interestingly, our MTC results show that shear moduli increase as epithelial cells go through the transition to become more mesenchymal. Cells became more resistant to the shear forces induced by twisting magnetic beads attached to the cell membrane, which indicates a stiffening of the cells. The moduli of the cells are highly influenced by cytoplasmic content and architectures; thus, the formation of long F-actin filaments observed may be the key contributor to this cell stiffening. The formation of long stress-fibers also affects cell morphology. As longer actin fibers are being formed, cells exhibit a more flattened morphology. We also found a similar compression behaviour in the nuclei of the cells, indicating that compression of cells and nuclei occur together. The cellular and nuclear thinning may allow cancer cells to travel through confined dense fiber matrices during metastasis. Previous reports showed that volume change of

nuclei is accompanied by volume change of the cells, and these volume changes are due to transport of water in and out of the cells.[145] How cell volume and nuclear volume are regulated and the role of water content in EMT are of great importance. Future experiments will define the role of efflux of water in mechanical changes of cells undergoing EMT. Finally, the motility changes follow the contractility and structural changes, indicating that all the biophysical changes observed here are contributing to the shift in migratory behaviours of the cells in EMT, driving enhanced motility of mesenchymal cells. In summary, we find that actin remodeling happens initially, increasing contractility and work, and resulting in cell and nuclei flattening, which in turn leads to increased moduli and faster ballistic motility characteristic of mesenchymal cells during cancer metastasis. Our work highlights the importance of studying EMT from a physical and mechanical point of view while taking different physical parameters into account.

Given the nature of the epithelial cells to form strong cell-cell adhesion with neighboring cells, communication with their neighbors is crucial to function and meet the needs of the cohort. To capture the multi-cellular nature of epithelial cells, we examined changes in physical parameters during EMT in monolayer sheets, finding that sheets of epithelial cells undergo physical and mechanical changes in an organized manner in transitioning to become more mesenchymal. During EMT, it is believed that the collection of cells lose their coherence and begin to function as more isolated units.[41] This means that cooperativity must change as these collective behaviors change during the transition. However, how neighboring epithelial cells work in harmony with each other and how they change this cooperative behavior as they go through EMT are not well understood. Future work focusing on cell-cell interactions, such as studying cadherins and intercellular stresses, will answer these questions.

Acknowledgments

The authors thank Denis Flipo for technical assistance, Adele Khavari for tracking code, Ramaswamy R. Krishnan, and Sumati Ram-Mohan for TFM code, Luv Srivastava for helpful discussions. AJE acknowledges support from NSERC RGPIN/05843-2014, FRQNT 191119, and CCS Grant #703930, CIHR Grant # 143327, NSERC EQPEQ/472339-2015. HY was supported by FRQS and FRQNT.

4.7 References

Butler, J. P., Tolic-Norrelykke, I. M., Fabry, B., & Fredberg, J. J. (2002). Traction fields, moments, and strain energy that cells exert on their surroundings. *Am J Physiol Cell Physiol, 282*(3), C595-605.

Carpenter, A. E., Jones, T. R., Lamprecht, M. R., Clarke, C., Kang, I. H., Friman, O., . . . Sabatini, D. M. (2006). CellProfiler: image analysis software for identifying and quantifying cell phenotypes. *Genome Biology, 7*(10), R100.

Chen, Y.-Q., Lan, H.-Y., Wu, Y.-C., Yang, W.-H., Chiou, A., & Yang, M.-H. (2018). Epithelial-mesenchymal transition softens head and neck cancer cells to facilitate migration in 3D environments. *Journal of Cellular and Molecular Medicine, 22*(8), 3837-3846.

Efremov, Y. M., Wang, W.-H., Hardy, S. D., Geahlen, R. L., & Raman, A. (2017). Measuring nanoscale viscoelastic parameters of cells directly from AFM force-displacement curves. *Scientific Reports, 7*(1), 1541.

Eltzner, B., Wollnik, C., Gottschlich, C., Huckemann, S., & Rehfeldt, F. (2015). The Filament Sensor for Near Real-Time Detection of Cytoskeletal Fiber Structures. *PLOS ONE, 10*(5), e0126346.

Fabry, B., Maksym, G. N., Butler, J. P., Glogauer, M., Navajas, D., & Fredberg, J. J. (2001). Scaling the Microrheology of Living Cells. *Physical Review Letters, 87*(14), 148102.

Felipe Lima, J., Nofech-Mozes, S., Bayani, J., & Bartlett, J. M. S. (2016). EMT in Breast Carcinoma—A Review. *Journal of Clinical Medicine, 5*(7), 65.

Guck, J., Schinkinger, S., Lincoln, B., Wottawah, F., Ebert, S., Romeyke, M., . . . Bilby, C. (2005). Optical Deformability as an Inherent Cell Marker for Testing Malignant Transformation and Metastatic Competence. *Biophysical Journal, 88*(5), 3689-3698.

Guo, M., Ehrlicher, A. J., Jensen, M. H., Renz, M., Moore, J. R., Goldman, R. D., . . . Weitz, D. A. (2014). Probing the stochastic, motor-driven properties of the cytoplasm using force spectrum microscopy. *Cell, 158*(4), 822-832.

Guo, M., Pegoraro, A. F., Mao, A., Zhou, E. H., Arany, P. R., Han, Y., . . . Weitz, D. A. (2017). Cell volume change through water efflux impacts cell stiffness and stem cell fate. *Proceedings of the National Academy of Sciences, 114*(41), E8618-E8627.

Hayer, A., Shao, L., Chung, M., Joubert, L.-M., Yang, H. W., Tsai, F.-C., . . . Meyer, T. (2016). Engulfed cadherin fingers are polarized junctional structures between collectively migrating endothelial cells. *Nature cell biology, 18*, 1311.

Haynes, J., Srivastava, J., Madson, N., Wittmann, T., & Barber, D. L. (2011). Dynamic actin remodeling during epithelial–mesenchymal transition depends on increased moesin expression. *Molecular Biology of the Cell, 22*(24), 4750-4764.

ImageJ. Retrieved from https://imagej.net

Institute, B. CellProfiler cell image analysis software. Retrieved from https://cellprofiler.org/

Iwano, M., Plieth, D., Danoff, T. M., Xue, C., Okada, H., & Neilson, E. G. (2002). Evidence that fibroblasts derive from epithelium during tissue fibrosis. *J Clin Invest, 110*(3), 341-350.

Kalluri, R., & Weinberg, R. A. (2009). The basics of epithelial-mesenchymal transition. *The Journal of Clinical Investigation, 119*(6), 1420-1428.

Kim, D. H., Xing, T., Yang, Z., Dudek, R., Lu, Q., & Chen, Y.-H. (2017). Epithelial Mesenchymal Transition in Embryonic Development, Tissue Repair and Cancer: A Comprehensive Overview. *Journal of Clinical Medicine, 7*(1), 1.

Kondo, M., Cubillo, E., Tobiume, K., Shirakihara, T., Fukuda, N., Suzuki, H., . . . Miyazono, K. (2004). A role for Id in the regulation of TGF-β-induced epithelial–mesenchymal transdifferentiation. *Cell Death & Differentiation, 11*(10), 1092-1101.

Kumar, S., Das, A., & Sen, S. (2014). Extracellular matrix density promotes EMT by weakening cell-cell adhesions. *Molecular bioSystems, 10*(4), 838-850.

Lamouille, S., Xu, J., & Derynck, R. (2014). Molecular mechanisms of epithelial–mesenchymal transition. *Nat Rev Mol Cell Biol, 15*(3), 178-196.

Lekka, M., Laidler, P., Gil, D., Lekki, J., Stachura, Z., & Hrynkiewicz, A. Z. (1999). Elasticity of normal and cancerous human bladder cells studied by scanning force microscopy. *European Biophysics Journal, 28*(4), 312-316.

Morikawa, M., Derynck, R., & Miyazono, K. (2016). TGF-beta and the TGF-beta Family: Context-Dependent Roles in Cell and Tissue Physiology. *Cold Spring Harb Perspect Biol, 8*(5).

Nalluri, S. M., O'connor, J. W., Virgi, G. A., Stewart, S. E., Ye, D., & Gomez, E. W. (2018). TGFbeta1-induced expression of caldesmon mediates epithelial-mesenchymal transition. *Cytoskeleton (Hoboken), 75*(5), 201-212.

Neve, R. M., Chin, K., Fridlyand, J., Yeh, J., Baehner, F. L., Fevr, T., . . . Gray, J. W. (2006). A collection of breast cancer cell lines for the study of functionally distinct cancer subtypes. *Cancer cell, 10*(6), 515-527.

Oakes, P. W., Banerjee, S., Marchetti, M. C., & Gardel, M. L. (2014). Geometry regulates traction stresses in adherent cells. *Biophysical Journal, 107*(4), 825-833.

Radisky, E. S., & Radisky, D. C. (2010). Matrix Metalloproteinase-Induced Epithelial-Mesenchymal Transition in Breast Cancer. *Journal of Mammary Gland Biology and Neoplasia, 15*(2), 201-212.

Roche, J. (2018). The Epithelial-to-Mesenchymal Transition in Cancer. *Cancers, 10*(2), 52.

Schneider, D., Baronsky, T., Pietuch, A., Rother, J., Oelkers, M., Fichtner, D., . . . Janshoff, A. (2013). Tension Monitoring during Epithelial-to-Mesenchymal Transition Links the Switch of Phenotype to Expression of Moesin and Cadherins in NMuMG Cells. *PLOS ONE, 8*(12), e80068.

Singla, M., Kumar, A., Bal, A., Sarkar, S., & Bhattacharyya, S. (2018). Epithelial to mesenchymal transition induces stem cell like phenotype in renal cell carcinoma cells. *Cancer cell international, 18*, 57-57.

Taylor, M. A., Parvani, J. G., & Schiemann, W. P. (2010). The Pathophysiology of Epithelial-Mesenchymal Transition Induced by Transforming Growth Factor-β in Normal and Malignant Mammary Epithelial Cells. *Journal of Mammary Gland Biology and Neoplasia, 15*(2), 169-190.

Trepat, X., Wasserman, M. R., Angelini, T. E., Millet, E., Weitz, D. A., Butler, J. P., & Fredberg, J. J. (2009). Physical forces during collective cell migration. *Nature Physics, 5*, 426.

Vuoriluoto, K., Haugen, H., Kiviluoto, S., Mpindi, J. P., Nevo, J., Gjerdrum, C., . . . Ivaska, J. (2011). Vimentin regulates EMT induction by Slug and oncogenic H-Ras and migration by governing Axl expression in breast cancer. *Oncogene, 30*(12), 1436-1448.

Wang, Y., & Zhou, B. P. (2013). Epithelial-mesenchymal Transition---A Hallmark of Breast Cancer Metastasis. *Cancer hallmarks, 1*(1), 38-49.

Yang, H. W., Chung, M., Kudo, T., & Meyer, T. (2017). Competing memories of mitogen and p53 signalling control cell-cycle entry. *Nature, 549*(7672), 404-408.

Yoshie, H., Koushki, N., Kaviani, R., Tabatabaei, M., Rajendran, K., Dang, Q., . . . Ehrlicher, A. J. (2018). Traction Force Screening Enabled by Compliant PDMS Elastomers. *Biophysical Journal, 114*(9), 2194-2199.

Yoshie, H., Koushki, N., Molter, C., Siegel, P. M., Krishnan, R., & Ehrlicher, A. J. (2019). High Throughput Traction Force Microscopy Using PDMS Reveals Dose-Dependent Effects of Transforming Growth Factor-β on the Epithelial-to-Mesenchymal Transition. *JoVE*(148), e59364.

Chapter 5 : General Discussion & Conclusion

In this work, I measured cellular traction stresses using a method called Traction Force Microscopy. Cellular traction stresses are the contractile stresses exerted by crawling adherent cells on to their environment when cells translocate across the substrate surface to which they are adhered. A wealth of research is revealing that these contractile forces are indicative of the cell state, and in cancer, can reveal the metastatic state of the cell.[36, 128]

I developed a traction force assay utilizing soft silicone materials (PDMS), offering a more stable assay than the more commonly utilized hydrogel-based assays. Soft PDMS enables the assembly of a plate in 96-well format, facilitating the performance of high throughput screening to study the dose-dependent contractile response of ASM cells with pharmaceutically relevant compounds. These results help transition TFM from a quantitative but slow lab approach to a deployable tool utilized to study different biological systems. This tool can also be utilized as a force screening assay, enabling clinicians and researchers to screen for malfunctioning cells based on the levels of contractile forces.

Utilizing the high-throughput silicone substrate-based assay, I investigated how epithelial cells change their physical behaviors in the breast cancer model, an EMT-inducible mammary gland cell line, NMuMG. Utilizing this system, I studied changes in contractile forces and total work done by single cells and monolayer cells. I observed significant increases in both contractile stresses and strain energies (2.5-fold and 13-fold, respectively) as cells became more mesenchymal. The increased contractile forces may explain the more migratory and invasive behaviors of mesenchymal cells; as epithelial cells transition to become more mesenchymal cells, they apply larger contractile forces on their environment to move forward and this stronger pulling allows them to migrate more easily in the body. This increase in contractility must also

be reflected in the underlying cytoskeletal structure, which does the work for cell movement: cells reorganize their actin fibers to transmit forces across the body, enabling to pull harder on the surfaces to which they are adhered, facilitating their migration. The increased tension further explains the increased spreading of the cells we observed during EMT. Furthermore, I observed a reduction in cell volume (70% reduction); indicating flattening of the cells during EMT. This "cell-thinning" and formation of F-actin bundles could potentially explain the increased complex shear moduli of TGF-β-treated cells (2.5-fold) we observed with MTC measurements. To investigate the additional effect of cell compression observed, I studied how morphology of the nucleus changes during EMT. Here, we observed the nucleus to be more spread in 2D and 3D upon TGF-β treatment. Interestingly but not surprisingly, flattening of the nucleus and flattening of the cell happen in a similar manner (approximately 70% volume reduction in both cases), and occur almost simultaneously. This reduction in nuclear volume may allow cells to move more easily through confined spaces between dense fiber mesh and during the processes of intravasation and extravasation. These observations suggest a mechanical role of EMT with epithelial cancer cells in which they become stronger, stiffer, and more invasive mesenchymal cells, ultimately increasing their motility in breast cancer progression. These mechanical changes are, therefore, key to the research of how cells become invasive. Future studies can clarify the role of nuclear volume regulation in cancer metastasis, and any impact on gene and protein regulation.

To understand how the physical changes influence cell motility, namely increased contractility, actin remodeling, cell stiffening, and flattening, I studied changes in cell motility in confluent cell monolayers by tracking nuclei of the cells with TGF-β treatment. Here, I found a transition in cell migratory behavior from slow diffusive motion to faster persistent movement

for cell monolayers during EMT. Together, these results suggest that actin remodeling of the epithelial cells occurs initially affecting cell morphology and contractility, making cells become more spread and apply larger contractile forces, further driving faster and more directed cell movement.

These findings highlight the importance of the biophysical research of cancer. By quantifying and comparing the various physical parameters in EMT and cancer, we can understand how these pieces function together to produce invasive cells, and this allows us to design targeted treatments to modify the behavior of metastatic cells. Targeting alterations of cellular activity in physical contexts, such as motility, cell-cell adhesions, cellular moduli, actin architecture, contractile forces, and total work, may provide an additional source of new therapeutic and pharmacological tools to slow down or inhibit the metastatic progression of the disease.

Although I primarily focused on studying physical changes in EMT, focusing on the aspects of cancer metastasis, these assays and insights can be utilized to study virtually any other physiological and pathological systems where mechanics play a role. I believe that this thesis, and continued work at the interface of biology and engineering, may yield tools for researchers, pathologists, and clinicians to investigate challenging questions in a high-throughput manner. Using the knowledge gained from this study, researchers can begin to develop a better understanding of the physical nature of cancer, which may lead to improved therapies for the treatment of the disease.

Appendix

Computation of the displacement field

To calculate the cell-induced deformation of the substrate, images of fluorescent particles embedded in soft PDMS substrates with and without cells are compared. To calculate the displacement of these particles, the analysis looks for pattern matches between the images to determine how one region has moved with respect to another. This is done by applying small displacement shifts of the image and observing if it matches the original, allowing us to calculate the cross-correlation of the images. When the maximum match between images is found, this has the highest cross-correlation value, and the values for this translation are assigned as the displacements. This process is repeated in small windows throughout the sequence of images to determine the local displacements. Images are first corrected for drifts by the same pattern matching algorithm described above, by finding the maximum cross-correlation between the two images and aligning the images.[17] From these displacements and the knowledge of the substrate stiffness, we calculate traction stresses that cells apply on the underlying substrate.

Computation of the traction field

To overcome more computationally intensive analysis originally introduced by Dembo and Wang [154], Butler *et al.*[17] introduced Fourier Transform Traction Cytometry (FTTC) approach. In FTTC, computations of traction forces are done in Fourier space. In Fourier space, the displacement field, given by convolution (Equation 1) of the tractions with Green's function (Equation 2) becomes a simple product of the two (Equation 3).[17] To calculate tractions from the calculated particle displacement, displacement field is transformed into Fourier space. This transformed displacement is then multiplied by Fourier transformed matrix (Equation 4) to

obtain the traction in Fourier space. Finally, the calculated traction is reverse transformed into real space.[17]

Equations shown below are adapted from Butler *et al.*[17].

Equation 1:

$\vec{u}(\vec{r}) = K \otimes \vec{T} = \int K(\vec{r} - \vec{r}')T(\vec{r}')d\vec{r}'$

$\vec{u}(\vec{r})$: displacement vector at a point $\vec{r}'$;

K: Kernal;

$\otimes$: integration over $d\vec{r}'$;

$T(\vec{r}')$: traction vector at $\vec{r}'$;

Equation 2:

$K(r) = \frac{A}{r^3}\begin{bmatrix}(1-v)r^2 + vx^2 & vxy \\ vxy & (1-v)r^2 + vy^2\end{bmatrix}$

$A = (1 + v)/\pi E$

v: Poisson's ratio

E: Young's modulus

Equation 3:

$\vec{\tilde{u}}(\vec{k}) = \tilde{K}(\vec{k})\vec{\tilde{T}}(\vec{k})$

~: Fourier transform with wave vector $\vec{k}$;

$\vec{k}$: wave vector in Fourier space;

Equation 4:

$\tilde{K}(\vec{k}) = A\frac{2\pi}{k^3}\begin{bmatrix}(1-v)k^2 + vk_y^2 & vk_xk_y \\ vk_xk_y & (1-v)k^2 + vk_x^2\end{bmatrix}$

References

1. Lauffenburger, D. A.; Horwitz, A. F., Cell Migration: A Physically Integrated Molecular Process. *Cell* **1996,** *84* (3), 359-369.

2. Kurosaka, S.; Kashina, A., Cell biology of embryonic migration. *Birth defects research. Part C, Embryo today : reviews* **2008,** *84* (2), 102-122.

3. Bray, D., *Cell movements : from molecules to motility*. 2nd ed. ed.; Garland Pub.: New York, 2001.

4. Stuelten, C. H.; Parent, C. A.; Montell, D. J., Cell motility in cancer invasion and metastasis: insights from simple model organisms. *Nature Reviews Cancer* **2018,** *18* (5), 296-312.

5. Alberts, B., *Molecular biology of the cell*. Sixth edition. ed.; Garland Science, Taylor and Francis Group: New York, NY, 2015.

6. Ananthakrishnan, R.; Ehrlicher, A., The Forces Behind Cell Movement. *International Journal of Biological Sciences* **2007,** *3* (5), 303-317.

7. Pollard, T. D.; Borisy, G. G., Cellular Motility Driven by Assembly and Disassembly of Actin Filaments. *Cell* **2003,** *112* (4), 453-465.

8. Welch, M. D.; Mullins, R. D., Cellular Control of Actin Nucleation. *Annual Review of Cell and Developmental Biology* **2002,** *18* (1), 247-288.

9. Pollard, T. D.; Cooper, J. A., Actin, a central player in cell shape and movement. *Science (New York, N.Y.)* **2009,** *326* (5957), 1208-1212.

10. Burridge, K.; Chrzanowska-Wodnicka, M., Focal adhesions, contractility, and signaling. *Annu Rev Cell Dev Biol* **1996,** *12*, 463-518.

11. Mousavi, S. J.; Doweidar, M. H., Role of Mechanical Cues in Cell Differentiation and Proliferation: A 3D Numerical Model. *PloS one* **2015,** *10* (5), e0124529-e0124529.

12. Brugués, A.; Anon, E.; Conte, V.; Veldhuis, J. H.; Gupta, M.; Colombelli, J.; Muñoz, J. J.; Brodland, G. W.; Ladoux, B.; Trepat, X., Forces driving epithelial wound healing. *Nature physics* **2014,** *10* (9), 683-690.

13. Fournier, M. F.; Sauser, R.; Ambrosi, D.; Meister, J.-J.; Verkhovsky, A. B., Force transmission in migrating cells. *The Journal of Cell Biology* **2010,** *188* (2), 287-297.

14. Harris, A.; Wild, P.; Stopak, D., Silicone rubber substrata: a new wrinkle in the study of cell locomotion. *Science* **1980,** *208* (4440), 177-179.

15. Zündel, M.; Ehret, A. E.; Mazza, E., Factors influencing the determination of cell traction forces. *PLOS ONE* **2017,** *12* (2), e0172927.

16. Schwarz, U. S.; Soiné, J. R. D., Traction force microscopy on soft elastic substrates: A guide to recent computational advances. *Biochimica et Biophysica Acta (BBA) - Molecular Cell Research* **2015,** *1853* (11, Part B), 3095-3104.

17. Butler, J. P.; Tolic-Norrelykke, I. M.; Fabry, B.; Fredberg, J. J., Traction fields, moments, and strain energy that cells exert on their surroundings. *Am J Physiol Cell Physiol* **2002,** *282* (3), C595-605.

18. Dembo, M.; Wang, Y.-L., Stresses at the Cell-to-Substrate Interface during Locomotion of Fibroblasts. *Biophysical Journal* **1999,** *76* (4), 2307-2316.

19. Pelham, R. J., Jr.; Wang, Y. l., Cell locomotion and focal adhesions are regulated by substrate flexibility. *Proceedings of the National Academy of Sciences of the United States of America* **1997,** *94* (25), 13661-13665.

20. Yeung, T.; Georges, P. C.; Flanagan, L. A.; Marg, B.; Ortiz, M.; Funaki, M.; Zahir, N.; Ming, W.; Weaver, V.; Janmey, P. A., Effects of substrate stiffness on cell morphology, cytoskeletal structure, and adhesion. *Cell Motility and the Cytoskeleton* **2005,** *60* (1), 24-34.

21. Mierke, C. T.; Institute of, P., Physics of cancer. Volume 1, Interplay between tumor biology, inflammation and cell mechanics. Second edition. ed.; IOP Publishing: Bristol [England] (Temple Circus, Temple Way, Bristol BS1 6HG, UK), 2018.

22. Janmey, P. A.; Miller, R. T., Mechanisms of mechanical signaling in development and disease. *Journal of cell science* **2011,** *124* (Pt 1), 9-18.

23. Ehrlicher, A. J.; Krishnan, R.; Guo, M.; Bidan, C. M.; Weitz, D. A.; Pollak, M. R., Alpha-actinin binding kinetics modulate cellular dynamics and force generation. *Proceedings of the National Academy of Sciences of the United States of America* **2015,** *112* (21), 6619-24.

24. An, S. S.; Fabry, B.; Trepat, X.; Wang, N.; Fredberg, J. J., Do biophysical properties of the airway smooth muscle in culture predict airway hyperresponsiveness? *American journal of respiratory cell and molecular biology* **2006,** *35* (1), 55-64.

25. Black, J. L.; Johnson, P. R., Airway smooth muscle in asthma. *Respirology (Carlton, Vic.)* **1996,** *1* (3), 153-8.

26. Fredberg Jeffrey, J. Bronchospasm and its biophysical basis in airway smooth muscle *respiratory research* [Online], 2004, p. 2. WorldCat.org.

27. JOHNSON, P. R. A.; ROTH, M.; TAMM, M.; HUGHES, M.; GE, Q.; KING, G.; BURGESS, J. K.; BLACK, J. L., Airway Smooth Muscle Cell Proliferation Is Increased in Asthma. *American Journal of Respiratory and Critical Care Medicine* **2001,** *164* (3), 474-477.

28. Wang, Y.; Lu, Y.; Luo, M.; Shi, X.; Pan, Y.; Zeng, H.; Deng, L., Evaluation of pharmacological relaxation effect of the natural product naringin on in vitro cultured airway smooth muscle cells and in vivo ovalbumin-induced asthma Balb/c mice. *Biomed Rep* **2016,** *5* (6), 715-722.

29. Barnes, P. J., Drugs for asthma. *Br J Pharmacol* **2006,** *147 Suppl 1* (Suppl 1), S297-S303.

30. Rabe, K. F.; Schmidt, D. T., Pharmacological treatment of asthma today. *European Respiratory Journal* **2001,** *18* (34 suppl), 34s-40s.

31. Waldeck, B., β-Adrenoceptor agonists and asthma—100 years of development. *European Journal of Pharmacology* **2002,** *445* (1), 1-12.

32. Chung, K. F., Airway smooth muscle in asthma and COPD : biology and pharmacology. John Wiley & Sons: Chichester, 2008.

33. Xu, W.; Mezencev, R.; Kim, B.; Wang, L.; McDonald, J.; Sulchek, T., Cell Stiffness Is a Biomarker of the Metastatic Potential of Ovarian Cancer Cells. *PLOS ONE* **2012,** *7* (10), e46609.

34. Swaminathan, V.; Mythreye, K.; O'Brien, E. T.; Berchuck, A.; Blobe, G. C.; Superfine, R., Mechanical Stiffness Grades Metastatic Potential in Patient Tumor Cells and in Cancer Cell Lines. *Cancer Research* **2011,** *71* (15), 5075-5080.

35. Li, Z.; Persson, H.; Adolfsson, K.; Abariute, L.; Borgstrom, M. T.; Hessman, D.; Astrom, K.; Oredsson, S.; Prinz, C. N., Cellular traction forces: a useful parameter in cancer research. *Nanoscale* **2017,** *9* (48), 19039-19044.

36. Casey, M. K.-R.; Joseph, P. C.; Cynthia, A. R.-K. Cellular Traction Stresses Increase with Increasing Metastatic Potential *PLOS ONE* [Online], 2012. WorldCat.org.

37. Kalluri, R.; Weinberg, R. A., The basics of epithelial-mesenchymal transition. *The Journal of Clinical Investigation* **2009,** *119* (6), 1420-1428.

38. Chitty, J. L.; Filipe, E. C.; Lucas, M. C.; Herrmann, D.; Cox, T. R.; Timpson, P., Recent advances in understanding the complexities of metastasis. *F1000Research* **2018,** *7*, F1000 Faculty Rev-1169.

39. Kalluri, R., EMT: When epithelial cells decide to become mesenchymal-like cells. *The Journal of Clinical Investigation* **2009,** *119* (6), 1417-1419.

40. Felipe Lima, J.; Nofech-Mozes, S.; Bayani, J.; Bartlett, J. M. S., EMT in Breast Carcinoma—A Review. *Journal of Clinical Medicine* **2016,** *5* (7), 65.

41. Lamouille, S.; Xu, J.; Derynck, R., Molecular mechanisms of epithelial–mesenchymal transition. *Nat Rev Mol Cell Biol* **2014,** *15* (3), 178-196.

42. Huang, R. Y.; Guilford, P.; Thiery, J. P., Early events in cell adhesion and polarity during epithelial-mesenchymal transition. *Journal of cell science* **2012,** *125* (Pt 19), 4417-22.

43. Yilmaz, M.; Christofori, G., EMT, the cytoskeleton, and cancer cell invasion. *Cancer and Metastasis Reviews* **2009,** *28* (1-2), 15-33.

44. Bax, N. A. M.; Pijnappels, D. l. A.; van Oorschot, A. A. M.; Winter, E. M.; de Vries, A. A. F.; van Tuyn, J.; Braun, J.; Maas, S.; Schalij, M. J.; Atsma, D. E.; Goumans, M.-J.; Gittenberger-de Groot, A. C., Epithelial-to-mesenchymal transformation alters electrical conductivity of human epicardial cells. *Journal of Cellular and Molecular Medicine* **2011,** *15* (12), 2675-2683.

45. Haynes, J.; Srivastava, J.; Madson, N.; Wittmann, T.; Barber, D. L., Dynamic actin remodeling during epithelial–mesenchymal transition depends on increased moesin expression. *Molecular Biology of the Cell* **2011,** *22* (24), 4750-4764.

46. Vuoriluoto, K.; Haugen, H.; Kiviluoto, S.; Mpindi, J. P.; Nevo, J.; Gjerdrum, C.; Tiron, C.; Lorens, J. B.; Ivaska, J., Vimentin regulates EMT induction by Slug and oncogenic H-Ras and migration by governing Axl expression in breast cancer. *Oncogene* **2011,** *30* (12), 1436-48.

47. Neve, R. M.; Chin, K.; Fridlyand, J.; Yeh, J.; Baehner, F. L.; Fevr, T.; Clark, L.; Bayani, N.; Coppe, J. P.; Tong, F.; Speed, T.; Spellman, P. T.; DeVries, S.; Lapuk, A.; Wang, N. J.; Kuo, W. L.; Stilwell, J. L.; Pinkel, D.; Albertson, D. G.; Waldman, F. M.; McCormick, F.; Dickson, R. B.; Johnson, M. D.; Lippman, M.; Ethier, S.; Gazdar, A.; Gray, J. W., A collection of breast cancer cell lines for the study of functionally distinct cancer subtypes. *Cancer cell* **2006,** *10* (6), 515-27.

48. Massagué, J., TGFb signalling in context. *Nature reviews. Molecular cell biology* **2012,** *13* (10), 616-30.

49. Taylor, M. A.; Parvani, J. G.; Schiemann, W. P., The Pathophysiology of Epithelial-Mesenchymal Transition Induced by Transforming Growth Factor-β in Normal and Malignant Mammary Epithelial Cells. *Journal of Mammary Gland Biology and Neoplasia* **2010,** *15* (2), 169-190.

50. Micalizzi, D. S.; Ford, H. L., Epithelial–mesenchymal transition in development and cancer. *Future Oncology* **2009,** *5* (8), 1129-1143.

51. Bryan, S.; Masoud, H.; Weir, H. K.; Woods, R.; Lockwood, G.; Smith, L.; Brierley, J.; Gospodarowicz, M.; Badets, N., Cancer in Canada: Stage at diagnosis. *Health reports* **2018,** *29* (12), 21-25.

52. Holliday, D. L.; Speirs, V., Choosing the right cell line for breast cancer research. *Breast cancer research : BCR* **2011,** *13* (4), 215.

53. Yersal, O.; Barutca, S., Biological subtypes of breast cancer: Prognostic and therapeutic implications. *World Journal of Clinical Oncology* **2014,** *5* (3), 412-424.

54. Sorlie, T.; Perou, C. M.; Tibshirani, R.; Aas, T.; Geisler, S.; Johnsen, H.; Hastie, T.; Eisen, M. B.; van de Rijn, M.; Jeffrey, S. S.; Thorsen, T.; Quist, H.; Matese, J. C.; Brown, P. O.; Botstein, D.; Lonning, P. E.; Borresen-Dale, A. L., Gene expression patterns of breast carcinomas distinguish tumor subclasses with clinical implications. *Proc Natl Acad Sci U S A* **2001,** *98* (19), 10869-74.

55. Schatten, H., Cell and molecular biology of breast cancer. Humana Press: New York, 2013.

56. Polyak, K., Breast cancer: origins and evolution. *The Journal of Clinical Investigation* **2007,** *117* (11), 3155-3163.

57. Allred, D. C.; Mohsin, S. K.; Fuqua, S. A., Histological and biological evolution of human premalignant breast disease. *Endocrine-related cancer* **2001**, 47-61.

58. Burstein, H. J.; Polyak, K.; Wong, J. S.; Lester, S. C.; Kaelin, C. M., Ductal Carcinoma in Situ of the Breast. *New England Journal of Medicine* **2004,** *350* (14), 1430-1441.

59. Mariotti, C., Ductal carcinoma in situ of the breast. Springer: Cham, Switzerland, 2018.

60. Ligresti, G.; Libra, M.; Militello, L.; Clementi, S.; Donia, M.; Imbesi, R.; Malaponte, G.; Cappellani, A.; McCubrey, J. A.; Stivala, F., Breast cancer: Molecular basis and therapeutic strategies (Review). *Mol Med Rep* **2008,** *1* (4), 451-8.

61. Steelman, L. S.; Navolanic, P. M.; Franklin, R. A.; Bonati, A.; Libra, M.; Stivala, F.; Martelli, A. M.; McCubrey, J. A., Combining chemo-, hormonal and targeted therapies to treat breast cancer (Review). *Mol Med Rep* **2008,** *1* (2), 139-60.

62. Smith, I. E.; Dowsett, M., Aromatase Inhibitors in Breast Cancer. *New England Journal of Medicine* **2003,** *348* (24), 2431-2442.

63. Munshi, A.; Singh, P.; Jalali, R., Trastuzumab: is the new evidence revolutionary? *Journal of cancer research and therapeutics* **2006,** *2* (3), 144-6.

64. Slamon, D. J.; Clark, G. M.; Wong, S. G.; Levin, W. J.; Ullrich, A.; McGuire, W. L., Human breast cancer: correlation of relapse and survival with amplification of the HER-2/neu oncogene. *Science* **1987,** *235* (4785), 177-82.

65. Huang, S.; Ingber, D. E., Cell tension, matrix mechanics, and cancer development. *Cancer Cell* **2005,** *8* (3), 175-176.

66. Levental, K. R.; Yu, H.; Kass, L.; Lakins, J. N.; Egeblad, M.; Erler, J. T.; Fong, S. F. T.; Csiszar, K.; Giaccia, A.; Weninger, W.; Yamauchi, M.; Gasser, D. L.; Weaver, V. M., Matrix Crosslinking Forces Tumor Progression by Enhancing Integrin Signaling. *CELL Cell* **2009,** *139* (5), 891-906.

67. Kai, F.; Laklai, H.; Weaver, V. M., Force Matters: Biomechanical Regulation of Cell Invasion and Migration in Disease. *Trends in Cell Biology* **2016,** *26* (7), 486-497.

68. Hayashi, K.; Iwata, M., Stiffness of cancer cells measured with an AFM indentation method. *Journal of the mechanical behavior of biomedical materials* **2015,** *49*, 105-11.

69. Cross, S. E.; Jin, Y. S.; Rao, J.; Gimzewski, J. K., Nanomechanical analysis of cells from cancer patients. *Nature nanotechnology* **2007,** *2* (12), 780-3.

70. Alibert, C.; Goud, B.; Manneville, J.-B., Are cancer cells really softer than normal cells? *Biology of the Cell* **2017,** *109* (5), 167-189.

71. Li, Z.; Persson, H.; Adolfsson, K.; Abariute, L.; Borgström, M. T.; Hessman, D.; Åström, K.; Oredsson, S.; Prinz, C. N., Cellular traction forces: a useful parameter in cancer research. *Nanoscale* **2017,** *9* (48), 19039-19044.

72. Koch, T. M.; Münster, S.; Bonakdar, N.; Butler, J. P.; Fabry, B., 3D Traction Forces in Cancer Cell Invasion. *PLOS ONE* **2012,** *7* (3), e33476.

73. Peschetola, V.; Laurent, V. r. M.; Duperray, A.; Michel, R.; Ambrosi, D.; Preziosi, L.; Verdier, C., Time-dependent traction force microscopy for cancer cells as a measure of invasiveness. *Cytoskeleton* **2013,** *70* (4), 201-214.

74. Lodish, H. F.; Berk, A.; Kaiser, C. A.; Krieger, M.; Bretscher, A.; Ploegh, H.; Amon, A.; Martin, K. C., *Molecular cell biology*. Eighth edition. ed.; W.H. Freeman-Macmillan Learning: New York, 2016.

75. Nieman, M. T.; Prudoff, R. S.; Johnson, K. R.; Wheelock, M. J., N-cadherin promotes motility in human breast cancer cells regardless of their E-cadherin expression. *The Journal of cell biology* **1999,** *147* (3), 631-44.

76. Hulit, J.; Suyama, K.; Chung, S.; Keren, R.; Agiostratidou, G.; Shan, W.; Dong, X.; Williams, T. M.; Lisanti, M. P.; Knudsen, K.; Hazan, R. B., N-cadherin signaling potentiates mammary tumor metastasis via enhanced extracellular signal-regulated kinase activation. *Cancer Res* **2007,** *67* (7), 3106-16.

77. Araki, K.; Shimura, T.; Suzuki, H.; Tsutsumi, S.; Wada, W.; Yajima, T.; Kobayahi, T.; Kubo, N.; Kuwano, H., E/N-cadherin switch mediates cancer progression via TGF-β-induced epithelial-to-mesenchymal transition in extrahepatic cholangiocarcinoma. *British Journal Of Cancer* **2011,** *105*, 1885.

78. Hazan, R. B.; Qiao, R.; Keren, R.; Badano, I.; Suyama, K., Cadherin switch in tumor progression. *Annals of the New York Academy of Sciences* **2004,** *1014*, 155-63.

79. Scarpa, E.; Szabó, A.; Bibonne, A.; Theveneau, E.; Parsons, M.; Mayor, R., Cadherin Switch during EMT in Neural Crest Cells Leads to Contact Inhibition of Locomotion via Repolarization of Forces. *Developmental Cell* **2015,** *34* (4), 421-434.

80. Friedl, P.; Alexander, S., Cancer invasion and the microenvironment: plasticity and reciprocity. *Cell* **2011,** *147* (5), 992-1009.

81. Friedl, P.; Locker, J.; Sahai, E.; Segall, J. E., Classifying collective cancer cell invasion. *Nature Cell Biology* **2012,** *14* (8), 777-783.

82. Friedl, P., Prespecification and plasticity: shifting mechanisms of cell migration. *Current Opinion in Cell Biology* **2004,** *16* (1), 14-23.

83. Fey, P.; Stephens, S.; Titus, M. A.; Chisholm, R. L., SadA, a novel adhesion receptor in Dictyostelium. *The Journal of Cell Biology* **2002,** *159* (6), 1109-1119.

84. Tamariz, E.; Grinnell, F., Modulation of Fibroblast Morphology and Adhesion during Collagen Matrix Remodeling. *Molecular Biology of the Cell* **2002,** *13* (11), 3915-3929.

85. O'Brien, L. E.; Jou, T.-S.; Pollack, A. L.; Zhang, Q.; Hansen, S. H.; Yurchenco, P.; Mostov, K. E., Rac1 orientates epithelial apical polarity through effects on basolateral laminin assembly. *Nature Cell Biology* **2001,** *3*, 831.

86. Yang, S.; Graham, J.; Kahn, J. W.; Schwartz, E. A.; Gerritsen, M. E., Functional Roles for PECAM-1 (CD31) and VE-Cadherin (CD144. in Tube Assembly and Lumen Formation in Three-Dimensional Collagen Gels. *The American Journal of Pathology* **1999,** *155* (3), 887-895.

87. Tambe, D. T.; Hardin, C. C.; Angelini, T. E.; Rajendran, K.; Park, C. Y.; Serra-Picamal, X.; Zhou, E. H.; Zaman, M. H.; Butler, J. P.; Weitz, D. A.; Fredberg, J. J.; Trepat, X., Collective cell guidance by cooperative intercellular forces. *Nature materials* **2011,** *10* (6), 469-475.

88. Tambe, D. T.; Corey Hardin, C.; Angelini, T. E.; Rajendran, K.; Park, C. Y.; Serra-Picamal, X.; Zhou, E. H.; Zaman, M. H.; Butler, J. P.; Weitz, D. A.; Fredberg, J. J.; Trepat, X., Collective cell guidance by cooperative intercellular forces. *Nature Materials* **2011,** *10*, 469.

89. Pourati, J.; Maniotis, A.; Spiegel, D.; Schaffer, J. L.; Butler, J. P.; Fredberg, J. J.; Ingber, D. E.; Stamenovic, D.; Wang, N., Is cytoskeletal tension a major determinant of cell deformability in adherent endothelial cells? *Am J Physiol* **1998,** *274* (5 Pt 1), C1283-9.

90. Wang, N.; Tolic-Norrelykke, I. M.; Chen, J.; Mijailovich, S. M.; Butler, J. P.; Fredberg, J. J.; Stamenovic, D., Cell prestress. I. Stiffness and prestress are closely associated in adherent contractile cells. *Am J Physiol Cell Physiol* **2002,** *282* (3), C606-16.

91. Stamenovic, D.; Suki, B.; Fabry, B.; Wang, N.; Fredberg, J. J., Rheology of airway smooth muscle cells is associated with cytoskeletal contractile stress. *J Appl Physiol* **2004,** *96* (5), 1600-5.

92. Balaban, N. Q.; Schwarz, U. S.; Riveline, D.; Goichberg, P.; Tzur, G.; Sabanay, I.; Mahalu, D.; Safran, S.; Bershadsky, A.; Addadi, L.; Geiger, B., Force and focal adhesion assembly: a close relationship studied using elastic micropatterned substrates. *Nature cell biology* **2001,** *3* (5), 466-72.

93. Chen, C. S.; Alonso, J. L.; Ostuni, E.; Whitesides, G. M.; Ingber, D. E., Cell shape provides global control of focal adhesion assembly. *Biochem Biophys Res Commun* **2003,** *307* (2), 355-61.

94. Lele, T. P.; Pendse, J.; Kumar, S.; Salanga, M.; Karavitis, J.; Ingber, D. E., Mechanical forces alter zyxin unbinding kinetics within focal adhesions of living cells. *Journal of cellular physiology* **2006,** *207* (1), 187-94.

95. Tan, J. L.; Tien, J.; Pirone, D. M.; Gray, D. S.; Bhadriraju, K.; Chen, C. S., Cells lying on a bed of microneedles: an approach to isolate mechanical force. *Proc Natl Acad Sci U S A* **2003,** *100* (4), 1484-9.

96. Kim, J. H.; Serra-Picamal, X.; Tambe, D. T.; Zhou, E. H.; Park, C. Y.; Sadati, M.; Park, J. A.; Krishnan, R.; Gweon, B.; Millet, E.; Butler, J. P.; Trepat, X.; Fredberg, J. J., Propulsion and navigation within the advancing monolayer sheet. *Nature materials* **2013,** *12* (9), 856-63.

97. Ghosh, K.; Thodeti, C. K.; Dudley, A. C.; Mammoto, A.; Klagsbrun, M.; Ingber, D. E., Tumor-derived endothelial cells exhibit aberrant Rho-mediated mechanosensing and abnormal angiogenesis in vitro. *Proc Natl Acad Sci U S A* **2008,** *105* (32), 11305-10.

98. Krishnan, R.; Park, C. Y.; Lin, Y. C.; Mead, J.; Jaspers, R. T.; Trepat, X.; Lenormand, G.; Tambe, D.; Smolensky, A. V.; Knoll, A. H.; Butler, J. P.; Fredberg, J. J., Reinforcement versus fluidization in cytoskeletal mechanoresponsiveness. *PLoS One* **2009,** *4* (5), e5486.

99. Chen, C.; Krishnan, R.; Zhou, E.; Ramachandran, A.; Tambe, D.; Rajendran, K.; Adam, R. M.; Deng, L.; Fredberg, J. J., Fluidization and resolidification of the human bladder smooth muscle cell in response to transient stretch. *PLoS One* **2010,** *5* (8), e12035.

100. Prager-Khoutorsky, M.; Lichtenstein, A.; Krishnan, R.; Rajendran, K.; Mayo, A.; Kam, Z.; Geiger, B.; Bershadsky, A. D., Fibroblast polarization is a matrix-rigidity-dependent process controlled by focal adhesion mechanosensing. *Nature cell biology* **2011,** *13* (12), 1457-65.

101. Chen, C. S.; Mrksich, M.; Huang, S.; Whitesides, G. M.; Ingber, D. E., Geometric control of cell life and death. *Science* **1997,** *276* (5317), 1425-8.

102. Harris, A. K.; Wild, P.; Stopak, D., Silicone rubber substrata: a new wrinkle in the study of cell locomotion. *Science* **1980,** *208* (4440), 177-9.

103. Steinwachs, J.; Metzner, C.; Skodzek, K.; Lang, N.; Thievessen, I.; Mark, C.; Munster, S.; Aifantis, K. E.; Fabry, B., Three-dimensional force microscopy of cells in biopolymer networks. *Nature methods* **2016,** *13* (2), 171-6.

104. Krishnan, R.; Tambe, D.; Steward, R.; Hardin, C.; Butler, J., Traction Microscopy. In *Cells, Forces, and the Microenvironment*, Pan Stanford: 2015; pp 75-96.

105. Trappmann, B.; Gautrot, J. E.; Connelly, J. T.; Strange, D. G.; Li, Y.; Oyen, M. L.; Cohen Stuart, M. A.; Boehm, H.; Li, B.; Vogel, V.; Spatz, J. P.; Watt, F. M.; Huck, W. T., Extracellular-matrix tethering regulates stem-cell fate. *Nat Mater* **2012,** *11* (7), 642-9.

106. Park, C. Y.; Zhou, E. H.; Tambe, D.; Chen, B.; Lavoie, T.; Dowell, M.; Simeonov, A.; Maloney, D. J.; Marinkovic, A.; Tschumperlin, D. J.; Burger, S.; Frykenberg, M.; Butler, J. P.; Stamer, W. D.; Johnson, M.; Solway, J.; Fredberg, J. J.; Krishnan, R., High-throughput screening for modulators of cellular contractile force. *Integrative biology : quantitative biosciences from nano to macro* **2015,** *7* (10), 1318-24.

107. Comer, B. S.; Camoretti-Mercado, B.; Kogut, P. C.; Halayko, A. J.; Solway, J.; Gerthoffer, W. T., MicroRNA-146a and microRNA-146b expression and anti-inflammatory function in human airway smooth muscle. *Am J Physiol Lung Cell Mol Physiol* **2014,** *307* (9), L727-34.

108. Trepat, X.; Wasserman, M. R.; Angelini, T. E.; Millet, E.; Weitz, D. A.; Butler, J. P.; Fredberg, J. J., Physical forces during collective cell migration. *Nat Phys* **2009,** *5* (6), 426-430.

109. Sturton, R. G.; Trifilieff, A.; Nicholson, A. G.; Barnes, P. J., Pharmacological characterization of indacaterol, a novel once daily inhaled 2 adrenoceptor agonist, on small airways in human and rat precision-cut lung slices. *The Journal of pharmacology and experimental therapeutics* **2008,** *324* (1), 270-5.

110. Battram, C.; Charlton, S. J.; Cuenoud, B.; Dowling, M. R.; Fairhurst, R. A.; Farr, D.; Fozard, J. R.; Leighton-Davies, J. R.; Lewis, C. A.; McEvoy, L.; Turner, R. J.; Trifilieff, A., In vitro and in vivo pharmacological characterization of 5-[(R)-2-(5,6-diethyl-indan-2-ylamino)-1-hydroxy-ethyl]-8-hydroxy-1H-quinolin-2-o ne (indacaterol), a novel inhaled beta(2) adrenoceptor agonist with a 24-h duration of action. *The Journal of pharmacology and experimental therapeutics* **2006,** *317* (2), 762-70.

111. Deshpande, D. A.; Wang, W. C.; McIlmoyle, E. L.; Robinett, K. S.; Schillinger, R. M.; An, S. S.; Sham, J. S.; Liggett, S. B., Bitter taste receptors on airway smooth muscle bronchodilate by localized calcium signaling and reverse obstruction. *Nature medicine* **2010,** *16* (11), 1299-304.

112. Saxena, H.; Deshpande, D. A.; Tiegs, B. C.; Yan, H.; Battafarano, R. J.; Burrows, W. M.; Damera, G.; Panettieri, R. A.; Dubose, T. D., Jr.; An, S. S.; Penn, R. B., The GPCR OGR1 (GPR68) mediates diverse signalling and contraction of airway smooth muscle in response to small reductions in extracellular pH. *British journal of pharmacology* **2012,** *166* (3), 981-90.

113. Sparrow, J. R.; Hicks, D.; Hamel, C. P., The retinal pigment epithelium in health and disease. *Current molecular medicine* **2010,** *10* (9), 802-23.

114. Klettner, A.; Kaya, L.; Flach, J.; Lassen, J.; Treumer, F.; Roider, J., Basal and apical regulation of VEGF-A and placenta growth factor in the RPE/choroid and primary RPE. *Mol Vis* **2015,** *21*, 736-48.

115. Penn, J. S.; Madan, A.; Caldwell, R. B.; Bartoli, M.; Caldwell, R. W.; Hartnett, M. E., Vascular endothelial growth factor in eye disease. *Progress in retinal and eye research* **2008,** *27* (4), 331-71.

116. Hanus, J.; Zhang, H.; Wang, Z.; Liu, Q.; Zhou, Q.; Wang, S., Induction of necrotic cell death by oxidative stress in retinal pigment epithelial cells. *Cell Death Dis* **2013,** *4*, e965.

117. Jager, R. D.; Mieler, W. F.; Miller, J. W., Age-related macular degeneration. *The New England journal of medicine* **2008,** *358* (24), 2606-17.

118. Notbohm, J.; Poon, B.; Ravichandran, G., Analysis of nanoindentation of soft materials with an atomic force microscope. *Journal of Materials Research* **2012,** *27* (1), 229-237.

119. Pham, J. T.; Schellenberger, F.; Kappl, M.; Butt, H.-J., From elasticity to capillarity in soft materials indentation. *Physical Review Materials* **2017,** *1* (1), 015602.

120. Zhang, W.; Dong, X.; Cruz, S. S.; Heris, H. K.; Mongeau, L. G.; Ehrlicher, A. J.; Liu, X. In *A cost-effective microindentation system for soft material characterization*, 2015 IEEE International Conference on Mechatronics and Automation (ICMA), 2-5 Aug. 2015; 2015; pp 825-830.

121. Klein, S. M.; Manoharan, V. N.; Pine, D. J.; Lange, F. F., Preparation of monodisperse PMMA microspheres in nonpolar solvents by dispersion polymerization with a macromonomeric stabilizer. *Colloid Polym Sci Colloid and Polymer Science : Kolloid-Zeitschrift und Zeitschrift für Polymere.* **2003,** *282* (1), 7-13.

122. Oliver, T.; Jacobson, K.; Dembo, M., Traction forces in locomoting cells. *Cell Motility* **1995,** *31* (3), 225-240.

123. Yoshie, H.; Koushki, N.; Kaviani, R.; Tabatabaei, M.; Rajendran, K.; Dang, Q.; Husain, A.; Yao, S.; Li, C.; Sullivan, J. K.; Saint-Geniez, M.; Krishnan, R.; Ehrlicher, A. J., Traction Force Screening Enabled by Compliant PDMS Elastomers. *Biophysical Journal* **2018,** *114* (9), 2194-2199.

124. Kraning-Rush, C. M.; Califano, J. P.; Reinhart-King, C. A., Cellular Traction Stresses Increase with Increasing Metastatic Potential. *PLOS ONE* **2012,** *7* (2), e32572.

125. The Physical Sciences - Oncology Centers, N.; Agus, D. B.; Alexander, J. F.; Arap, W.; Ashili, S.; Aslan, J. E.; Austin, R. H.; Backman, V.; Bethel, K. J.; Bonneau, R.; Chen, W.-C.; Chen-Tanyolac, C.; Choi, N. C.; Curley, S. A.; Dallas, M.; Damania, D.; Davies, P. C. W.; Decuzzi, P.; Dickinson, L.; Estevez-Salmeron, L.; Estrella, V.; Ferrari, M.; Fischbach, C.; Foo, J.; Fraley, S. I.; Frantz, C.; Fuhrmann, A.; Gascard, P.; Gatenby, R. A.; Geng, Y.; Gerecht, S.; Gillies, R. J.; Godin, B.; Grady, W. M.; Greenfield, A.; Hemphill, C.; Hempstead, B. L.; Hielscher, A.; Hillis, W. D.; Holland, E. C.; Ibrahim-Hashim, A.; Jacks, T.; Johnson, R. H.; Joo, A.; Katz, J. E.; Kelbauskas, L.; Kesselman, C.; King, M. R.; Konstantopoulos, K.; Kraning-

Rush, C. M.; Kuhn, P.; Kung, K.; Kwee, B.; Lakins, J. N.; Lambert, G.; Liao, D.; Licht, J. D.; Liphardt, J. T.; Liu, L.; Lloyd, M. C.; Lyubimova, A.; Mallick, P.; Marko, J.; McCarty, O. J. T.; Meldrum, D. R.; Michor, F.; Mumenthaler, S. M.; Nandakumar, V.; O'Halloran, T. V.; Oh, S.; Pasqualini, R.; Paszek, M. J.; Philips, K. G.; Poultney, C. S.; Rana, K.; Reinhart-King, C. A.; Ros, R.; Semenza, G. L.; Senechal, P.; Shuler, M. L.; Srinivasan, S.; Staunton, J. R.; Stypula, Y.; Subramanian, H.; Tlsty, T. D.; Tormoen, G. W.; Tseng, Y.; van Oudenaarden, A.; Verbridge, S. S.; Wan, J. C.; Weaver, V. M.; Widom, J.; Will, C.; Wirtz, D.; Wojtkowiak, J.; Wu, P.-H., A physical sciences network characterization of non-tumorigenic and metastatic cells. *Scientific Reports* **2013,** *3*, 1449.

126. Guo, M.; Ehrlicher, A. J.; Jensen, M. H.; Renz, M.; Moore, J. R.; Goldman, R. D.; Lippincott-Schwartz, J.; Mackintosh, F. C.; Weitz, D. A., Probing the stochastic, motor-driven properties of the cytoplasm using force spectrum microscopy. *Cell* **2014,** *158* (4), 822-32.

127. Ngan, E.; Northey, J. J.; Brown, C. M.; Ursini-Siegel, J.; Siegel, P. M., A complex containing LPP and α-actinin mediates TGFβ-induced migration and invasion of ErbB2-expressing breast cancer cells. *Journal of Cell Science* **2013,** *126* (9), 1981-1991.

128. Nalluri, S. M.; O'Connor, J. W.; Virgi, G. A.; Stewart, S. E.; Ye, D.; Gomez, E. W., TGFbeta1-induced expression of caldesmon mediates epithelial-mesenchymal transition. *Cytoskeleton (Hoboken, N.J.)* **2018,** *75* (5), 201-212.

129. Yoshie, H.; Koushki, N.; Molter, C.; Siegel, P. M.; Krishnan, R.; Ehrlicher, A. J., High Throughput Traction Force Microscopy Using PDMS Reveals Dose-Dependent Effects of Transforming Growth Factor-β on the Epithelial-to-Mesenchymal Transition. *JoVE* **2019,** (148), e59364.

130. Kim, D. H.; Xing, T.; Yang, Z.; Dudek, R.; Lu, Q.; Chen, Y.-H., Epithelial Mesenchymal Transition in Embryonic Development, Tissue Repair and Cancer: A Comprehensive Overview. *Journal of clinical medicine* **2017,** *7* (1), 1.

131. Iwano, M.; Plieth, D.; Danoff, T. M.; Xue, C.; Okada, H.; Neilson, E. G., Evidence that fibroblasts derive from epithelium during tissue fibrosis. *J Clin Invest* **2002,** *110* (3), 341-50.

132. Wang, Y.; Zhou, B. P., Epithelial-mesenchymal Transition---A Hallmark of Breast Cancer Metastasis. *Cancer hallmarks* **2013,** *1* (1), 38-49.

133. Radisky, E. S.; Radisky, D. C., Matrix Metalloproteinase-Induced Epithelial-Mesenchymal Transition in Breast Cancer. *Journal of Mammary Gland Biology and Neoplasia* **2010,** *15* (2), 201-212.

134. Kumar, S.; Das, A.; Sen, S., Extracellular matrix density promotes EMT by weakening cell-cell adhesions. *Molecular bioSystems* **2014,** *10* (4), 838-50.

135. Roche, J., The Epithelial-to-Mesenchymal Transition in Cancer. *Cancers* **2018,** *10* (2), 52.

136. Chen, Y.-Q.; Lan, H.-Y.; Wu, Y.-C.; Yang, W.-H.; Chiou, A.; Yang, M.-H., Epithelial-mesenchymal transition softens head and neck cancer cells to facilitate migration in 3D environments. *Journal of cellular and molecular medicine* **2018,** *22* (8), 3837-3846.

137. Morikawa, M.; Derynck, R.; Miyazono, K., TGF-beta and the TGF-beta Family: Context-Dependent Roles in Cell and Tissue Physiology. *Cold Spring Harb Perspect Biol* **2016,** *8* (5).

138. Kondo, M.; Cubillo, E.; Tobiume, K.; Shirakihara, T.; Fukuda, N.; Suzuki, H.; Shimizu, K.; Takehara, K.; Cano, A.; Saitoh, M.; Miyazono, K., A role for Id in the regulation of TGF-β-induced epithelial–mesenchymal transdifferentiation. *Cell Death & Differentiation* **2004,** *11* (10), 1092-1101.

139. Lekka, M.; Laidler, P.; Gil, D.; Lekki, J.; Stachura, Z.; Hrynkiewicz, A. Z., Elasticity of normal and cancerous human bladder cells studied by scanning force microscopy. *European Biophysics Journal* **1999,** *28* (4), 312-316.

140. Guck, J.; Schinkinger, S.; Lincoln, B.; Wottawah, F.; Ebert, S.; Romeyke, M.; Lenz, D.; Erickson, H. M.; Ananthakrishnan, R.; Mitchell, D.; Käs, J.; Ulvick, S.; Bilby, C., Optical Deformability as an Inherent Cell Marker for Testing Malignant Transformation and Metastatic Competence. *Biophysical Journal* **2005,** *88* (5), 3689-3698.

141. Singla, M.; Kumar, A.; Bal, A.; Sarkar, S.; Bhattacharyya, S., Epithelial to mesenchymal transition induces stem cell like phenotype in renal cell carcinoma cells. *Cancer Cell Int* **2018,** *18*, 57-57.

142. Efremov, Y. M.; Wang, W.-H.; Hardy, S. D.; Geahlen, R. L.; Raman, A., Measuring nanoscale viscoelastic parameters of cells directly from AFM force-displacement curves. *Scientific Reports* **2017,** *7* (1), 1541.

143. Schneider, D.; Baronsky, T.; Pietuch, A.; Rother, J.; Oelkers, M.; Fichtner, D.; Wedlich, D.; Janshoff, A., Tension Monitoring during Epithelial-to-Mesenchymal Transition Links the Switch of Phenotype to Expression of Moesin and Cadherins in NMuMG Cells. *PLOS ONE* **2013,** *8* (12), e80068.

144. Fabry, B.; Maksym, G. N.; Butler, J. P.; Glogauer, M.; Navajas, D.; Fredberg, J. J., Scaling the Microrheology of Living Cells. *Physical Review Letters* **2001,** *87* (14), 148102.

145. Guo, M.; Pegoraro, A. F.; Mao, A.; Zhou, E. H.; Arany, P. R.; Han, Y.; Burnette, D. T.; Jensen, M. H.; Kasza, K. E.; Moore, J. R.; Mackintosh, F. C.; Fredberg, J. J.; Mooney, D. J.; Lippincott-Schwartz, J.; Weitz, D. A., Cell volume change through water efflux impacts cell stiffness and stem cell fate. *Proceedings of the National Academy of Sciences* **2017,** *114* (41), E8618-E8627.

146. Oakes, P. W.; Banerjee, S.; Marchetti, M. C.; Gardel, M. L., Geometry regulates traction stresses in adherent cells. *Biophysical journal* **2014,** *107* (4), 825-33.

147. Yang, H. W.; Chung, M.; Kudo, T.; Meyer, T., Competing memories of mitogen and p53 signalling control cell-cycle entry. *Nature* **2017,** *549* (7672), 404-408.

148. Hayer, A.; Shao, L.; Chung, M.; Joubert, L.-M.; Yang, H. W.; Tsai, F.-C.; Bisaria, A.; Betzig, E.; Meyer, T., Engulfed cadherin fingers are polarized junctional structures between collectively migrating endothelial cells. *Nature Cell Biology* **2016,** *18*, 1311.

149. Trepat, X.; Wasserman, M. R.; Angelini, T. E.; Millet, E.; Weitz, D. A.; Butler, J. P.; Fredberg, J. J., Physical forces during collective cell migration. *Nature Physics* **2009,** *5*, 426.

150. Institute, B. CellProfiler cell image analysis software. https://cellprofiler.org/ (accessed Sep 26, 2019).

151. Carpenter, A. E.; Jones, T. R.; Lamprecht, M. R.; Clarke, C.; Kang, I. H.; Friman, O.; Guertin, D. A.; Chang, J. H.; Lindquist, R. A.; Moffat, J.; Golland, P.; Sabatini, D. M., CellProfiler: image analysis software for identifying and quantifying cell phenotypes. *Genome Biology* **2006,** *7* (10), R100.

152. Eltzner, B.; Wollnik, C.; Gottschlich, C.; Huckemann, S.; Rehfeldt, F., The Filament Sensor for Near Real-Time Detection of Cytoskeletal Fiber Structures. *PLOS ONE* **2015,** *10* (5), e0126346.

153. ImageJ. https://imagej.net (accessed Sep 26, 2019).

154. Dembo, M.; Wang, Y. L., Stresses at the cell-to-substrate interface during locomotion of fibroblasts. *Biophysical journal* **1999,** *76* (4), 2307-16.